Synthesis of Missile Autopilots Robust to the Presence of Parametric Variations

by

Thomas John Urban

S.B. Aeronautics and Astronautics
Massachusetts Institute of Technology (1989)

Submitted to the Department of Aeronautics and Astronautics
in Partial Fulfillment of the Requirements for the Degree of
Master of Science in Aeronautics and Astronautics

at the

Massachusetts Institute of Technology
September 1991

Signature of Author _____
Department of Aeronautics and Astronautics
July 15, 1991

Certified by _____
Professor Lena Valavani
Thesis Supervisor

Accepted by _____
Professor Harold Y. Wachman
Chairman, Department Graduate Committee

Synthesis of Missile Autopilots
Robust to the Presence of
Parametric Variations

by

Thomas John Urban

Submitted to the Department of Aeronautics and Astronautics
on July 15, 1991 in partial fulfillment of the requirements
for the degree of Master of Science in
Aeronautics and Astronautics.

Abstract

A variety of H_∞ techniques to develop tactical missile autopilots robust to the presence of parametric variations have been analyzed. Three different H_∞ techniques are compared: H_∞ mixed sensitivity, H_∞ with modelled parametric uncertainty, and H_∞ with inner loop compensation. The importance of dynamic scaling (μ–analysis and μ–synthesis) to reduce conservatism when the H_∞ problem has a block diagonal uncertainty structure is also evaluated.

The results demonstrate the importance of the structured singular value (ssv) for the reduction of conservatism when a block diagonal perturbation structure exists. The extension of the ssv to the synthesis of H_∞ designs (μ–synthesis) also proves to be a valuable synthesis tool. Controllers synthesized using classical H_∞ optimization techniques are found to have poor robustness to parameter variations. Controllers synthesized using the H_∞ inner loop technique exhibit excellent parameter robustness, but poor robust performance in the presence of unstructured uncertainty. Controllers synthesized using H_∞/μ–synthesis techniques with modelled parameter uncertainty demonstrate adequate parameter robustness while providing the best framework for simultaneously satisfying multiple uncertainty criterion.

Thesis Supervisor: Dr. Lena Valavani

Title: Associate Professor of Aeronautics and Astronautics

This work was sponsored by the Department of the Air Force.

Acknowledgements

I would like to express my gratitude to Professor Lena Valavani and Carl Much for giving me the opportunity to pursue a Master's degree at M.I.T.

I would also like to thank Group 76, especially Dr. Appa Madiwale and Tony Hotz, for providing me with the best atmosphere for performing my graduate studies; their friendship and guidance were greatly appreciated.

To my friends and family, I would like to thank you for all the times you were there when I needed you and for all the memories we have shared. I hope that I can return the love you have given to me. It is to all of you that I dedicate my life.

A special thanks goes to Tony Hotz whose friendship and guidance have helped me through some very difficult times. I am sure that the time he spent helping me learn about academics and life will have a profound influence on me for years to come. Thank you.

Finally, a very special thanks go to my parents for their love and support throughout the years. I know that they are proud of me, but I'm not sure if they realize how proud I am of them.

Table of Contents

List of Figures

List of Tables

Chapter One:

Introduction

One of the most challenging of guidance and control problems is that of a modern tactical air-to-air missile in pursuit of a highly maneuverable aircraft. The missile, in an attempt to intercept the aircraft, undergoes dramatic changes in flight conditions and experiences high accelerations capable of exciting a multitude of unmodelled high frequency dynamics. The parametric variations associated with these changes in flight conditions and the possible excitation of high frequency unmodelled dynamics can cause the missile's control system to degrade, and in many cases to become unstable.

Because of this potential for instabilities, the performance one can extract from a missile control system must be offset by the requirement that the closed loop system remain stable in the presence of model uncertainties and parametric variations. The conflicting requirements between performance and stability have been the focus of much research in the past several years, [1] thru [7].

The H_∞ design methodology has recently arisen as one of the more popular modern control techniques. Its popularity stems from its ability to formulate the control problem as a frequency domain optimization problem [8]-[10]. This technique first appeared in literature in a paper by Zames [11], in which the emphasis was placed on sensitivity optimization. A simple extension of this optimization problem led to the

development of the *mixed sensitivity problem*, in which the optimal controller minimizes a weighted sensitivity cost function subject to stability robustness constraints. The stability robustness constraints were developed from classical design techniques and extended to the multi input multi output framework by utilizing singular values and norm bounds on expected model errors [1],[3],[12],[13]. The error models assumed, were based on worst case model uncertainty and made no attempt to incorporate direction or phase information — for this reason the error models are called unstructured uncertainties. The mixed sensitivity problem was the first attempt to incorporate known model uncertainty directly into the design process. Others methods which have recently been developed to incorporate model uncertainty in the design process include [2],[4],[5].

The application of the H_∞ methodology to research problems soon showed that while the closed loop system demonstrated excellent robustness to unstructured uncertainty, it had poor robustness to structured uncertainties; such as parametric variations. The lack of robustness to parameter variations manifests itself as instabilities of the closed loop system [14]-[16].

In the mid 1980's it was shown that analysis of linear systems with block diagonal perturbation structures using the H_∞ norm produced overly conservative results. It was proven that by optimally scaling the transfer functions of the closed loop system, to minimize its directionality, the conservatism of the maximum singular value could be significantly reduced [17], [18]. This measure became known as the structured singular value (μ).

When the H_∞ problem was formulated with multiple uncertainty requirements and desired performance criteria, the conservatism experienced in the application of the H_∞

norm also produced controllers that were conservative in nature. The optimistic results of the structured singular value were incorporated into the H_∞ design procedure to reduce conservatism. This led to the development of the newest robust control algorithm: μ Synthesis [19].

1.2 Contribution of Thesis

The purpose of this thesis is to demonstrate the use of different H_∞ methodologies to the development of a missile control system that is robust to the presence of both unmodelled dynamics and parametric variations. The thesis will compare four separate missile autopilot designs: H_∞ mixed sensitivity, H_∞ with modelled parametric variation, classical, and H_∞ with inner loop compensation.

This thesis will demonstrate the effectiveness of utilizing the structured singular value to reduce conservatism in the presence of multiple uncertainties, as well as performance requirements. Since the synthesis of controllers using the H_∞ optimization is sensitive to scaling effects, the thesis will also demonstrate the effectiveness of incorporating the results of the structured singular value directly into the design process (μ synthesis).

1.3 Organization of Thesis

This thesis consists of five chapters. Chapter Two discusses the important theories that underlie an understanding of the development of robust control systems using the H_∞ theory and the small gain theorem. This discussion includes:

- Small Gain Theorem
- Structured Singular Value (μ–analysis)
- H_∞ optimization
- μ Synthesis

In Chapter Three, the dynamic model of the missile is developed, while Chapter Four covers the actual synthesis of the missile control system. The first half of Chapter Four discusses the choice of performance criterion, the specification of uncertainty models, and the importance of μ-analysis and μ-synthesis. The second half of Chapter Four covers the development of the four different autopilot designs. A discussion of the important similarities and differences between these designs is included in the last section of Chapter Four.

Finally, Chapter Five summarizes the thesis and suggests possible directions for future research.

Chapter Two:

Robust Control Theory

Two of the most important purposes of feedback in a control system are the stabilization of unstable plants, and the reduction of uncertainty in the system's response. A certain amount of uncertainty is always present both in the environment in which the system operates as well as in the description of the system itself. When the presence of external disturbances are accurately known, then their effects can be accounted for during the design process. In most cases, however, it is not possible to know *a priori* the specific nature of such disturbances or their possible effects on the system. Accordingly, it is often necessary to design control systems with adequate disturbance rejection properties.

Similar to the effects of disturbances, uncertainties in the description of the plant affect the system's closed loop performance. This resulting degradation in performance may manifest as a slightly more oscillatory system, or it may result in an unstable system. Uncertainties of this nature arise because infinite dimensional nonlinear time varying systems are often approximated by finite dimensional linear time invariant models.

The ability of a system to adequately reject external disturbances and noisy measurements is an indication of it's *performance* capabilities. The performance of a

system is generally measured by how well the system is capable of tracking command signals and/or regulating specific outputs. The effects of these uncertainties on the system is a degradation in the desired output response of the system. When properly formulated, tracking properties can be considered a form of disturbance rejection since it is desired to regulate the tracking error to zero.

The assessment of how resilient a system is to internal changes due to parametric variations and unmodelled dynamics is a measure of how robust the system is. As noted above, if not properly developed, feedback control systems can become unstable in the presence of modelling errors. Systems which exhibit stability in the face of significant changes in plant structure are said to have good *stability robustness* properties.

In general there is a tradeoff between the performance of a system and its robustness properties. Tracking requirements and disturbance rejection properties require increased closed loop bandwidths, while robustness to unmodelled dynamics requires smaller bandwidths. When no uncertainties exist in a model, high performance control laws capable of following command signals with very high frequency content can be developed. In all practical situations, however, linear models neglect high frequency dynamics which result in significant errors between the model and the actual plant. When the control system has the ability to respond to frequencies where unmodelled dynamics have appreciable magnitude, the system may become unstable. This potential for instability requires that the bandwidth of the closed loop system be restricted in such a way as to prevent the control system from responding to signals above a critical frequency.

The majority of analysis and design techniques assume that a sufficiently accurate model of the plant to be controlled has been formulated. Although some methods draw conclusions about the effects of uncertainty on the response of the closed loop system, only a few have made attempts to directly incorporate the knowledge of uncertainty into the design procedure.

One of the primary objectives of robust control theory is the development of methodologies that explicitly formulate the control problem so as to account for uncertainties in the modelled system. By accounting for known plant variations and possible model errors, the control systems will be provide closed loop stability not only for the nominal model, but also for a range of plants characterized by the nominal model together with its uncertainties.

Another aim of robust control theory is to extend the application of linear feedback control into areas of nonlinear and time varying processes. By incorporating information concerning the differences between the nonlinear time varying model and the linearized approximation, it may be possible to develop feedback control laws using linear time invariant (LTI) models that respond just as well for the non-linear system.

The next few sections discuss some of the most important advances in robust control theory to date. The first section discusses the importance of the *small gain theorem* in the establishing sufficient conditions to guarantee stability in the presence of expected model errors, as necessary and sufficient conditions to insure adequate performance, and finally as a measure of robust performance. After an appropriate controller has been determined, the robustness of a system can be verified in the frequency domain by applying the small gain theorem.

The second section introduces the structured singular value and demonstrates its importance to the reduction of conservatism when the uncertainty has a block diagonal structure. The third section introduces the importance of the H_∞ problem and addresses how its results allow the designer to explicitly formulate the control problem to satisfy both performance and robustness criteria simultaneously.

Finally, the last section of this chapter discusses the newest addition to robust control theory, μ-synthesis. Section 2.2 demonstrates the importance of using the structured singular value to reduce conservatism in the small gain theorem, while Section 2.4 shows how μ–Synthesis utilizes the results of the structured singular value to reduce conservatism in the solution to the H_∞ problem.

2.1 Small Gain Theorem

In classical designs, the stability of the closed loop system is measured by means of gain and phase margins. The Bode plot of the open loop transfer function G(s)K(s) indicates how much uncertainty in gain and phase characteristics a system can withstand before its stability is affected. The Nyquist Stability Theorem provides necessary and sufficient conditions for determining the stability of the closed loop system:

Theorem 1. Nyquist Stability Criterion [20]

> *The closed loop system is stable if and only if the graph of $G(j\omega)K(j\omega)$ for $-\infty$ to ∞ encircles the point -1+0j as many times anticlockwise as $G(j\omega)K(j\omega)$ has right hand plane poles.*

The gain margin of the system is defined to be the minimum change in gain (either up or down) which alters the number of encirclements of the point -1+0j. The phase margin has a similar definition: the minimum phase shift a system could experience without changing the number of encirclements of the point -1+0j.

The Generalized Nyquist Criterion (GNC) attempted to extend the fundamentals of the classical Nyquist Criterion to the multi-input multi-output (MIMO) framework of modern control theory. In the MIMO framework, the Generalized Nyquist Criterion established similar rules, but looked at the plot of det[I+G(s)K(s)]. As in the classical theorem, changes in the number of encirclements of the point -1+0j was the criterion for establishing stability margins.

In the MIMO framework, changes in gain were not as simple to assess as they were in the single input single output (SISO) case. This difficulty led to the development of error models which provided information regarding the maximum possible error bound for the model at each point in frequency. The stability of the system was then verified by plotting circles, or Gershgorin bands, around a discrete set of points in the frequency domain. The radius of the circle was the magnitude of the largest error expected at that frequency. If one of the bands overlapped the point -1+0j, the stability of the system was uncertain. This provided only a sufficient condition for stability, since it assumed no phase characteristics, and also assumed that the largest possible model error could occur in any direction in the space of the system.

A simple extension of the Generalized Nyquist Criterion, the small gain theorem is perhaps the most utilized theorem in the field of robust control. Given a stable closed loop system M(s), the small gain theorem provides a measure of how stable the system is to a particular model uncertainty Δ(s). This theorem provides the same sufficient conditions as the GNC and the Gershgorin bands, but it's application is simpler and more structured.

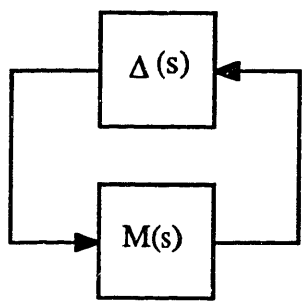

Figure 2.1 Small Gain Block Diagram

Based on the feedback system of Figure 2.1, the small gain theorem states that:

Theorem 2. Small Gain Theorem [20]

If M(s) is stable, the closed loop system of Figure 2.1 is stable for all functions Δ which satisfy:

- $\Delta(s)$ *is a stable function*
- $\|\Delta(s)\|_\infty \leq 1$ *for all* $s = jw$

if and only if $\|M(s)\|_\infty < 1$ *for all* $s=j\omega$

Proof: *If M(s) is stable and Δ(s) is stable, then the feedback system of Figure 2.1 can only become unstable if one or more of the characteristic loci of -ΔM encircles the point -1+0j or equivalently,*

$\det(I+\Delta M)=0$. If the characteristic loci, $\lambda_i(M(s)\Delta(s))$, the spectral radius, $\rho(\bullet)$, the maximum singular value, $\bar{\sigma}(\bullet)$, and

$$|\lambda_i(M\Delta)| \leq \rho(M\Delta) \leq \bar{\sigma}(M\Delta) \tag{2.1}$$

then no encirclements of -1+0j can occur if $\bar{\sigma}(M\Delta) \leq 1$ at each point in frequency or, equivalently if,

$$\|M\Delta\|_\infty \leq 1 \tag{2.2}$$

Using the triangle rule, and the fact that $\|\Delta\|_\infty \leq 1$,

$$\|M(s)\|_\infty \leq 1 \tag{2.3}$$

Based on the results of the small gain theorem, if the maximum singular value of the closed loop transfer function is less than the inverse of the minimum singular value of the uncertainty, the system is guaranteed to be stable. Note that this theorem is only a sufficient condition for stability; if the condition is violated, the system may or may not be unstable.

Stability requirements as well as performance specifications may be formulated as small gain problems. By finding the appropriate transfer functions for M(s) a designer can verify performance goals, stability requirements and robust performance.

2.1.1 Stability Robustness

When the model of a system is known exactly, there is no need to determine stability margins. If however, the model is a linearized reduced order approximation to a complex system, significant modelling uncertainty exists. There are several ways of

representing this uncertainty. Three of the most popular methods for capturing uncertainty due to unmodelled dynamics are:

- Multiplicative Input Uncertainty

$$G_a = G_{nom}(1 + W_i\Delta_i) \tag{2.4}$$

- Multiplicative Output Uncertainty

$$G_a = (1 + W_o\Delta_o)G_{nom} \tag{2.5}$$

- Additive Uncertainty

$$G_a = G_{nom} + dG \quad \text{where } dG = W_a\Delta_a \tag{2.6}$$

In the representation of the uncertainty, W is a real rational stable transfer function which represents the maximum model error over all frequency. The uncertainty block, Δ, is a stable transfer function whose $\|\Delta\|_\infty \leq 1$. The Δ block contains all the phase information, i.e. it represents any possible phase variation.

Using the results of the small gain theorem, sufficient conditions for robust stability of the system of Figure 2.2 can be expressed as either

$$\bar{\sigma}((I + GK)^{-1}GK) \leq \underline{\sigma}(W_i\Delta_i)^{-1} \tag{2.7}$$

or,

$$\|W_i(I + GK)^{-1}GK\|_\infty \leq 1 \tag{2.8}$$

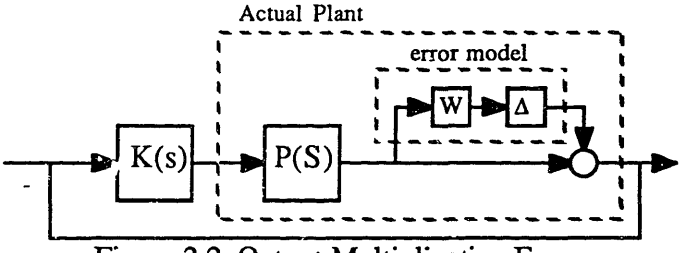

Figure 2.2 Output Multiplicative Error

The first result is a statement of the small gain problem while the second is expressed as a requirement for satisfying the small gain problem of Figure 2.1.

In many instances one error model will not be sufficient to capture the differences between the real plant and the model. In such cases, additional error models may be incorporated into the block diagram of Figure 2.2. For example, the system shown in Figure 2.3 has multiplicative modelling errors at both the input and output of the plant.

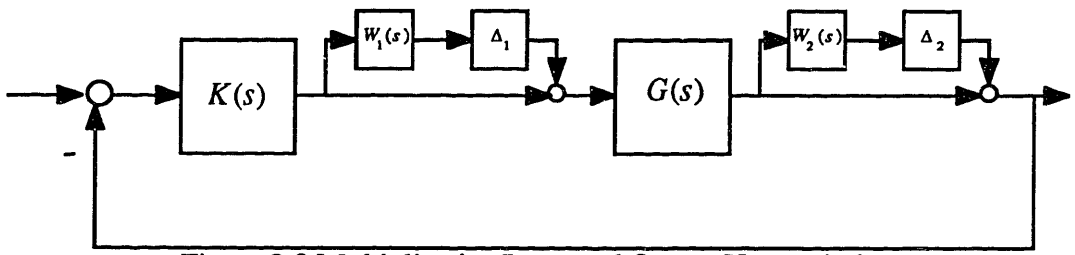

Figure 2.3 Multiplicative Input and Output Uncertainties

This problem may arise when there is uncertainty in the actuator and in the output of the plant. Here, the small gain theorem must be applied using both uncertainty models simultaneously. It is not sufficient to verify the norm inequalities for the transfer functions of Δ_1 and Δ_2 separately.

In order to apply the small gain theorem to a multiple uncertainty problem, the engineer must redraw the block diagram as shown in Figure 2.4.

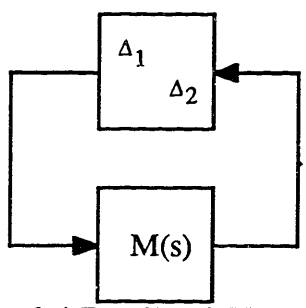

Figure 2.4 Two Block Uncertainty

The transfer function, M(s) is represented by

$$M(s)=\begin{bmatrix} W_1(I+KG)^{-1}KG & W_1(I+KG)^{-1}K \\ W_2(I+GK)^{-1}G & W_2(I+GK)^{-1}GK \end{bmatrix} \tag{2.9}$$

Satisfaction of the small gain theorem requires that $\|M(s)\|_\infty \leq 1$.

The uncertainty structure represented by Figure 2.4 has a block diagonal structure. The straightforward application of the H_∞ norm provides a very conservative result. Section 2.2 will discuss a method to reduce the conservatism of this result.

2.1.2 Performance Optimization

In the design of control systems performance criteria are generally specified as input output relations. Typical performance criteria include:

- Disturbance Rejection
- Command Following
- Minimum Control Use
- Zero Steady State Error

One way of attempting to meet certain performance specifications is to augment the plant with weighting filters. For example, an integrator is placed on the tracking error, a high pass filter is used for low frequency disturbance rejection, and a low pass filter is used for high frequency noise attenuation.

Once a feedback control law has been determined, satisfaction of the performance requirements can be assessed by application of the small gain theorem. Unlike the case

of robust stability, when the problem is properly formulated, the application of the small gain theorem provides both necessary and sufficient conditions for verification of frequency specified performance criterion.

Figure 2.5 shows the small gain formulation for performance; w represents all external disturbances, and z represents all performance variables to be minimized.

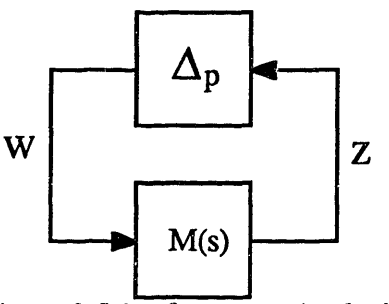

Figure 2.5 Performance Analysis

When $\|M(s)\|_\infty \leq 1$ the desired performance criterion has been achieved. If there exists a region in which $\|M(s)\|_\infty \geq 1$, then the performance is degraded at that frequency band. The $\|\bullet\|_\infty$ norm provides a measure of the degradation. If $\|M(s)\|_\infty = 1.5$, then the performance specifications are degraded by 50% of their desired level.

2.1.3 Robust Performance

It is generally desirable to guarantee a minimum level of performance over a range of plant variations. This can be achieved by combining the results of sections 2.1.1 and 2.1.2. A closed loop system can be analyzed by placing weighting functions and error models on all appropriate transfer functions and then applying the small gain theorem. It is important however, for the designer to remember that there are conflicting requirements between high performance and good robustness. In particular, the system is constrained by:

$$S(s) + C(s) = 1,$$

where S(s) is the sensitivity function and C(s) is the complementary sensitivity function. In order to guarantee a minimum stable performance in the presence of modelling uncertainty, the system must satisfy the small gain theorem of Figure 2.6.

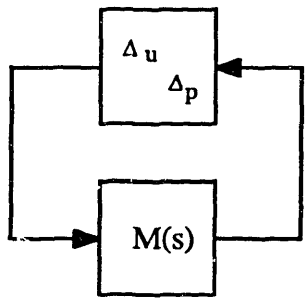

Figure 2.6 Robust Performance

where Δ_u and Δ_p represent the unstructured uncertainty and performance requirements respectively. Whenever a problem contains unstructured uncertainties and performance requirements it will have the block diagonal structure of Figure 2.6.

2.2 μ–Analysis

The application of the small gain theorem to problems which contain multiple uncertainty blocks, (see Figure 2.3) or to problems with a mixture of performance and stability robustness specifications (see Figure 2.6) introduces one of the most serious limitations in the application of the $\|\bullet\|_\infty$ norm. When more than one specification is given, the uncertainty block, Δ, takes on a block diagonal structure. By blindly applying the $\|\bullet\|_\infty$ norm, no attempt is made to utilize this structure. The result is an excessively conservative estimate of the minimum perturbation that can destabilize the system.

When the uncertainty block has a diagonal structure, the inputs and outputs of the system are related in sets defined by the block structure.

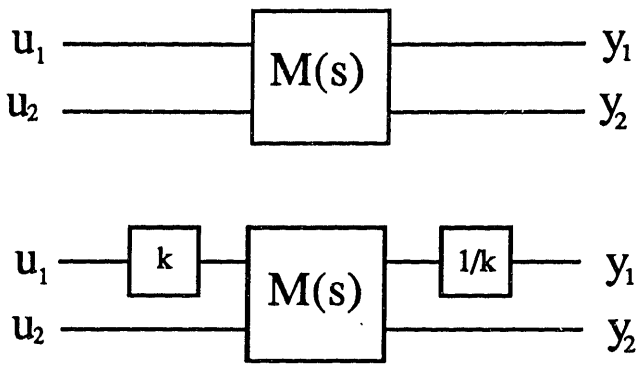

Figure 2.7 Effects of Scaling

When considering simultaneous perturbations, there is no way of eliminating the cross effect of the input u_1 to the output y_2. In Figure 2.7, the input u_1 is related to the output y_1, but not to the output y_2. In determining the $\|M(s)\|_\infty$ it is mathematically assumed that all the inputs are meaningfully related to all outputs. The conservatism in the $\|\bullet\|_\infty$ norm arises because of the relative difference in scales between inputs and outputs which are not associated with the same uncertainty block. Since $\|\bullet\|_\infty$ calculates the largest magnification of a signal between all inputs and all outputs, this scaling problem may exaggerate the relative importance of one input set to an unrelated output set.

Figure 2.7 shows the effect of scaling on the input/output nature of the system. In the top picture, the relations between $\vec{u}$ and $\vec{y}$ are simply

$$\begin{aligned} y_1 &= M_{11}u_1 + M_{12}u_2 \\ y_2 &= M_{21}u_1 + M_{22}u_2 \end{aligned} \tag{2.10}$$

When the transfer function between u_1 and y_1 is scaled, the relations between $\vec{u}$ and $\vec{y}$ become

$$\begin{aligned} y_1 &= M_{11}u_1 + \frac{1}{k}M_{12}u_2 \\ y_2 &= kM_{21}u_1 + M_{22}u_2 \end{aligned} \tag{2.11}$$

In the above example, it is obvious that for certain choices of k, the input u_1 has an exaggerated effect on the output y_2. This demonstrates the severe limitation of $\|\bullet\|_\infty$. While it is important to consider the effects of simultaneous perturbations, the scaling between unrelated input /output sets may result in overly conservative estimates of $\|M(s)\|_\infty$.

In 1982, John Doyle [17] introduced the *structured singular value* as a method of reducing the conservativeness associated with block diagonal perturbations. The structured singular value utilizes the uncertainty structure of Δ to optimally scale the inputs and outputs of the system, minimizing the influence one input set has upon an unrelated output set.

There are two types of uncertainties which arise in problem formulations: repeated scalar blocks and full blocks. Let S denote the number of repeated scalar blocks and F the number of full blocks present in a specific problem. Repeated scalar blocks have dimension r associated with the number of places the scalar uncertainty arises in the problem, so the ith scalar block has dimension r_i. Like repeated scalars, full blocks can be of any dimension and are not necessarily square matrices. To simplify the explanation of the structured singular value, however, it will be assumed that all full blocks are square matrices. In this case, the dimension of the jth full block is $m_j x m_j$.

The total perturbation Δ is a compilation of all scalar uncertainties, δ, and full block uncertainties, Δ. Given the S scalar uncertainties and the F full block uncertainties, Δ is defined as

$$\Delta = \left\{ \text{diag}(\delta_1 I_{r_1}, \ldots\ldots, \delta_S I_{r_S}, \Delta_1, \ldots\ldots, \Delta_F) \mid \delta_i \in C,\ \Delta_j \in C^{m_j \times m_j} \right\} \tag{2.12}$$

For consistency, the dimension of Δ should be the same as that of M.

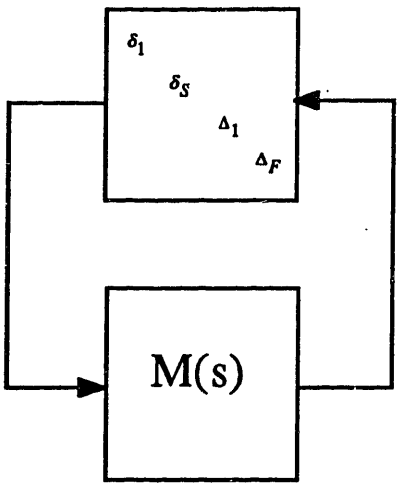

Figure 2.8 General Interconnection

Having defined the total structured uncertainty form Δ, μ is defined as the inverse of the smallest Δ which makes the feedback system of Figure 2.8 unstable, i.e. $\det(I+M\Delta)=0$.

$$\mu(M)=\left\{\begin{array}{l}0 \text{ if no } \Delta \text{ solves } \det(I+M\Delta)=0\\ \dfrac{1}{\left(\min\limits_{\Delta}\{\bar{\sigma}(\Delta)\mid \det(I+M\Delta)=0\}\right)}\end{array}\right\} \tag{2.13}$$

There are two degenerative cases to which the definition of μ is expected to simplify to:

- Δ represents a single full block uncertainty

$$\Delta \in C^{m\times m} \qquad \mu(M)=\bar{\sigma}(M) \tag{2.14}$$

- Δ represents a single repeated scalar uncertainty

$$\Delta \in C \text{ s.t. } \Delta=\delta I \qquad \mu(M)=\rho(M) \tag{2.15}$$

These relations are consistent with the expected solution of the small gain problem using the appropriate norm bounds.

Some other properties associated with μ are

- There exists a D, $D\Delta D^{-1} = \Delta$
- $\mu(M) = \mu(MU) = \mu(UM)$
- $\mu(DMD^{-1}) = \mu(M)$

where D has a block diagonal structure similar to Δ, and U is a unitary matrix.

The first property above states that there exists a matrix D that has the same block structure as and commutes with Δ. Since Δ is block diagonal, each entry on its diagonal commutes with the same entry of D. Therefore, D has the following structure

$$D = diag(D_1,....,D_s,d_1 I_{m_1},...d_F I_{m_f}) \tag{2.16}$$

In this way, D_i commutes with repeated scalar blocks $\delta_i I_{r_i}$, and $d_j I_{m_j}$ commutes with Δ_{m_j} .

It was shown in [17] that the value of $\mu(M)$ is bounded above and below by

$$\max_{U} \rho(UM) \leq \mu(M) \leq \inf_{D} \overline{\sigma}(DMD^{-1}) \tag{2.17}$$

It was further proved that the lower bound is always an equality. Unfortunately, the maximization problem is not guaranteed to converge to the global minimum. There are problems that exist which contain many local maxima, and gradient techniques have been known to converge to the nonoptimal solution.

Doyle also proved that in certain special cases the upper bound is also an equality. This equality is important, since it can be shown that the minimization of DMD^{-1} has no local minima which are not global. These special cases occur when Δ has no more than three blocks; where each block represents a separate uncertainty or performance

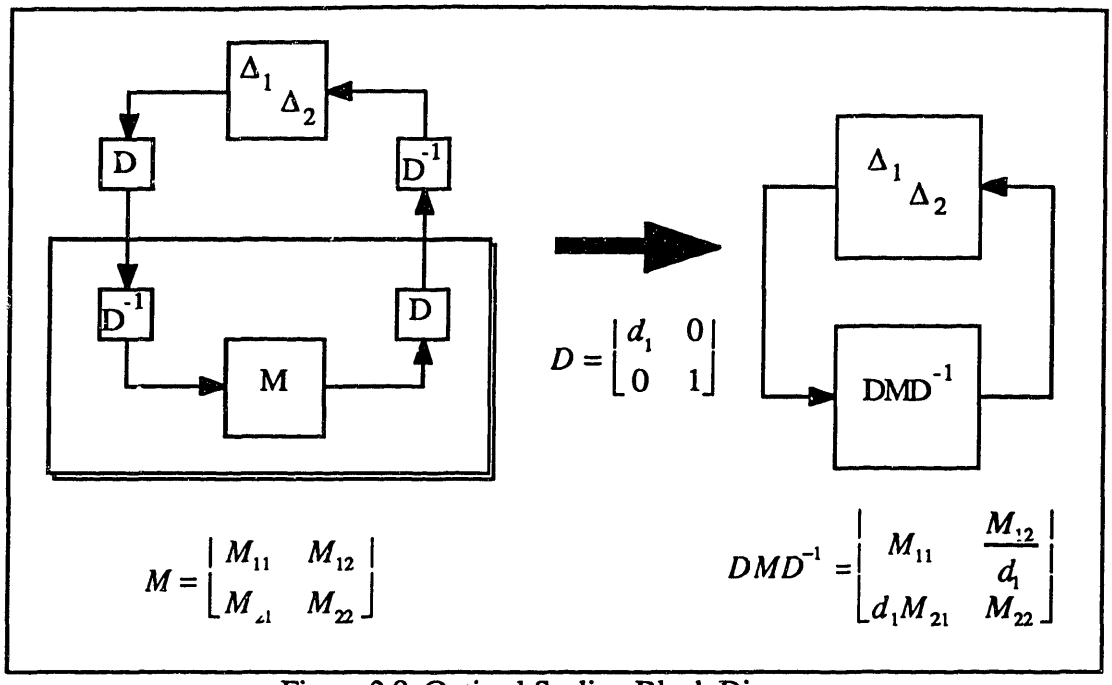

Figure 2.9 Optimal Scaling Block Diagram

specification. For cases in which Δ contains more than three blocks it has been shown that the upper bound remains reasonably tight. In fact worst case convergences have had accuracies of 85%, whereas most others have been approximately 95% correct.

It is generally simpler to intuitively understand the function of μ when one considers the case of three or fewer blocks and uses the upper bound as the definition of μ. The scaling matrix, D, is represented point by point in the frequency domain as a diagonal matrix of frequency-varying scales. As noted, D commutes with Δ, however, D does not commute with M(s). As shown in Figure 2.9, the appropriate choice of D, scales the off-diagonal terms of the matrix DMD^{-1}. By searching for the D that minimizes the maximum singular value of DMD^{-1} , the conservatism of the $\|\bullet\|_\infty$ norm is reduced.

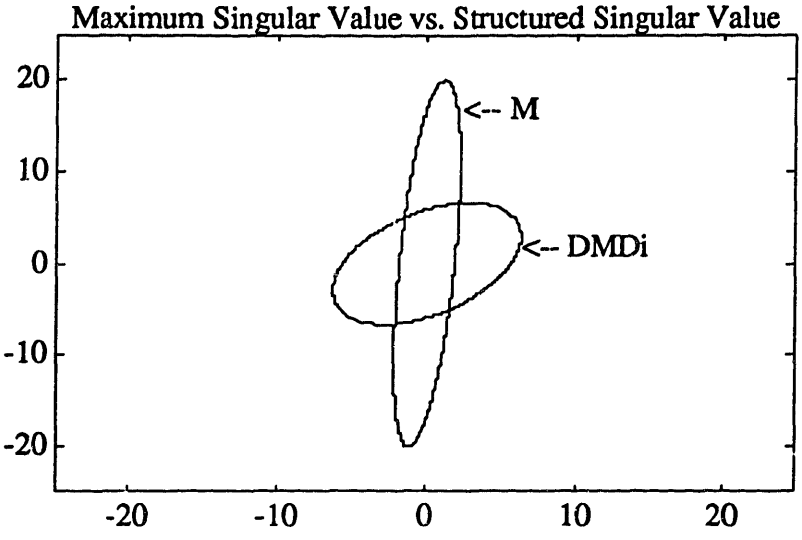

Figure 2.10 Maximum vs. Structured Singular Value

A brief example may be helpful at this point: Given a two-by-two constant matrix M,

$$M = \begin{bmatrix} 1 & 2 \\ 20 & 2 \end{bmatrix}$$

$$\overline{\sigma}(M) = 20.1355$$

the maximum singular value of M equals 20.1355. Figure 2.10 plots an ellipse that represents the locus of possible amplifications of the matrix M as a function of the input direction. It is obvious that the maximum singular value is much greater than the minimum singular value. This is evidenced by the elongation of the ellipse.

To apply the small gain theorem to this matrix would require that the maximum singular value of M be less than some prespecified magnitude. Satisfaction of this requirement produces extremely conservative results for directions other than that of the maximum singular value.

Using a gradient search supplied in the μ Tools software package, the D scale is found to be

$$D = \begin{bmatrix} .316 & 0 \\ 0 & 1 \end{bmatrix} \qquad D^{-1} = \begin{bmatrix} 3.16 & 0 \\ 0 & 1 \end{bmatrix}.$$

so that,

$$DMD^{-1} = \begin{bmatrix} 1 & 6.32 \\ 6.32 & 2 \end{bmatrix}$$

$$\overline{\sigma}(DMD^{-1}) = \mu(M) = 7.84$$

When the system matrix M is scaled by this optimal D, the maximum singular value is reduced to 7.84. This shows clearly that without scaling, the results of the $\|\bullet\|_\infty$ norm are quite conservative. Figure 2.10 shows the loci of amplifications of DMD^{-1} as a function of input direction. In this case, the scaling has reduced the elongation considerably. The off-diagonal terms of DMD^{-1} have been equalized as much as possible, given that they are equivalent. Application of the small gain theorem to the matrix DMD^{-1} results in a much less conservative estimate of stability. As an item of comparison, the locus of amplifications of the system matrix with the least amount of conservatism is represented by a circle, so that every direction has the same amount of magnification.

2.3 H_∞ Design Methodology

The H_∞ design methodology has become in recent years one of the most popular of the modern control techniques. The reason for its popularity is its ability to formulate the control problem as a frequency domain optimization process. This technique first appeared in the literature in a paper by Zames [11], in which the emphasis was placed on sensitivity optimization. In 1988, Keith Glover and John Doyle published results

which generalized the sensitivity optimization process and provided a direct state space solution [21].

Previously, researchers in the field of modern control investigated time domain optimization techniques. These techniques assumed a specific nature of the inputs and the disturbances of the system — primarily, that they assumed a certain spectral distribution as well as specific probabalistic magnitudes such as covariance intensity [22], [23]. In cases where nothing was known about the inputs and disturbances, except that they contained a finite amount of energy, it became more meaningful to pose the problem as a minimization of the maximum possible energy amplification of the system's output .

Further research showed that minimizing the appropriate weighted transfer function norms made the H_∞ optimization a powerful tool for loop shaping techniques [9]. This utility had great appeal to classical designers, as they now had the ability to formulate the control problem as a weighted sensitivity optimization process. Moreover, it allowed them to explicitly augment the system with information about bandwidth limitations based on norm bounded unmodelled dynamic error models.

The following sections give a concise overview of the H_∞ methodology. More detailed information on the theory behind H_∞ solutions can be found in the works of B. A. Francis [24] and Glover and Doyle [21].

2.3.1 The H_∞ Norm

The H_∞ norm is one of several operator norms used to describe the possible amplification of a signal entering a system. The H_∞ norm is defined as

$$\|G(s)\|_\infty = \sup_\omega \bar{\sigma}(G(jw)) \tag{2.18}$$

where $\|G(s)\|_\infty$ satisfies the usual properties of norms — namely,

$$\|G\| \geq 0 \text{ with } \|G\| = 0 \text{ iff } G = 0$$
$$\|aG\| = |a|\|G\| \text{ for any scalar } \alpha$$
$$\|G + H\| \leq \|G\| + \|H\|$$
$$\|GH\|_\infty \leq \|G\|_\infty \|H\|_\infty$$

The H_∞ norm is referred to as an operator norm because it represents the greatest possible amplification of the mapping of the operator, G(s), which maps a function, the input signal, into another function, the output signal.

To fully understand the meaning of the H_∞ norm, consider the input signal u(t) which is known to have a finite amount of energy as measured by

$$\|u\|_2 = \sqrt{\int_{-\infty}^{\infty} u^T u \, dt} \tag{2.19}$$

but no other information regarding the signal is available. The H_∞ norm describes the greatest increase in energy that can occur between the input, u, and the output, y, for a given system, G. This was proven in a theorem by Vidyasagar, 1985 and Francis, 1987 and is stated as

Theorem: 3

If $\|u\|_2 < \infty$ and y(s)=G(s)u(s) and G(s) is stable and proper and has no poles on the imaginary axis then:

$$\sup_{\omega} \frac{\|y\|_2}{\|u\|_2} = \|G\|_\infty \tag{2.20}$$

Proof: omitted. see [24]

Intuitively, the H_∞ norm can be realized as the peak point in a maximum singular value plot of the transfer function G(s) as shown in Figure 2.11.

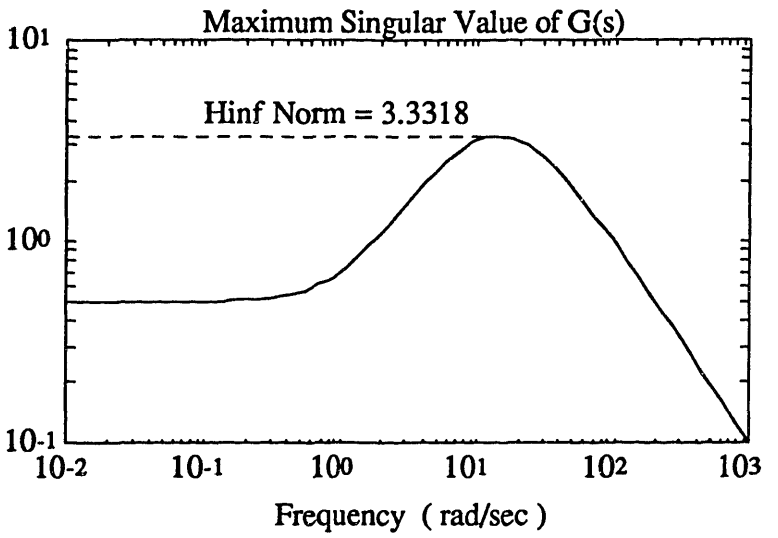

Figure 2.11 Maximum Singular Value and H_∞

2.3.2 The H_∞ Problem Formulation

A block diagram depicting the H_∞ problem formulation is shown in Figure 2.12. This diagram is often referred to as a linear fractional transformation.

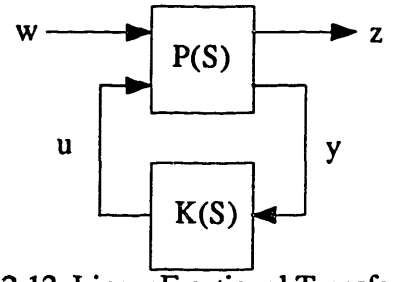

Figure 2.12 Linear Fractional Transformation

The vector w, represents external inputs to the system and the vector z represents signals which mathematically describe design objectives. Since the transfer function relationship between w and z represents a set of mathematical relations characterizing the desired system response, it often contains weighting functions which represent various performance objectives and norm bounds on error models.

The vector y contains all measured variables that will be used to provide the controller with information about the plant. The controller, K(s), generates a feedback signal represented by the vector u.

If P(s) is partitioned as

$$P(s)=\begin{bmatrix} P_{11}(s) & P_{12}(s) \\ P_{21}(s) & P_{22}(s) \end{bmatrix}$$

then the relatior between the inputs and the outputs of the system can be expressed as

$$z = P_{11}w + P_{12}u \tag{2.21}$$

$$y = P_{21}w + P_{22}u \tag{2.22}$$

Using the relationship u=Ky, equations 2.21 and 2.22 can be combined to obtain:

$$z = [P_{11} + P_{12}K(I - P_{22}K)^{-1}P_{21}]w \tag{2.23}$$

The expression in brackets is often denoted as $F_l(P,K)$, so that 2.23 can be expressed as

$$z = F_l(P,K)w \tag{2.24}$$

From this expression, the H_∞ optimization process is stated as: *Find K(s) which stabilizes the closed loop system and minimizes* $\|F_l(P,K)\|_\infty$.

The term H_∞ is defined as the set of transfer functions of asymptotically stable, realizable systems. Therefore $X \in H_\infty$ means that X is an asymptotically stable realizable system. The H_∞ problem arises because it is desirable to minimize $\|F_l(P,K)\|_\infty$ over all $F_l(P,K)$, such that $F_l(P,K) \in H_\infty$ and the feedback combination of P and K is internally stable [20].

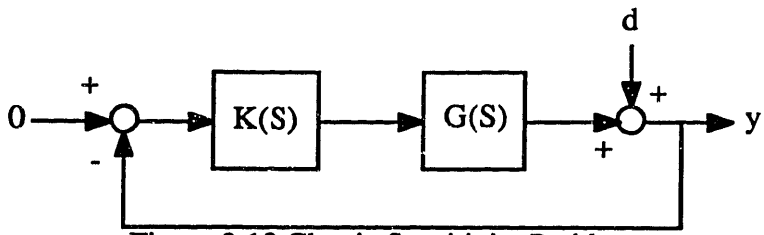

Figure 2.13 Classic Sensitivity Problem

2.3.3 Loop Shaping and Plant Augmentation

The original H_∞ problem was formulated as a sensitivity optimization problem (Figure 2.13) In that case, the optimization criterion was

$$\text{minimize } \|S\|_\infty \text{ where } S = (I + PK)^{-1}$$

It was soon found that this minimization could be improved upon by augmenting the output y with a weighting filter. An appropriate choice of weighting filter was one that had unity gain at frequencies at which the sensitivity minimization was important and attenuated the signal above the cutoff frequency. The new problem was formulated as

$$\text{minimize } \|W(s)S(s)\|_\infty$$

where W(s) represented the weighting filter.

The solution to the above minimization problem had one complication: it produced controllers with infinite bandwidth systems; there was no explicit criterion in the problem formulation to limit the bandwidth of the system. This led to the formulation of the mixed sensitivity problem:

$$\text{minimize } \left\| \begin{matrix} W_p(s)S(s) \\ W_u(s)C(s) \end{matrix} \right\|_\infty$$

where $W_u(s)$ represented a bound on the expected modelling error of the open loop plant and C(s) was the closed loop transfer function.

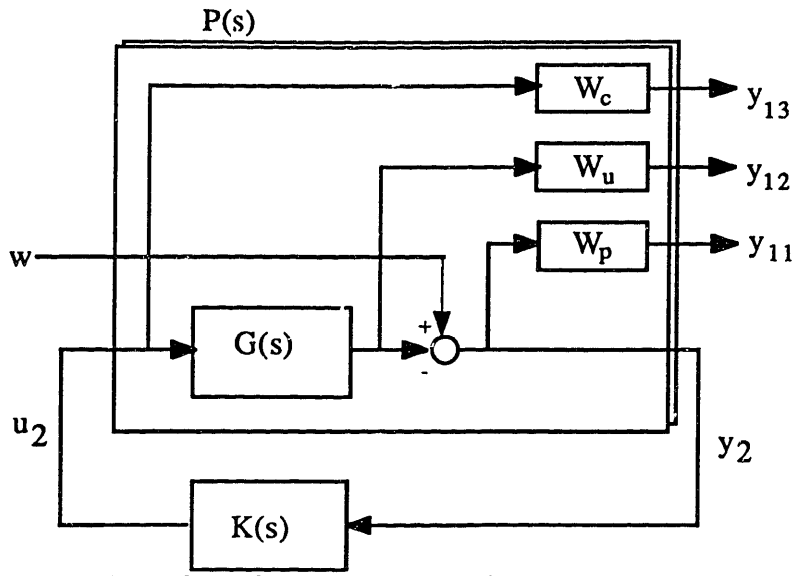

Figure 2.14 Standard H_∞ Feedback Formulation

This problem optimized the sensitivity of the system for disturbance rejection while satisfying the stability robustness criterion for stability in the presence of unstructured modelling uncertainty.

The standard H_∞ problem formulation is depicted in Figure 2.14. The minimization criterion is

$$\text{minimize} \left\| \begin{matrix} W_p(s)S(s) \\ W_u(s)C(s) \\ W_c(s)R(s) \end{matrix} \right\|_\infty$$

where *R(S)* is the transfer function from w to the control u. Typically, the weights W_u and W_C tend to perform the same objective: bandlimit the closed loop system. W_u is the appropriate filter to use if the plant uncertainty is specified as a multiplicative output error, while the weight W_C tends to model uncertainties which are additive in nature.

There are some requirements on the structure of P(s) in order to insure that the solution to the H_∞ problem is proper. P_{12} and P_{21} must be proper transfer functions. P_{21} can be made proper by providing a noise signal to each measured variable. P_{12} can be made proper by either weighting the control transfer function, R(s), with a proper weight, $W_C(s)$, or selecting a $W_U(s)G(s)$ combination that is proper. If $W_U(s)G(s)$ is not proper, a relatively small weight can be placed on the control TFM R(s) without interfering with the general solution of a mixed sensitivity/weighted output design.

2.3.4 The Glover-Doyle H_∞ Solution

In 1988, Keith Glover and John Doyle published a paper which provided a state space formula for determining all stabilizing controllers that satisfy an H_∞ norm bound [21]. Specifically, the solution to their algorithm provided the set of all stabilizing controllers K(s) such that

$$\|F_l(P,K)\|_\infty < \gamma \tag{2.25}$$

for some prespecified $\gamma \in \Re$.

The following state space solution to the H_∞ problem is taken directly from the paper published by Glover and Doyle in 1988. This solution minimizes the H_∞ norm for the linear system represented by

$$\dot{x} = Ax + B_1 w + B_2 u \tag{2.26}$$
$$z = C_1 x + D_{11} w + D_{12} u \tag{2.27}$$
$$y = C_2 x + D_{21} w + D_{22} u \tag{2.28}$$

where $w \in \Re^{m_1}$, $u \in \Re^{m_2}$, $z \in \Re^{p_1}$, $y \in \Re^{p_2}$.

In order to determine the solution to 2.25, the system of 2.26-2.28 must satisfy the following assumptions:

- $(A, B2)$ is stabilizable and $(A, C2)$ is detectable.
  (This is required for the existence of a stabilizing controller K)
- $D12$ is full column rank and $D21$ is full row rank
  (This is sufficient to ensure that the controllers are proper)
- $\begin{bmatrix} A - j\omega I & B_2 \\ C_1 & D_{12} \end{bmatrix}$ has full column rank for all ω
- $\begin{bmatrix} A - j\omega I & B_1 \\ C_2 & D_{21} \end{bmatrix}$ has full row rank for all ω

Along with these above assumptions, a scaling of u and y and a unitary transformation of w and z are necessary in order to simplify the algorithm notation. The scaling assumes that it is possible to arrange D_{12}, D_{21} and D_{11} as they are shown below:

$$D_{12} = \begin{bmatrix} 0 \\ I \end{bmatrix} \qquad D_{21} = [0 \quad I]$$

$$\begin{bmatrix} D_{1111} & D_{1112} \\ D_{1121} & D_{1122} \end{bmatrix}$$

where D_{1122} has m_2 rows and p_2 columns. The following notation is introduced to simplify the equations:

$$R = D_{1\bullet}^{*} D_{1} - \begin{bmatrix} \gamma^2 I_{m_1} & 0 \\ 0 & 0 \end{bmatrix} \text{ where } D_{1\bullet} = [D_{11}\ D_{12}]$$

$$\tilde{R} = D_{\bullet 1} D_{\bullet 1}^{*} - \begin{bmatrix} \gamma^2 I_{p_1} & 0 \\ 0 & 0 \end{bmatrix} \text{ where } D_{\bullet 1} = [D_{11}^{*}\ D_{21}^{*}]^{*}$$

Based on the results of Glover and Doyle, the solution to the H_∞ problem is solved by finding the solution to the following two Riccati equations, denoted X_∞ and Y_∞ respectively:

$$X_\infty(A-BR^{-1}D_{1\bullet}^*C_1)+(A-BR^{-1}D_{1\bullet}^*C_1)^*X_\infty - X_\infty BR^{-1}B^*X_\infty + C_1^*(I-D_{1\bullet}R^{-1}D_{1\bullet}^*)C_1 = 0 \qquad (2.29)$$

$$Y_\infty(A-B_1D_{\bullet 1}^*\tilde{R}^{-1}C)^*+(A-B_1D_{\bullet 1}^*\tilde{R}^{-1}C)^*Y_\infty - Y_\infty C^*\tilde{R}^{-1}CY_\infty + B_1(I-D_{\bullet 1}^*\tilde{R}^{-1}D_{\bullet 1})B_1^* = 0 \qquad (2.30)$$

The state feedback and output injection matrices are defined as:

$$F = -R^{-1}(D_{1\bullet}^*C_1 + B^*X_\infty) \quad \text{partitioned as } F=[F_{11}^* \;\; F_{12}^* \;\; F_2^*]^*$$

$$H = -(B_1D_{\bullet 1}^* + Y_\infty C^*)\tilde{R}^{-1} \quad \text{partitioned as } H=[H_{11} \;\; H_{12} \;\; H_2].$$

Given the Riccati equations 2.29 and 2.30, the solution to the H_∞ problem is stated on the following pages without proof. This solution is taken directly from [21].

Theorem 4 Glover and Doyle Algorithm

For the system described by 2.29 to 2.30 and satisfying the above assumptions:

a) There exists an internally stabilizing controller K(s) such that $\|F_l(P,K)\|_\infty < \gamma$ *if and only if,*

i) $\gamma > max(\overline{\sigma}[D_{1111}, D_{1112}],\ \sigma[D_{1111}^*, D_{1121}^*])$

and,

ii) there exists $X_\infty \geq 0$ *and* $Y_\infty \geq 0$ *satisfying 2.29 and 2.30 respectively and such that* $\rho(X_\infty Y_\infty) < \gamma^2$

b) *Given that the conditions of part a are satisfied, then all stabilizing controllers K(s) satisfying* $\|F_l(P,K)\|_\infty < \gamma$ *are given by*

$K = F_l(K_a, \Phi)$ *for arbitrary* $\Phi \in RH_\infty$ *such that* $\|\Phi\|_\infty < \gamma$

where,

$$K_a = \begin{bmatrix} \hat{A} & \hat{B}_1 & \hat{B}_2 \\ \hat{C}_1 & \hat{D}_{11} & \hat{D}_{12} \\ \hat{C}_2 & \hat{D}_{21} & 0 \end{bmatrix}$$

$$\hat{D}_{11} = -D_{1121} D_{1111}^{*} (\gamma^2 I - D_{1111} D_{1111}^{*})^{-1} D_{1112} - D_{1122}$$

$\hat{D}_{12} \in R^{m_2 \times m_2}$ *and* $\hat{D}_{21} \in R^{p_2 \times p_2}$ *are any matrices satisfying*

$$\hat{D}_{12} \hat{D}_{12}^{*} = I - D_{1121} (\gamma^2 I - D_{1111}^{*} D_{1111})^{-1} D_{1121}^{*}$$

$$\hat{D}_{21}^{*} \hat{D}_{21} = I - D_{1112}^{*} (\gamma^2 I - D_{1111} D_{1111}^{*})^{-1} D_{1112}$$

and

$$\hat{B}_2 = (B_2 + H_{12}) \hat{D}_{12}$$

$$\hat{C}_2 = -\hat{D}_{21} (C_2 + F_{12}) Z$$

$$\hat{B}_1 = -H_2 + \hat{B}_2 \hat{D}_{12}^{-1} \hat{D}_{11}$$

$$\hat{C}_1 = F_2 Z + \hat{D}_{11} \hat{D}_{21}^{-1} \hat{C}_2$$

$$\hat{A} = A + HC + \hat{B}_2 \hat{D}_{12}^{-1} \hat{C}_1$$

where

$$Z = (I - \gamma^{-2} Y_\infty X_\infty)^{-1}$$

Using the Glover and Doyle algorithm, one can find the controller which minimizes $\|F_l(P,K)\|_\infty$ by successively reducing the value of γ until the limiting value γ_o is reached, such that $\rho(X_\infty Y_\infty) = \gamma_o^2$, or until one of the two Ricatti equations fails to have a positive semi-definite solution.

The solution to the above set of nonlinear equations provides the set of all stabilizing controllers, where Φ is arbitrary, which minimizes equation (2.25). One solution, called the maximum entropy controller, is found by setting $\Phi = 0$. It has the realization

$$K = (\hat{A}, \hat{B}_1, \hat{C}_1, \hat{D}_{11}) \tag{2.31}$$

and therefore has the same dimension as the augmented plant P(s).

The above solution is determined for the case where $D_{22}=0$, which can be validly assumed in this particular problem formulation. The addition of D_{22} can be performed by applying the algorithm to the plant

$$\hat{P} = P - \begin{bmatrix} 0 & 0 \\ 0 & D22 \end{bmatrix} \tag{2.32}$$

and obtaining the controller $\hat{K}$. The desired controller is then of the form:

$$K = \hat{K}(I + D_{22}\hat{K})^{-1} \tag{2.33}$$

2.3.5 H_∞ Insight

There are two results of the H_∞ process which warrant further discussion. The first is the loop shaping capability, and the second is the nature of the controller.

Because the H_∞ optimization process minimizes the cost function $\|F_l(P,K)\|_\infty$ less than some prespecified value of γ, the designer has the ability to shape certain performance loops as desired, so long as he/she chooses weights that are not conflicting in nature. The best way to understand how loop shaping is accomplished is to assume that given the appropriate choice of weightings a minimum value of γ=1 is achieved. In this case, the optimization process guarantees that

$$\left\| \begin{matrix} W_p(s)S(s) \\ W_u(s)C(s) \end{matrix} \right\|_\infty \leq 1$$

This solution insures that for all frequencies, the following relationships also hold:

$$\|W_p(s)S(s)\|_\infty \leq 1 \quad \text{and,}$$
$$\|W_u(s)C(s)\|_\infty \leq 1$$

Using the above relationships and the properties of norms, it is easy to prove that

$$\bar{\sigma}(S(s)) \leq \left|W_p(s)^{-1}\right| \text{ and,}$$
$$\bar{\sigma}(\mathrm{C(c)}) \leq \left|\mathrm{W_u}(s)^{-1}\right| \text{ for all } \omega$$

The choice of weighting filters should be the inverse of what the designer actually wants the loop shape to be. In the case of unstructured uncertainty, the weighting filters should be an error model which represents a bound on the maximum expected plant uncertainty. In that case, the solution to the H_∞ problem would be one that satisfies the small gain stability robustness criterion.

The H_∞ optimization procedure is an excellent method for synthesizing controllers where the performance objectives and stability requirements can be expressed as functions of frequency loop shapes. In such cases, formulation of the H_∞ problem and minimization of $\gamma<1$ guarantee that all design objectives have been met and satisfy the small gain theorem. There is difficulty, however, when one desires a specific transient response to input commands. Choices of weighting filters to accomplish time domain transient goals are much more difficult and generally require several iterations before the designer receives a response which satisfies his/her specific goals.

The basic idea behind the H_∞ compensator is that it inverts the stable dynamics of the plant and substitutes in their place desirable dynamics prescribed by the weighting filters. In the inversion process, the stable poles are cancelled by zeroes and the stable zeroes are cancelled by poles. Unstable poles and zeroes are replaced by mirror image stable poles and zeroes [16].

This plant inversion process has been shown to provide results which are sensitive to parametric variations when the poles being inverted are lightly damped resonant pole pairs [14]. The purpose of this thesis is to suggest alternative problem formulations which provide H_∞ solutions that are robust to the parametric variation that influences the location of lightly damped poles.

2.4 μ–Synthesis

The primary objective of H_∞ theory is to minimize $\|F_l(P,K)\|_\infty$ over all frequencies. It has been shown above that there are specific types of problem formulations in which the $\|\bullet\|_\infty$ norm produces conservative estimates of the maximum amplification. These conservative results in the application of the $\|\bullet\|_\infty$ norm to the solution of the H_∞ problem suggest that solutions of the H_∞ problem may also be conservative in nature.

Indeed, the above statement has proven true [6]. When determining a controller K(s) for the H_∞ problem, the solution is extremely sensitive to the scalings of inputs, in relation both to one another and to their corresponding outputs. When the H_∞ algorithm is formulated to satisfy a small gain problem that has a block diagonal structure, the results may be extremely conservative.

Section 2.2 demonstrated the effectiveness of applying an optimal scaling procedure to the analysis of the small gain problem. This section discusses the newest theory in robust modern control, μ-synthesis. μ-Synthesis utilizes the optimal scaling procedure of the structured singular value to reduce the conservatism of the H_∞ problem solution. The μ-Synthesis problem becomes one of finding a stabilizing controller K(s) *and* a scaling matrix D(s) such that

$$\|DF_l(P,K)D^{-1}\|_\infty$$

is minimized. The specific solution to the μ-Synthesis problem has not been analytically determined. However in [19], Doyle recommends the so-called D-K iteration as a method of approximating the solution to the μ-synthesis problem. The D-K iteration is a systematic way of calculating the controller K(s) and the dynamic scales

D(s) to converge to a sub-optimal solution. The first step in the μ-synthesis problem to formulate the original H_∞ problem as a minimization of

$$\|F_l(P,K)\|_\infty .$$

If the synthesis of the controller K(s) meets the required specifications, there is no need to proceed further. If the H_∞ norm is not less than the desired value, the closed loop block of Figure 2.15 is analyzed using the structured singular value.

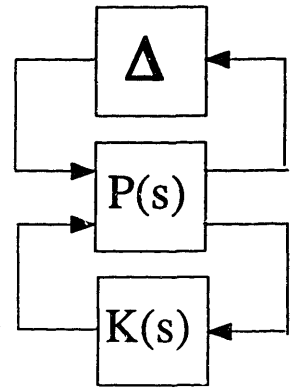

Figure 2.15 μ Analysis

In the analysis of the structured singular value, optimal D scales are calculated to improve the scaling of the system matrix. These D scales are approximated with real, minimum phase invertible transfer function weighting matrices. If the μ bound meets the specified criterion, then the procedure is complete. If, however, it does not, the D-scales are absorbed into the open loop plant as demonstrated by Figure 2.16.

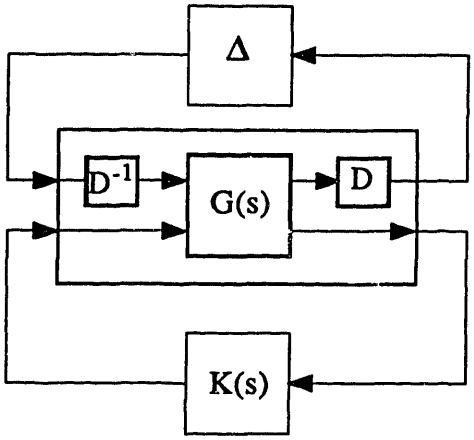

Figure 2.16 μ-Synthesis

Once the D-scales are absorbed into the plant, a new controller K(s) is determined. This new controller will have an increased number of states, since the D-scales have states of their own. The increase in the order of states is four times the number of states used in the D-scale approximation. Half of the states are present in the controller, and half in the plant's D-scales. After the controller K(s) is determined, the structured singular value is assessed again. If the design goals are met, the procedure is stopped, if not, the procedure continues to iterate on the selection of K(s) and D(s). Hence the name D-K iteration.

It should be noted that the solution to the μ-synthesis problem using the D-K iteration does not guarantee convergence to the optimal solution. Although each step in the process is guaranteed to solve the appropriate optimization process; K(s) minimizes $\|F_l(P,K)\|_\infty$ and D(s) minimizes $\|DF_l(P,K)D^{-1}\|_\infty$, the joint minimization of $\|DF_l(P,K)D^{-1}\|_\infty$ is not guaranteed based on this stepwise approach.

Another difficulty present in the μ-problem is that of developing D-scales for repeated scalar uncertainties. When the uncertainty is a repeated scalar of dimension r, the D scale which optimally scales the uncertainty constitute a full matrix of dimension r.

There is currently no method for implementing a full matrix D-scale with real rational transfer functions. Therefore, in the μ-synthesis problem, the calculation of D-scales for repeated scalars must be a suboptimal approach. The approach used is to assume for the synthesis problem that the uncertainty of dimension r actually represents r different scalar uncertainties of dimension 1. This assumption produces conservative results, but the conservatism of this approach is still much less than that of ignoring the block diagonal structure.

Chapter Three:

The Model: Tactical Missiles

One of the most challenging problems in the area of guidance and control is that of a modern tactical air to air missile in pursuit of a highly maneuverable aircraft. The missile's dynamic motion is characterized by a set of nonlinear, time varying, coupled differential equations. The inability to directly develop control systems for differential equations of this nature makes the design of high performance robust control systems extremely difficult.

The missile, in an attempt to intercept the aircraft, often undergoes dramatic changes in flight conditions and experiences high acceleration rates capable of exciting a multitude of unmodelled high frequency dynamics. The parametric variations associated with the changes in flight conditions and the possible excitation of high frequency unmodelled dynamics may cause the performance of a missile's control system to degrade and in many cases, to become unstable.

The changes in flight conditions affect the nominal operating point around which the missile's control system is designed. In general, a series of control laws are developed which are scheduled as a function of flight condition. One of the more difficult of parameters to schedule is angle of attack. Along with being difficult to measure, the

angle of attack changes rapidly during the pursuit of an aircraft and hence is difficult to schedule accurately, necessitating robust design techniques.

The following sections discuss the development of the linear time invariant model used for synthesizing a longitudinal missile control system.

3.1 The Dynamic Model

The synthesis of missile autopilots requires the characterization of the dynamic motion of the missile in flight. There are six equations of motion which describe a body in three dimensional space: three force equations and three moment equations. When the mass and moments of inertia are assumed constant the equations of kinematic rigid body motion can be expressed as the Euler's equations below.

Translational Dynamics

$$m(\dot{u}+qw-rv)=\sum F_x+g_x \tag{3.1}$$

$$m(\dot{v}+ru-pw)=\sum F_y+g_y \tag{3.2}$$

$$m(\dot{w}+pv-qu)=\sum F_z+g_z \tag{3.3}$$

Rotational Dynamics

$$I_{xx}\dot{p}-(I_{yy}-I_{zz})qr+I_{yz}(r^2-q^2)-I_{xz}(pq+\dot{r})+I_{xy}(rp-\dot{q})=\sum T_L \tag{3.4}$$

$$I_{yy}\dot{q}-(I_{zz}-I_{xx})rp+I_{xz}(p^2-r^2)-I_{xy}(qr+\dot{p})+I_{yz}(pq-\dot{r})=\sum T_M \tag{3.5}$$

$$I_{zz}\dot{r}-(I_{xx}-I_{yy})qp+I_{xy}(q^2-p^2)-I_{yz}(rp+\dot{q})+Ixz(qr-\dot{p})=\sum T_N \tag{3.6}$$

where g_X,g_Y, and g_Z are the components of gravity along each axis.

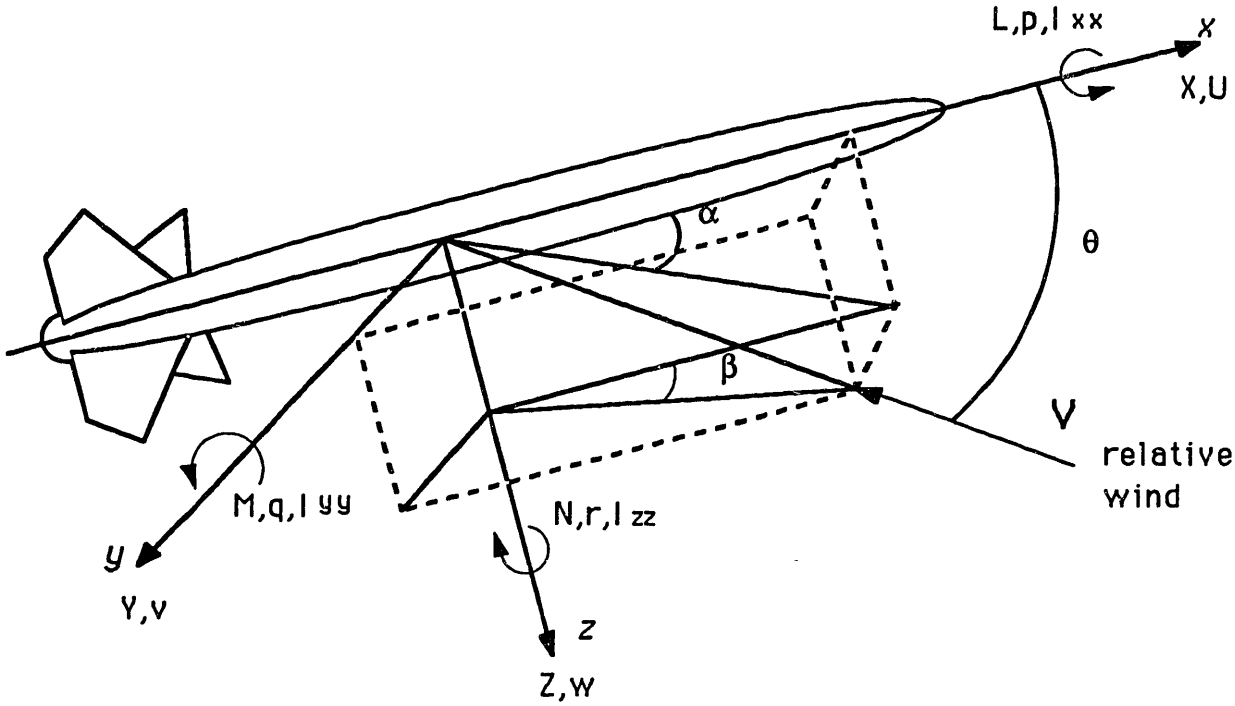

Figure 3.1 Missile Body Axis System

	Roll axis	Yaw axis	Pitch axis
Angular rates	p	q	r
Component of velocity on axis	U	v	w
Force along each axis	X	Y	Z
Moments about each axis	L	M	N
Moments of Inertia	I_{xx}	I_{yy}	I_{zz}

Table 3.1 Body Axis Notation

The Euler equations (3.1) to (3.6) are expressed in the body axis of the missile. Figure 3.1 shows the standard axis system used to describe the axis relative to the missile body, while Table 3.1 lists the symbols which denote the various components of force, moments, and velocities along each of the three axes.

In order to simplify the equations (3.1) to (3.5), several assumptions are made:

1) The missile's mass is symmetric with respect to the xy, yz, and xz axis. This eliminates the cross products of inertia. ($I_{xy} = I_{yz} = I_{xz} = 0$)
2) Gravity is ignored. This omission will be compensated for in the implementation by introducing a DC bias into the system.
3) In order to design a linear control system for the longitudinal motion of the missile, it is assumed that motions in the longitudinal plane do not influence motions in the lateral plane (p=r=v=0).

The above simplifications reduce Euler's equations to the following three nonlinear, coupled differential equations:

$$m(\dot{u} + qw) = \sum F_x \qquad (3.1a)$$

$$m(\dot{w} - qu) = \sum F_z \qquad (3.3a)$$

$$I_{yy}\dot{q} = \sum T_M \qquad (3.5a)$$

If pitch rate were integrated to give the pitching angle θ, these equations would represent a set of fourth order coupled differential equations describing the motion of the missile in the longitudinal plane. There are two modes associated with these equations: the phugoid mode and the short period mode. The phugoid mode, in general, is a slowly varying mode and will be compensated for in the guidance system. Therefore it is only necessary to develop a control system to control the short period mode of the missile.

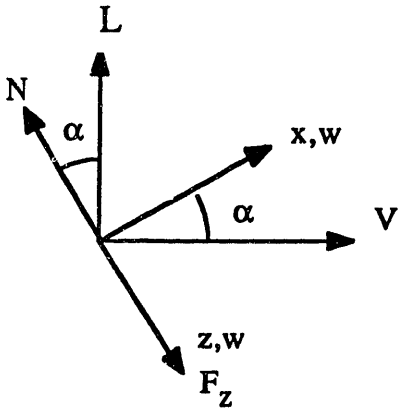

Figure 3.2 Axis Transformations

In the short period approximation to the missile's longitudinal motion, it is assumed that the forward velocity u is constant, u = U. This assumption eliminates the need for equation (3.1a). Since there are only two differential equations left, two states are sufficient to accurately model the short period mode of a tactical missile: angle of attack, α, and pitch rate q.

3.1.1 Aerodynamic Forces

The force F_Z and moment T_m are generated by the lifting and control surfaces of the missile. In order to characterize the aerodynamic response of the missile, the forces and moments are represented by the normalized aerodynamic coefficients, C_n and C_m, respectively:

$$N = \tfrac{1}{2}\rho V^2 S C_n \tag{3.6}$$

$$M = \tfrac{1}{2}\rho V^2 S l C_m. \tag{3.7}$$

The lifting force, L, is defined as perpendicular to the velocity vector V. The force F_Z is related to the lifting force by equation (3.8) (see Figure 3.2):

$$F_z = -L\cos\alpha \tag{3.8}$$

The aerodynamic coefficient C_n is measured in the inertial axis normal to the wing. It is therefore related to lift by equation (3.9):

$$C_l = C_n \cos\alpha. \tag{3.9}$$

Finally, the force in the z direction, F_Z, can be represented as

$$F_z = -N\cos^2\alpha. \tag{3.10}$$

The velocities w and u can be represented as functions of the total velocity, as seen in Figure 3.2. These relations are

$$w = V\sin\alpha \tag{3.11}$$
$$u = V\cos\alpha. \tag{3.12}$$

The rate of change of angle of attack can be represented as

$$\dot{\alpha} = \frac{\dot{w}}{u} = \frac{\dot{w}}{V\cos\alpha} \tag{3.13}$$

Dividing equation (3.3a) through by mass, m, and u, and using the relations (3.10), (3.12) and (3.13), equation (3.3a) can be written as

$$\dot{\alpha} = q - \frac{QSC_n\cos\alpha}{mV} \tag{3.14}$$

where Q is the dynamic pressure. Dividing equation (3.5a) through by the moment of inertia I_y, and using the relation (3.7), equation (3.5a) can be written as

$$\dot{q} = \frac{QSdC_m}{I_y}. \tag{3.15}$$

Since the aerodynamic coefficients Cn and Cm are nonlinear functions of many different variables (e.g., mach number and angle of attack), the coefficients of Cn and

Cm are expanded using a Taylor series to approximate the contribution of each parameter to the total force. In this example, angle of attack and elevator deflection are the only variables accounted for explicitly:

$$C_n = C_{no} + C_{n\alpha}\alpha + C_{ndq}dq \tag{3.16}$$

$$C_m = C_{mo} + C_{m\alpha}\alpha + C_{mdq}dq \tag{3.17}$$

where *dq* represents the deflection of the elevator.

After representing the aerodynamic coefficients by a Taylor series approximation, (3.14) thru (3.17) can be combined and linearized around a trim operating point. This analysis provides a linear representation of the dynamic equations for the short period mode.

$$\dot{\alpha} = \frac{Z_\alpha}{V}\alpha + q + \frac{Z_{dq}}{V}dq \tag{3.18}$$

$$\dot{q} = M_\alpha \alpha + M_{dq}dq \tag{3.19}$$

where,

$$Z_\alpha = -\frac{QSC_{n\alpha}\cos\alpha}{m} \tag{3.20}$$

$$Z_{dq} = -\frac{QSC_{zdq}\cos\alpha}{m} \tag{3.21}$$

$$M_\alpha = \frac{QSdC_{m\alpha}}{I_{yy}} \tag{3.22}$$

$$M_{dq} = \frac{QSdC_{mdq}}{I_{yy}} \tag{3.23}$$

3.1.2 Actuators

A linear actuator is used to move the control surface when commanded. This actuator can be modelled as a second order system with a natural frequency of ω_n=283 (rad/sec) and a damping ratio of ζ=.707.

$$dq = \frac{\omega_n^2}{s^2 + 2\xi\omega_n s + \omega_n^2} dq_c \tag{3.24}$$

The actuators are limited to 55° deflection and 300 deg/sec deflection rate.

3.1.3 State Space Representation

Combining equations (3.18), (3.19), (3.24) together, the dynamic equations used to describe the short period motion of a missile in flight can be represented in state space form as:

$$\begin{bmatrix} \dot{\alpha} \\ \dot{q} \\ \dot{dq} \\ \ddot{dq} \end{bmatrix} = \begin{bmatrix} \frac{Z_\alpha}{V} & 1 & \frac{Z_{dq}}{V} & 0 \\ M_\alpha & 0 & M_{dq} & 0 \\ 0 & 0 & 0 & 1 \\ 0 & 0 & -\omega^2 & -2\zeta\omega \end{bmatrix} \begin{bmatrix} \alpha \\ q \\ dq \\ \dot{dq} \end{bmatrix} + \begin{bmatrix} 0 \\ 0 \\ 0 \\ \omega^2 \end{bmatrix} dq_c \tag{3.25}$$

$$\begin{bmatrix} A_z \\ q \end{bmatrix} = \begin{bmatrix} Z_\alpha & 0 & Z_{dq} & 0 \\ 0 & 1 & 0 & 0 \end{bmatrix} X + \begin{bmatrix} 0 \\ 0 \end{bmatrix} dq_c \tag{3.26}$$

Where the stability derivatives Z_α, M_α, Z_{dq},M_{dq}, are nonlinear functions of angle of attack and mach number. The outputs, vertical acceleration and pitch rate, are measured by an accelerometer placed at the C.G. and a rate gyro, respectively. This state space representation is both controllable and observable.

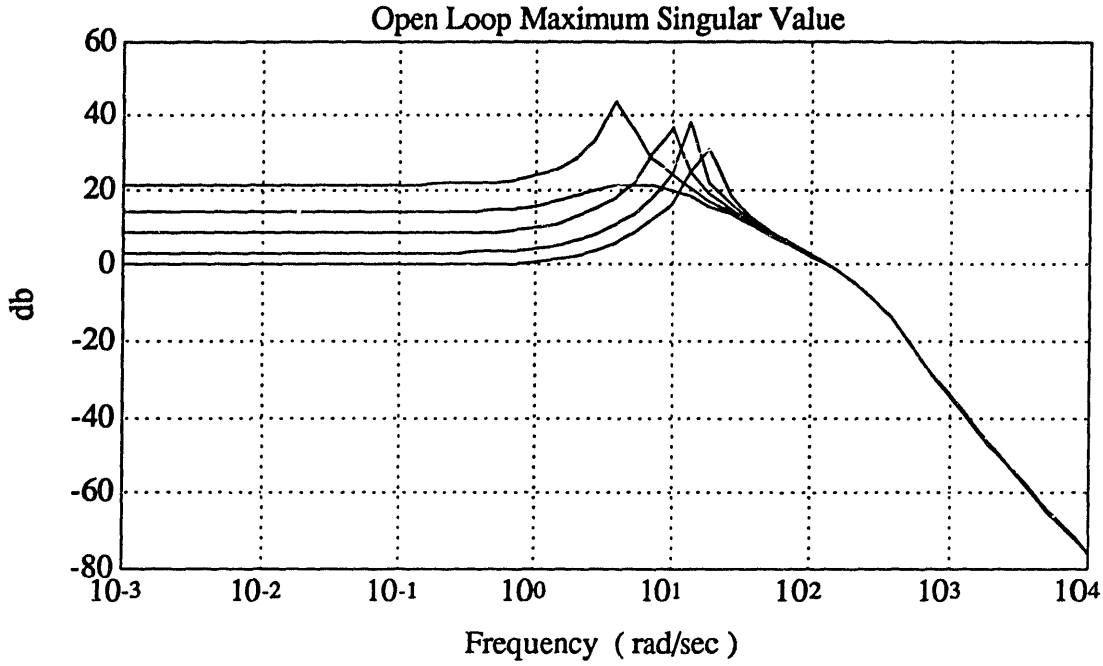

Figure 3.3 Plant Variation with Angle of Attack

3.2 Model Analysis

Figure 3.3 shows the open loop plant's maximum singular value variation as the angle of attack changes from 0° to 20°. As the Figure shows, the resonant peak of the short period mode shifts in frequency from approximately 3 rad/sec to 17.5 rad/sec.

This shift will make designing a robust controller extremely challenging. The H_∞ design methodology tends to invert the stable poles and zeros of the plant and add additional poles and zeros to satisfy the design criterion. This pole-zero cancellation technique will certainly produce unfavorable results in this case. Even classical designs where notch filters are developed are difficult to implement on plants whose dynamics vary so drastically with parameter changes.

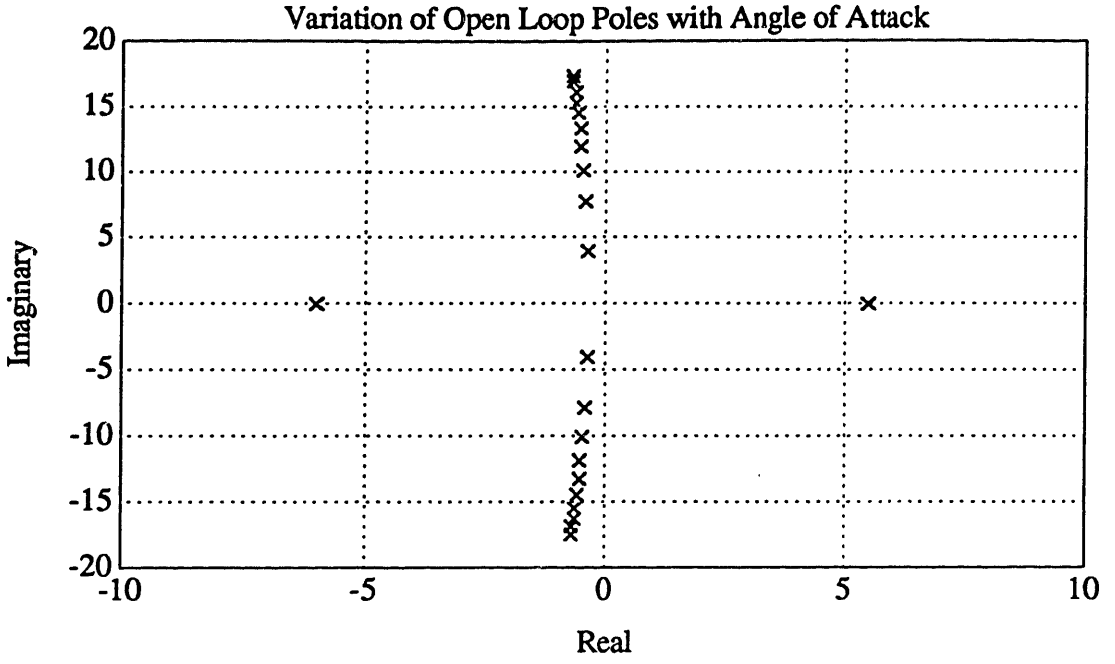

Figure 3.4 Root Locus of Open Loop Poles

Figure 3.4 shows the root locus plot of the short period poles as the angle of attack is varied. At $\alpha = 0°$, there is an unstable right hand plane pole. This is because Cm_α is positive at 0° angle of attack, and the sign of Cm_α determines the stability of the open loop airframe: when Cm_α is positive, the airframe is unstable. Positive values for Cm_α occur when the aerodynamic center is forward of the center of gravity.

Since the open loop plant's parameters vary significantly with changes in angle of attack, it is necessary to define a nominal model upon which a robust controller will be developed. The nominal model was determined by examining the stability derivatives over the range of angle of attack and choosing an average value for each parameter.

Appendix A contains a list of the parameter values at a discrete number of angle's of attack for the desired flight condition along with the average and center values of each parameter.

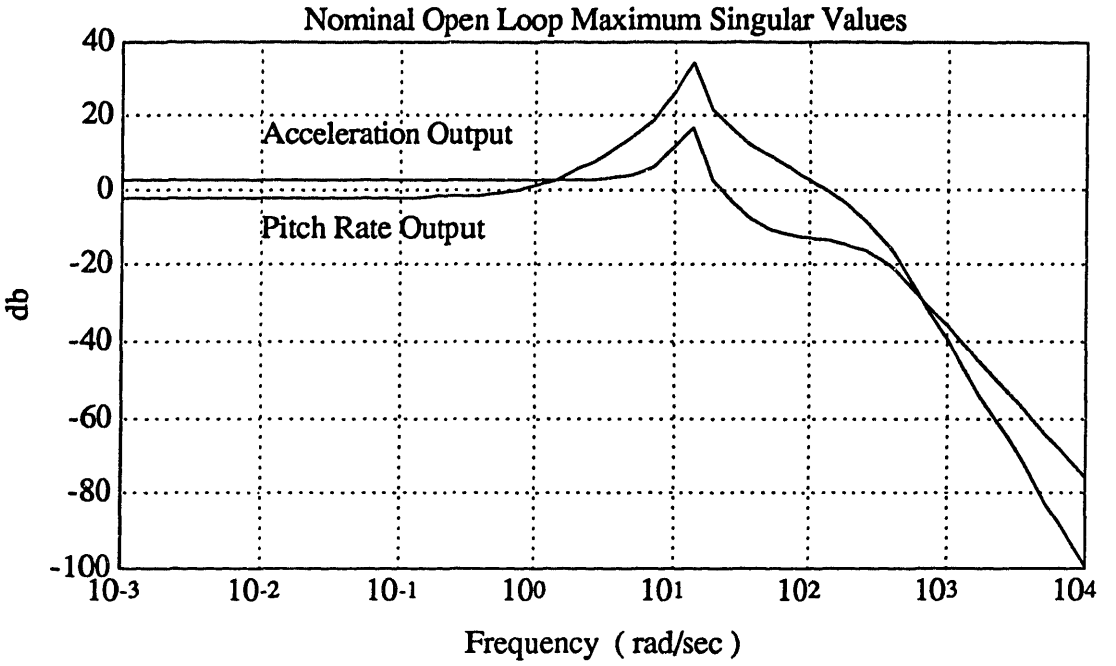

Figure 3.5 Bode Plot of Nominal Plant

The nominal model was chosen using the average values of the parameters as listed in Appendix A. The output of acceleration was normalized by gravity and all angles were measured in degrees. Figure 3.5 shows the nominal plant open loop bode plot for each output channel.

The eigenvalues of the nominal plant are:

real	imaginary	frequency	damping
-.5516	-12.641i	12.653	.0436
-.5516	+12.641i	12.653	.0436
-200.08	-200.14i	283	.7070
-200.08	+200.14i	283	.7070

Table 3.2 Poles of Nominal Plant

There are no multivariable transmission zeros present in the plant, however there are zeros in each of the output channels. These zeros are located at:

Pitch Channel	-.95913
Acceleration Channel	-32.6466 +32.6466

Table 3.3 Zeros of Nominal Plant

Notice that the pitch channel has a pole very close to the origin. This will make it difficult to have tight inner loop performance in the design synthesis. It should also be noticed that the acceleration channel has a non-minimum phase zero. This right hand plane zero is the result of the missile being controlled by surfaces aft of the center of gravity. When an acceleration command generates a controlled fin deflection, the missile's elevator surface produces an initial lift in the direction opposite of that commanded, however, the moment due to the fin deflection will eventually result in an acceleration in the desired direction. This will be evident as an initial undershoot in a step response time history.

Chapter Four:

Design Synthesis

This chapter discusses some of the important issues in the development of a missile control system capable of providing robustness to both unstructured uncertainties and variations in the angle of attack.

In the first section, the important issues concerning the choice of performance weights will be discussed. The second section discusses the relevant facts about unmodelled dynamics and demonstrates the importance of the structured singular value for reducing conservatism in both the analysis and synthesis of optimal H_∞ designs. The last section compares four problem formulations which attempt to satisfy a set of robust performance criterion over a range of angles of attack.

4.1 Performance Objectives

The first task in developing a control system is determining the appropriate performance criteria. In the case of the tactical missile problem, performance specifications are

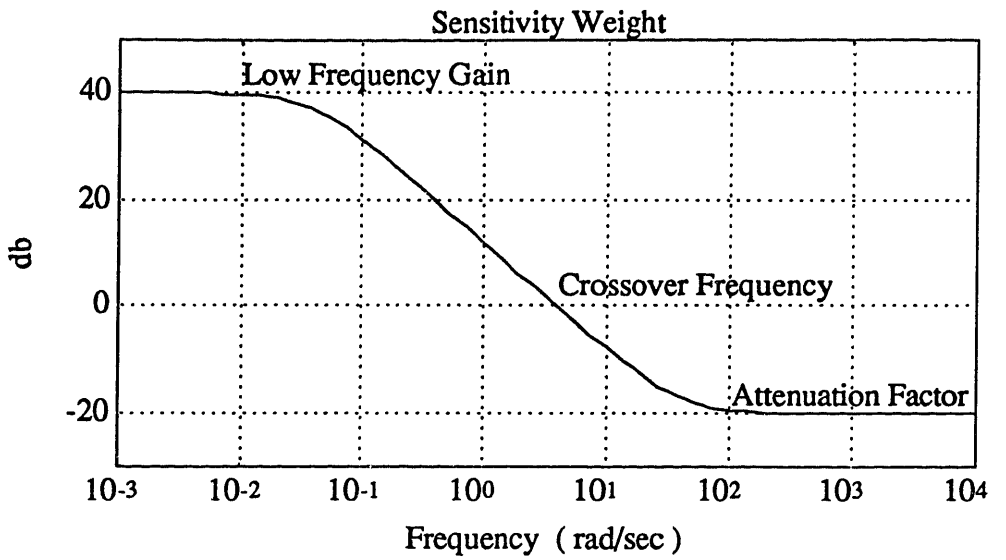

Figure 4.1 Performance Weight

generally in the form of a time constant of the response to a unit step command as well as certain disturbance rejection properties.

The performance specification for this specific problem is:

> *Design a controller to track commanded acceleration maneuvers with a steady state error of no more than one percent and a time constant of less than .4 secs. The controller must provide robust performance over a wide range of angles of attack and must avoid saturating tail deflection actuator rates as well as avoid high frequency unmodelled dynamics.*

Weighting functions which mathematically describe the performance requirements are determined from the above specification. Figure 4.1 shows a bode plot of a typical performance weight. The three parameters which define the weighting function are: the low frequency gain, the crossover frequency, and the high frequency attenuation factor. Satisfaction of the performance criteria can be achieved by appropriately choosing the values for each of these parameters. In this example, the performance critieria are

specified in the time domain so it is difficult to choose specific values for these parameters. The choice of each parameter must be made by iteratively selecting the values until the required performance specifications are achieved. In cases where the performance specifications are expressed in the frequency domain, the choice of values for the parameters are more obvious.

The steady state error requirement determines the low frequency gain of the sensitivity weight. If it is desired to track commands with no more than a 1% error then it necessary for the sensitivity transfer function, S(s), to have a low frequency gain smaller than .01. In section 2.3.5 it was shown that the appropriate choice of performance weight was the inverse of the desired sensitivity loop shape. Therefore, in order to insure that the low frequency gain of S(s) will be less than .01, the performance weight, W_p, must have a low frequency gain of 1/.01 or 100.

After determining the low frequency gain, it is necessary to fix the crossover frequency. This will set the minimum bandwidth for tracking command signals. In this case, it is desired to have a time constant of .4 secs or better. A crossover frequency of 4 rad/sec was chosen to meet the performance requirement. This value was determined by trial and error. The bandwidth of the performance weight was varied in order to determine the minimum crossover frequency necessary for satisfying the time response specification. In cases where it is known what the desired tracking bandwidth is, the problem is more straight forward.

The final requirement in the specification of a performance weight is the high frequency attenuation factor. The attenuation factor penalizes the high frequency portion of the tracking error. In general, small attenuation factors result in systems where the output contains significant amounts of high frequency energy. This usually results in large

overshoots and high actuator control rates. When the attenuation factor is increased to values closer to one, the system's output response slows down and less control effort is used. The results of increasing the attenuation factor is an apparent increase in the damping of the system. This can be evidenced as a reduction in the overshoot of the step response and less control energy. The placement of a pole to fix the attenuation factor at a certain gain is similar to using a proportional as well as integral feedback in the outer tracking loop of classical designs.

For this specific problem, the performance weight W_p was chosen to be

$$Wp = \frac{.2(s+20)}{(s+.04)}. \tag{4.1}$$

This choice of performance weight will provide a low frequency gain of 100 for a tracking accuracy of 99%, a crossover frequency of 4 rad/sec for a time constant of .4 secs. or better, and a high frequency attenuation factor of .02 to limit overshoot and excessive use of controls.

Along with placing a performance weight on the tracking error, small disturbances were injected into the system to satisfy other necessary performance requirements. A small gyro noise (.001 rad/sec) was modelled as a disturbance to the pitch rate measurement to account for any noise which may be inherent in the gyro. This is also necessary in order to insure that the H_∞ problem is properly formulated.

A small pitch rate disturbance (.01 rad/sec/sec) was modelled as a disturbance to the plant. This was done to provide process noise to the system. Without the addition of process noise, the state estimator will assume that the dynamics of the plant are undisturbed by outside sources. Such an assumption would produce a controller that has poor performance in the presence of external disturbances.

4.2 Unmodelled Dynamics and μ-Synthesis

The synthesis of missile control systems begins with the development of a linearized model of the missile. The missile, in general, is a complex, high order, nonlinear and time varying system with many high frequency structural modes. The linear dynamic model as derived in chapter three, is a simple approximation of the short period mode. Many assumptions were made in order to arrive at the low order linear model. The assumption which played the largest role in the simplification of the missile dynamics was the rigid body assumption used to develop Euler's equations.

The rigid body assumption is that the missile has no structural body modes. The missile, on the contrary, has a very slender body with many low frequency bending modes. When a control system is designed without taking into account signals which might excite these bending modes a dynamic instability may result. This instability is similar to that of the flutter problem associated with aircraft.

The instability arises because excitation of the bending modes produces high frequency feedback signals which are detected by the sensors used to measure the motion of the missile. If these signals have significant amplitudes at frequencies below the cutoff frequency of the control system, they will cause spurious corrective forces to be applied to the vehicle. The structural feedback loops thus established may produce an undesirable waste of power or even a dynamic aeroelastic instability [26].

The interaction of the elastic modes on the output of the missile can be visualized in Figure 4.2. In order to insure that the elastic modes will not affect the stability of the system, their influence must be assessed in relation to the bandwidth of the closed loop response of the linear system.

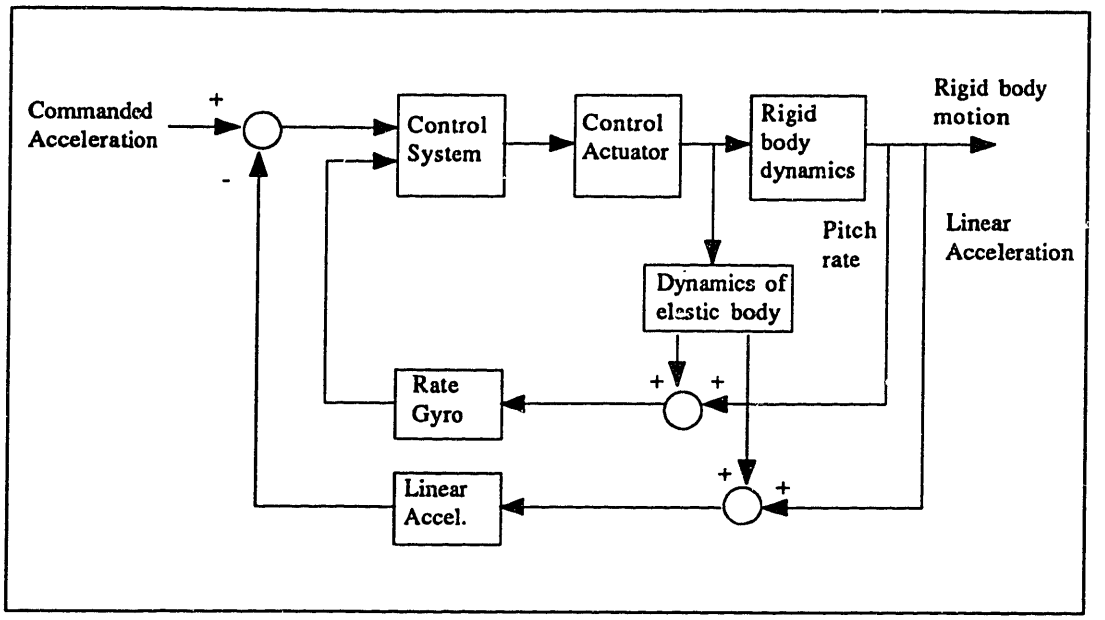

Figure 4.2 Block Diagram of Missile Control System

The error introduced by neglecting elastic modes in the linear model can be modeled as additive inputs between the deflection of the elevator and the output of the missile as shown in Figure 4.2. The uncertainties dG_a and dG_q of Figure 4.3 are stable transfer functions which are used to bound the expected magnitude of the unmodelled elastic mode dynamics.

Other forms of uncertainty which may arise in the development of a linear model are uncertainties in the actuator dynamics. The actuators are assumed to be perfect linear models. This is true for frequencies below their operating bandwidth, but as the operation of the actuator reaches the cutoff frequency, nonlinearities may occur.

The uncertainty structure at the input to the actuator of Figure 4.3 represents uncertainty in the gain and phase characteristics of the linear model. Using a normalizing factor of k=.6, this uncertainty structure is chosen to represents as much as 35 degrees of phase uncertainty and a gain variation of .6 to 2.5.

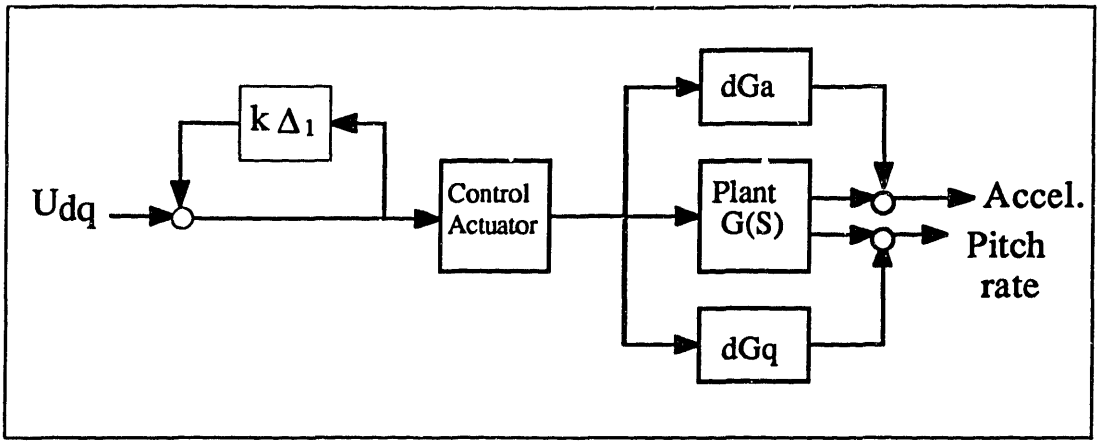

Figure 4.3 Modelled Uncertainties in the Linear Model

After determining the magnitudes and locations of the uncertainties in the linear model, the closed loop system is analyzed using the small gain theorem. If the small gain theorem is satisfied, $\|M(s)\|_\infty \leq 1$, then the stability of the closed loop system to these unmodelled dynamics is assured. Since the small gain theorem is only a sufficient condition for stability, violation of the small gain theorem makes no statement about the stability. In the general, however, when there exists unstructured uncertainties in the model, it is desirable that the small gain theorem be satisfied.

Because it is desired to satisfy the small gain theorem whenever there exists unstructured uncertainties, it is important to utilize the modelling error information during the design process. The H_∞ optimization method is one of the only methods which can be formulated to guarantee satisfaction of the small gain theorem for unstructured uncertainties a priori: if such a solution exists.

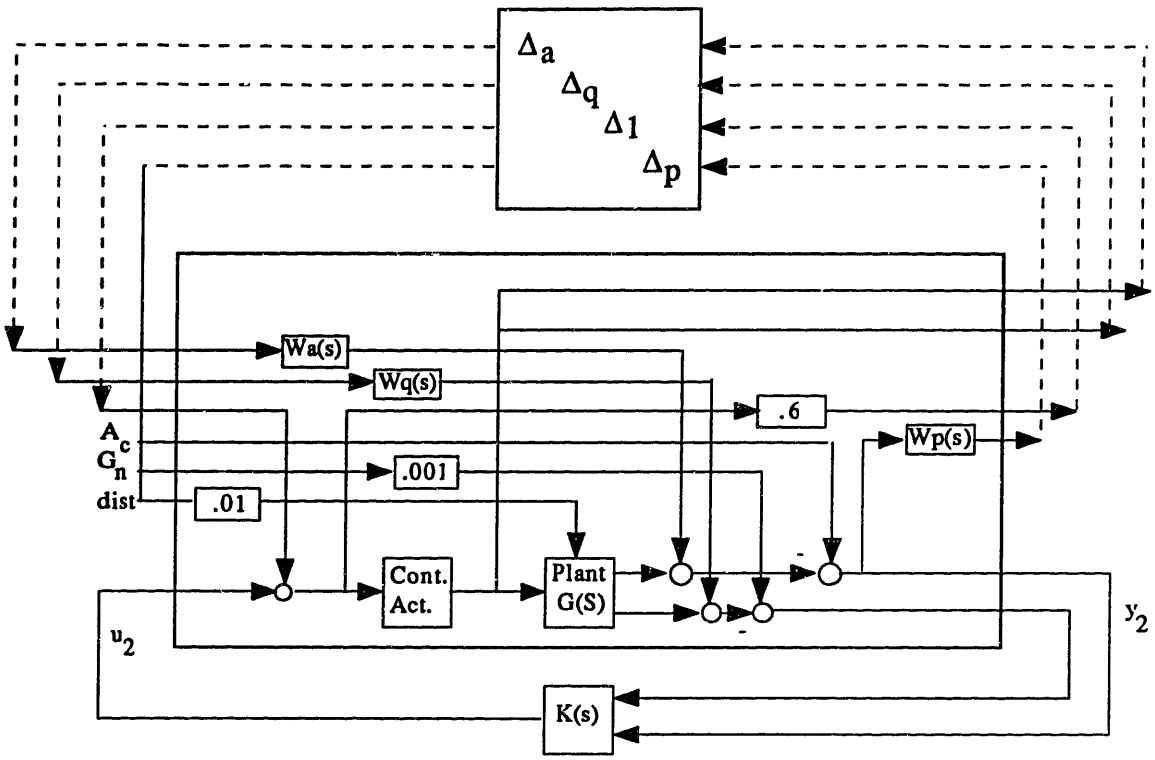

Figure 4.4 H_∞ Problem Formulation

The additive uncertainties dG_a and dG_q can be represented by the following two equations:

$$dG_a = W_a(s)\Delta_a \tag{4.2}$$

$$dG_q = W_q(s)\Delta_q \tag{4.3}$$

where W represents all the magnitude characteristics of the uncertainty and Δ represents all the possible phase uncertainty.

Since the uncertainty blocks are represented by magnitude and phase characteristics, the order in which the magnitude and phase are represented is arbitrary. For example, the same uncertainty can be represented as WΔ or ΔW. Figure 4.4 shows one possible H_∞ problem formulation which could be used to satisfy the small gain theorem.

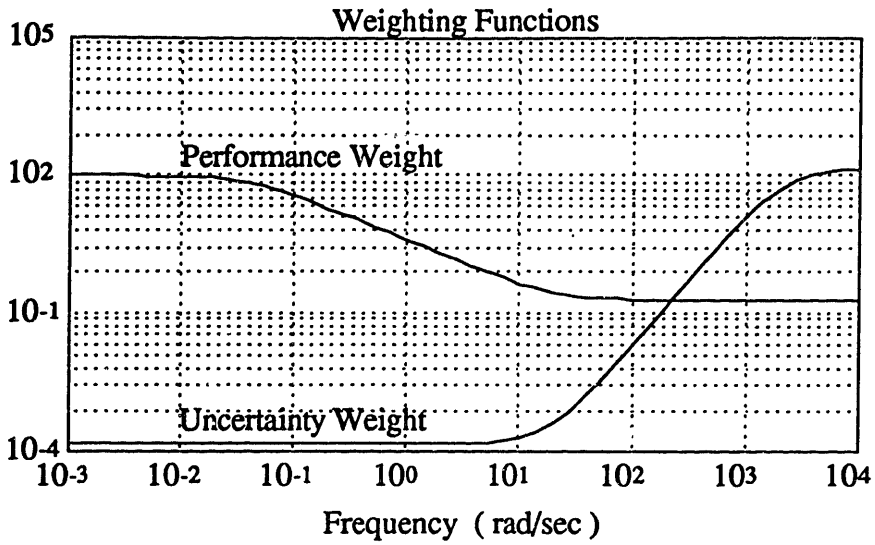

Figure 4.5 Weighting Functions

4.2.1 Example One

As section 2.4 discussed, when the H_∞ problem is formulated with a block diagonal structure, such as Figure 4.4, the resulting solution may be overly conservative. This conservatism arises because of the relative scaling difference between the different input/output sets. The following example shows the conservatism of an H_∞ design and demonstrates the effectiveness of utilizing dynamic scaling to reduce this conservatism.

For this specific example, the performance weight used is defined by equation (4.1). The problem is formulated similar to that of Figure 4.4 except that in this case the uncertainty dGa is assumed negligible and will therefore be ignored. The uncertainty dGq is assumed bounded by the transfer function

$$W_q = \frac{150(s+20)(s+20)(s+20)}{(s+2000)(s+2000)(s+2000)} \qquad (4.4)$$

Figure 4.5 shows the bode plot of the two weighting functions used for this example.

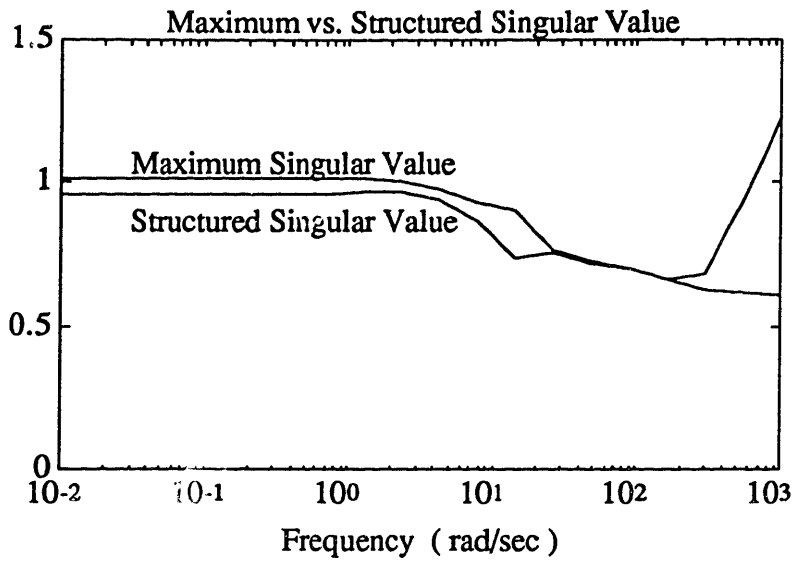

Figure 4.6 Maximum vs. Structured Singular Value

An H_∞ algorithm supplied in the μ-Tools software package [25] was used to determine the optimal H_∞ solution. For the problem of figures 4.4 and 4.5 the minimum γ achievable was 1.3164. This result is not sufficiently close to the required performance and robustness specifications.

The uncertainty structure is represented as a three block diagonal perturbation so the closed loop system of Figure 4.4 was analyzed using the ssv. Figure 4.6 shows the plot of the maximum versus structured singular value. As Figure 4.6 demonstrates, the maximum singular value provides a slightly conservative measure of the robust performance for this problem: The maximum singular value being 1.3164 while μ is .9685. Despite the fact that the closed loop transfer function satisfies the small gain theorem, it would be interesting to see what improvement in performance can be achieved when the optimal scales from the ssv analysis are incorporated into the design procedure.

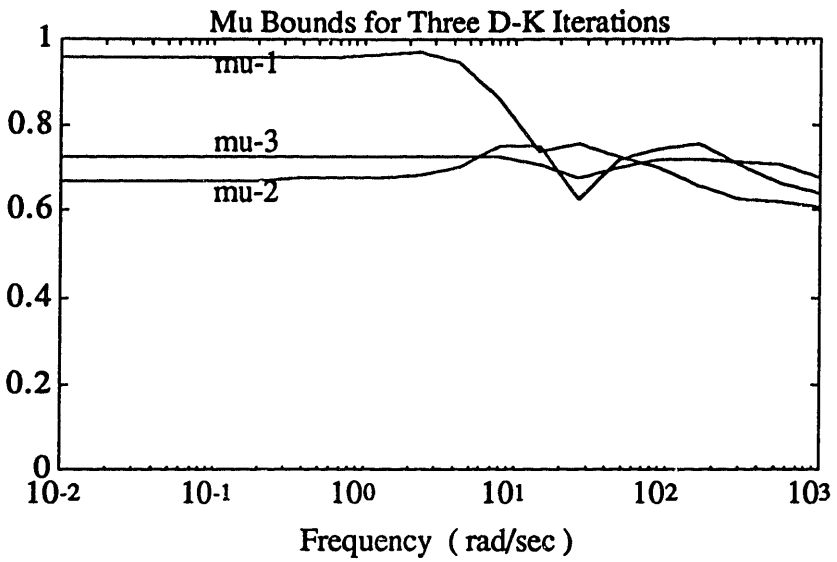

Figure 4.7 Three Iterations of μ-Synthesis

For this purpose, the D-scales determined in the μ–analysis were fit with 3rd order stable transfer functions. Since this specific problem had three uncertainty blocks, it was necessary to determine two sets of D scales: These scales normalized two of the input/output sets to that of the third set.

After appending the D-scales to the open loop plant, a second iteration of H_∞ was performed. This time, the minimum value of γ was .7578. Figure 4.7 shows the value of μ for three successive D-K iterations.

Table 4.1 shows the value of γ and μ for each iteration.

Iteration	γ	μ
1	1.3164	.9685
2	.7578	.7489
3	.7256	.7251

Table 4.1 D-K Iterations (Ex I)

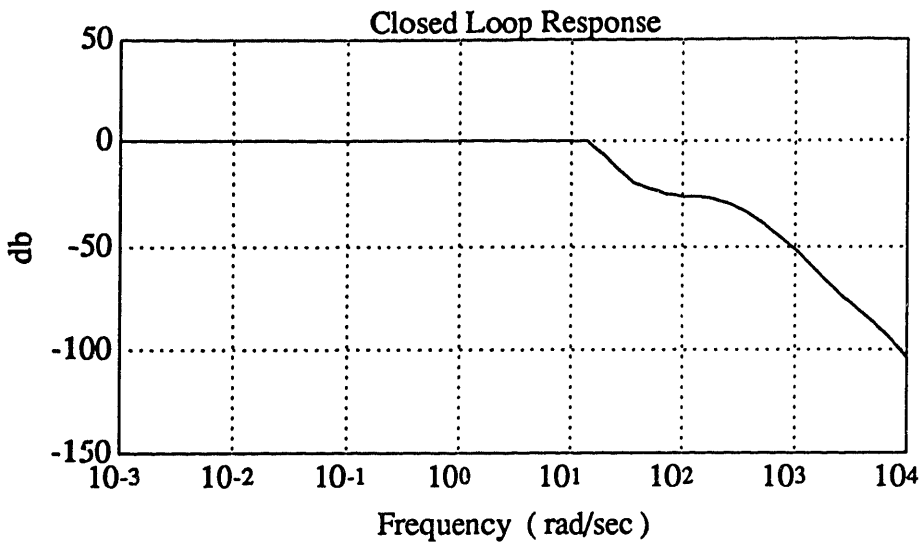

Figure 4.8 Complementary Sensitivity (Ex I)

The final value of μ was .7251, this represents a 45% improvement over the original H_∞ performance measure, and a 24% improvement over the first value of μ. The final controller has 20 states, 12 more than the original H_∞ design. The 24% improvement in performance may or may not warrant the increase in state order.

Figures 4.8 and 4.9 show the maximum singular value plot for the complementary sensitivity and the sensitivity functions. Figure 4.10 shows the step response to a 1g command signal. As 4.10 shows, the closed loop system meets all the necessary performance criterion.

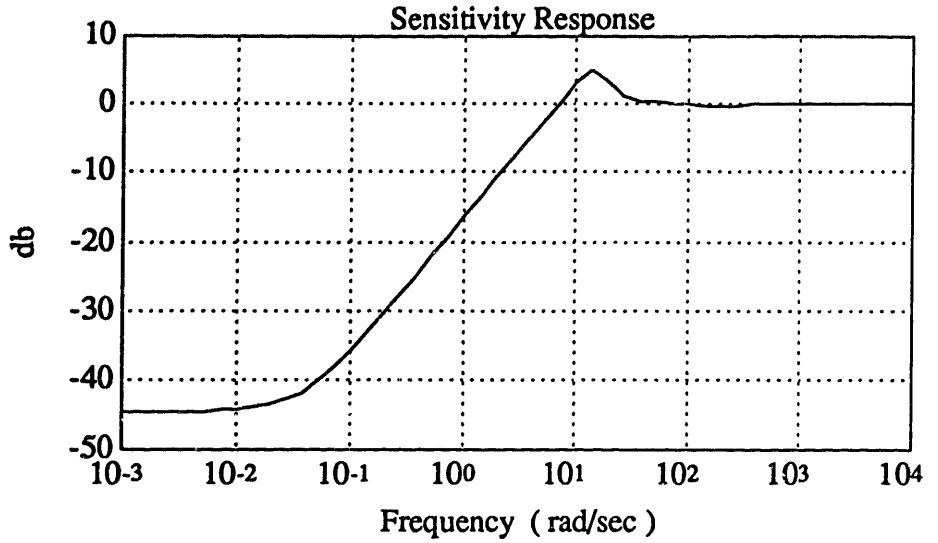

Figure 4.9 Sensitivity (Ex I)

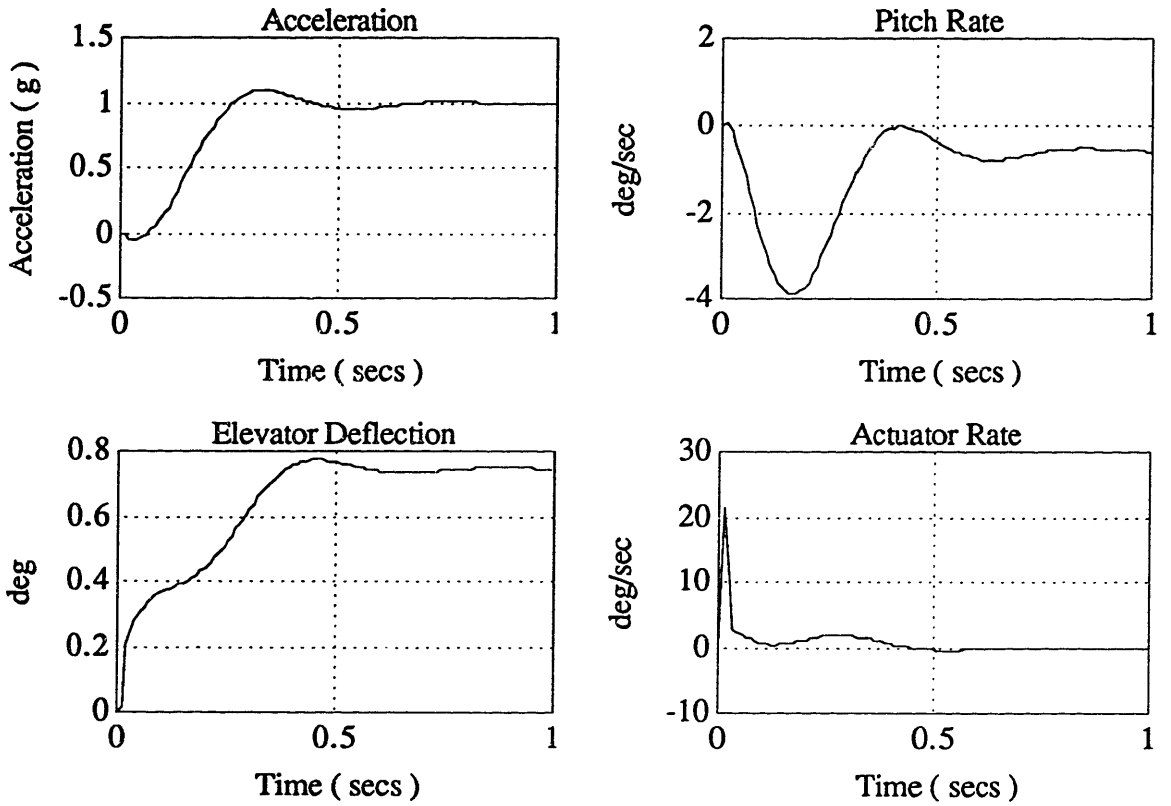

Figure 4.10 Step Response (Ex I)

4.2.2 Example two

During the D-K iterations, an interesting phenomena was observed. One of the D-scales appended to the open loop plant was noticed to be almost the exact inverse of the uncertainty weight, Wq.

The fact that the Δ scale seemed to invert the uncertainty weight Wq, indicated there may be a better way of formulating the problem. It was commented earlier that the order of the uncertainty $W\Delta$ or ΔW was arbitrary. In example one, the order was chosen to be $W\Delta$. In this case, the weight Wq was placed on the input channel as shown in Figure 4.4. Since the optimal D scale took on the inverse of this filter, it appeared that the problem might be better formulated if the uncertainty were arranged as ΔW. In this case, the weight W_q would be placed on the output channel as shown in Figure 4.11.

The minimum γ achievable for this problem using the H_∞ algorithm was 1.1453. Moving the weight W_q immediately resulted in a 13% improvement. After determining the first H_∞ solution, the μ-synthesis procedure was carried out using constant D scaling matrices; no additional states were added to the system.

Figure 4.12 shows the plot of the three successive D-K iterations. The values of γ for each iteration are listed in Table 4.2. Since no additional states were used for the D-scales, the total size of the controller was 8 states.

Iteration	γ	μ
1	1.1453	.9183
2	.7695	.7577
3	.7695	.7656

Table 4.2 D-K Iterations (II)

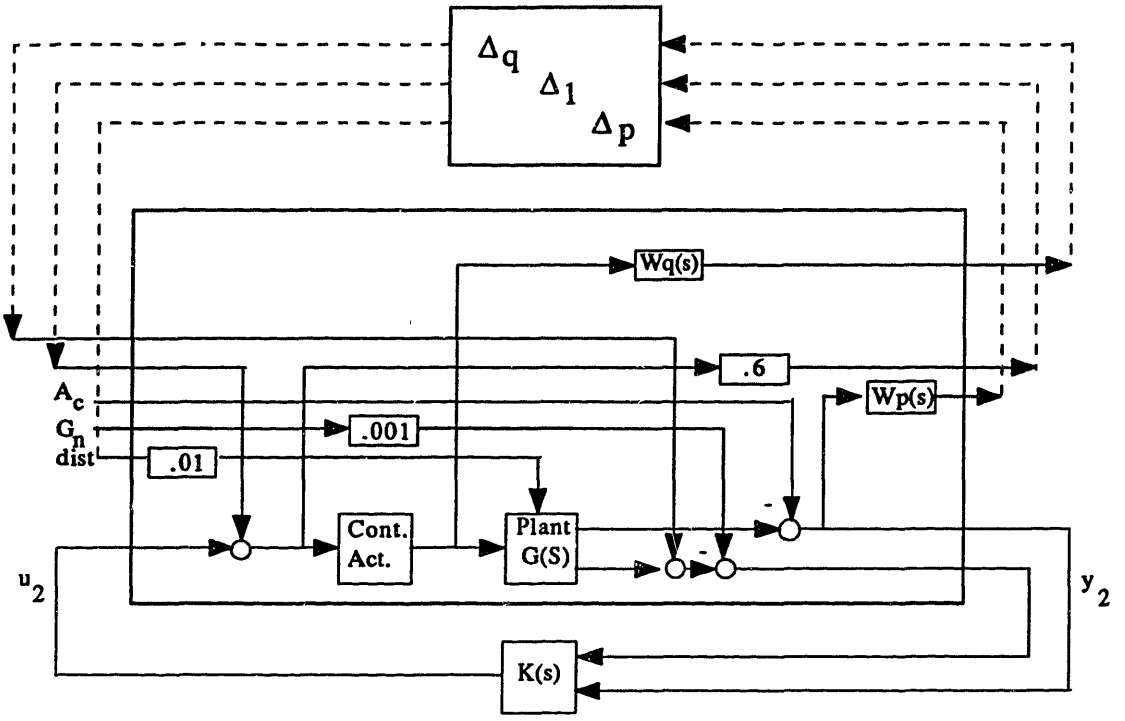

Figure 4.11 H_∞ Problem Formulation (Ex. II)

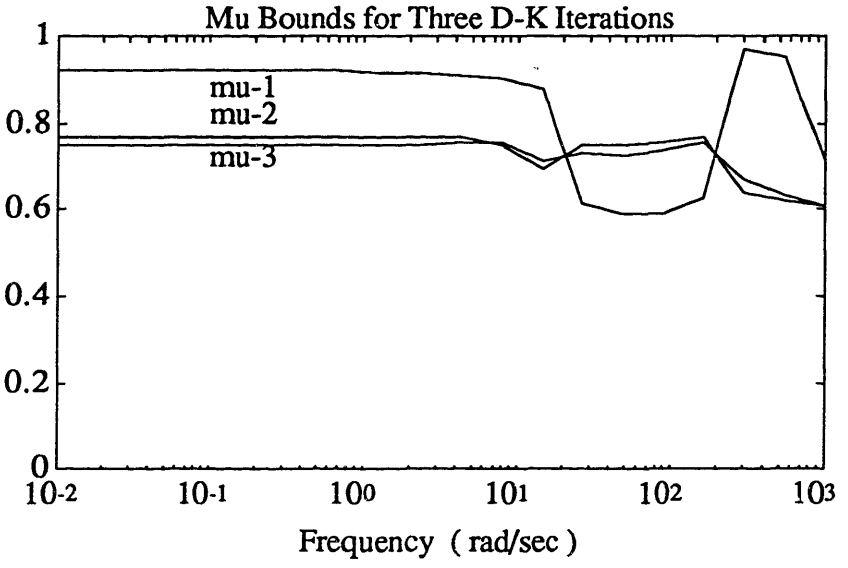

Figure 4.12 μ plots for Three D-K Iterations

It is important to comment at this time that the constant D scaling procedure was attempted for example one with no improvement in performance. The relocation of the weight W_q made it possible to perform all necessary scaling with constant D scales.

The final value of μ for the second design was .7654. This represents a 20% improvement from the initial value of μ in example one without any increase in state order. The results of example one with increased state order only achieved a 24% increase in performance: by properly formulating this problem, it was possible to recover most of the increase in performance without any additional increase in state size.

Figures 4.13 and 4.14 show the maximum singular value plots for the resulting complementary sensitivity and the sensitivity transfer functions. Figure 4.15 shows the step response to a 1g command signal. According to Figure 4.15, the closed loop system meets all the necessary performance criterion.

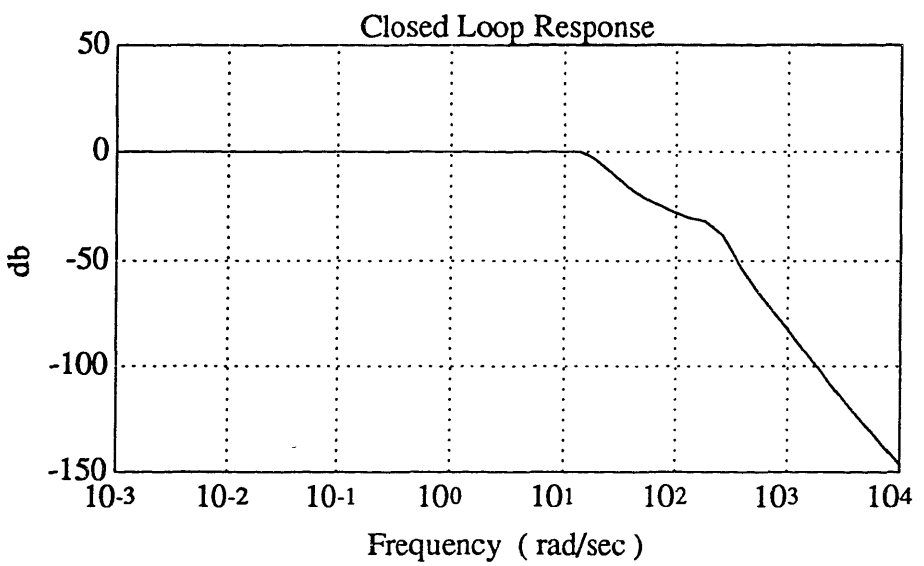

Figure 4.13 Complementary Sensitivity (Ex II)

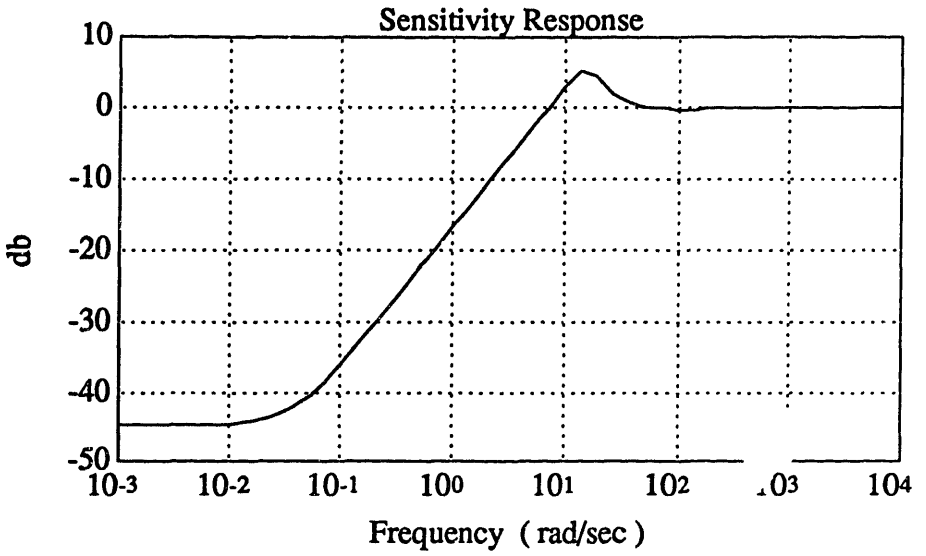

Figure 4.14 Sensitivity (Ex II)

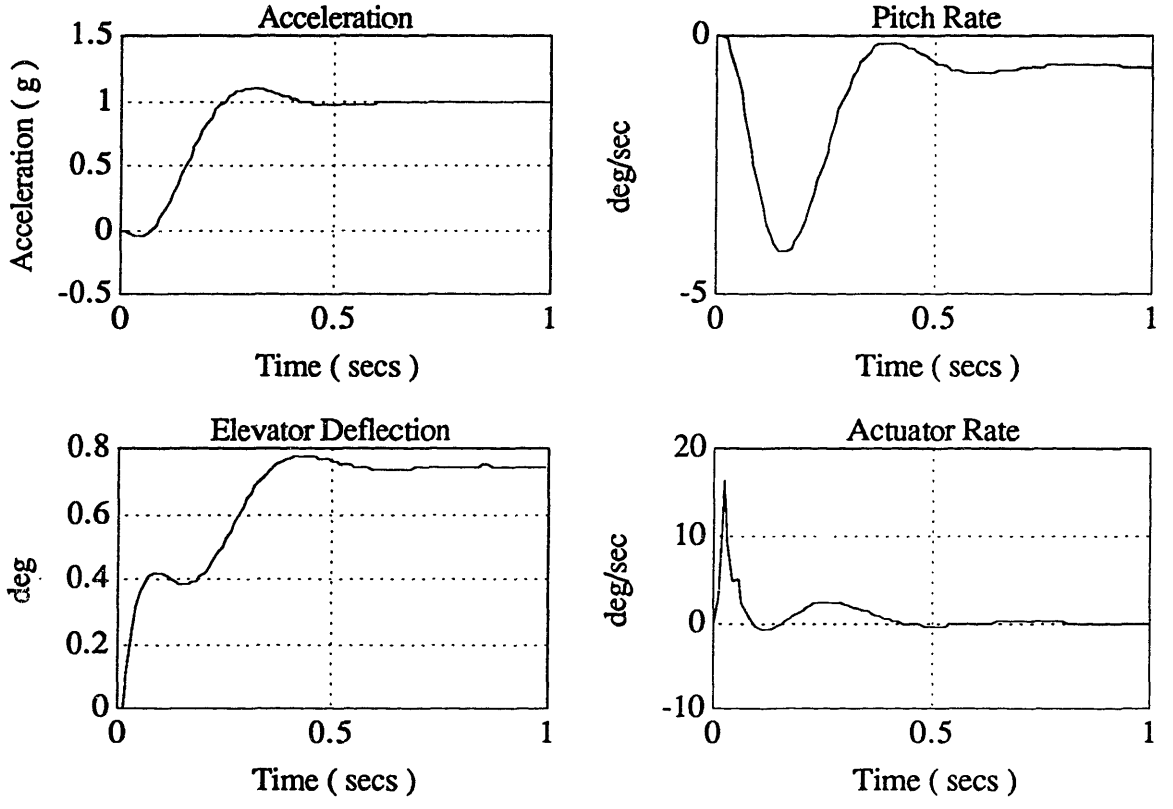

Figure 4.15 Step Response (Ex II)

The effect of moving the uncertainty weight, Wq, has been a substantial increase in performance without an increase in the order of the system. In fact, some cases were developed where moving the uncertainty weight actually provided better results than using the dynamic scales to invert the uncertainty weight. This is probably due to the fact that a curve fitting algorithm approximates the optimal D-scale whereas if the change is done by the designer, no approximation takes place.

In order to avoid this problem, the control systems engineer should pay close attention to the shape of the D-scales with each iteration. If the D-scales begin to take on the same shape as one of the uncertainty blocks, then the problem may be better formulated, without increasing the final order of the controller, by rearranging the location of the uncertainty weights.

4.3 H_∞ Designs and Parametric Uncertainty

The following sections discuss the development of a longitudinal autopilot using four different problem formulations. While each is required to satisfy the same performance specifications, the approach to handling parametric variations is different. The four design methods which will be compared are:

- Design I: H_∞ Optimization
- Design II: H_∞ Optimization with Parameter Uncertainty
- Design III: Classical
- Design IV: H_∞ Inner Loop.

The performance requirement for the four designs as developed in section 4.1 is:

$$Wp = \frac{.2(s+20)}{(s+.04)} \tag{4.3}$$

In order to insure that the missile will be stable in the presence of unmodelled dynamics, each control system must have at least -20 db of attenuation in the open loop pitch actuator branch and at least a two pole roll off. This criterion is derived from classical designs to insure that high frequency signals generated by the body bending modes are adequately attenuated.

For the H_∞ designs, a multiplicative input error, Wu, was chosen to provide the -20 db of attenuation at 200 rad/sec with a two pole roll off. The performance and model uncertainty weights are illustrated in Figure 4.16

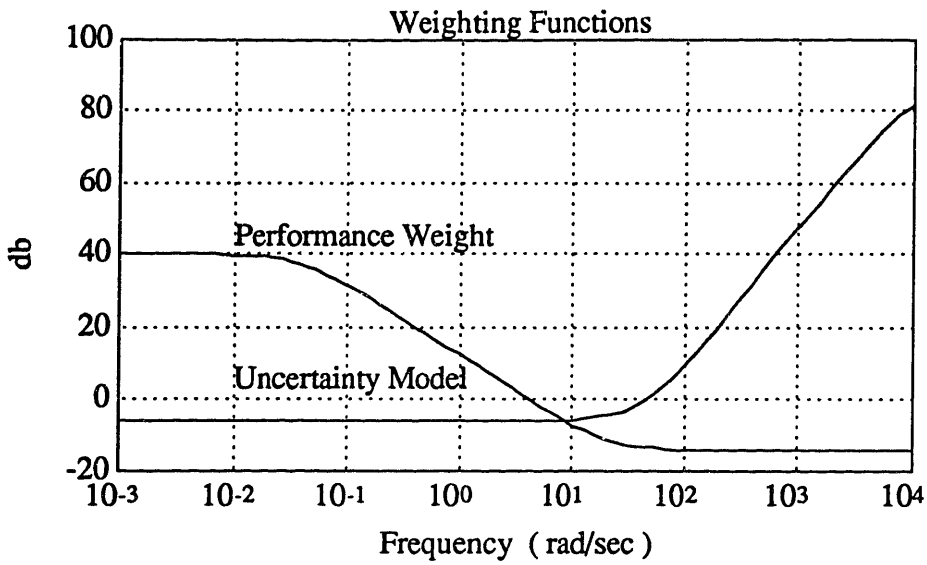

Figure 4.16 Weighting Functions

4.3.1 H_∞ Optimization

The first problem to be addressed is the classic H_∞ mixed sensitivity problem. The objective of the mixed sensitivity problem is the minimization of the weighted sensitivity function subject to the constraints placed on the system by the unstructured multiplicative input uncertainty model. In this case, the optimal solution is the one which provides the best sensitivity performance while maintaining stability in the presence of unstructured multiplicative perturbations. The problem is formulated as a two block small gain problem since it is desired to maintain nominal performance in the presence of the unstructured uncertainty.

After specifying the weights, the optimal solution is achieved by minimizing the sensitivity as much as possible while satisfying the unstructured uncertainty requirement. This is accomplished by iteratively reducing γ in the H_∞ solution until the minimum γ is achieved. Because the problem is formulated with a block diagonal structure, the results of the previous section demonstrate the importance of utilizing the

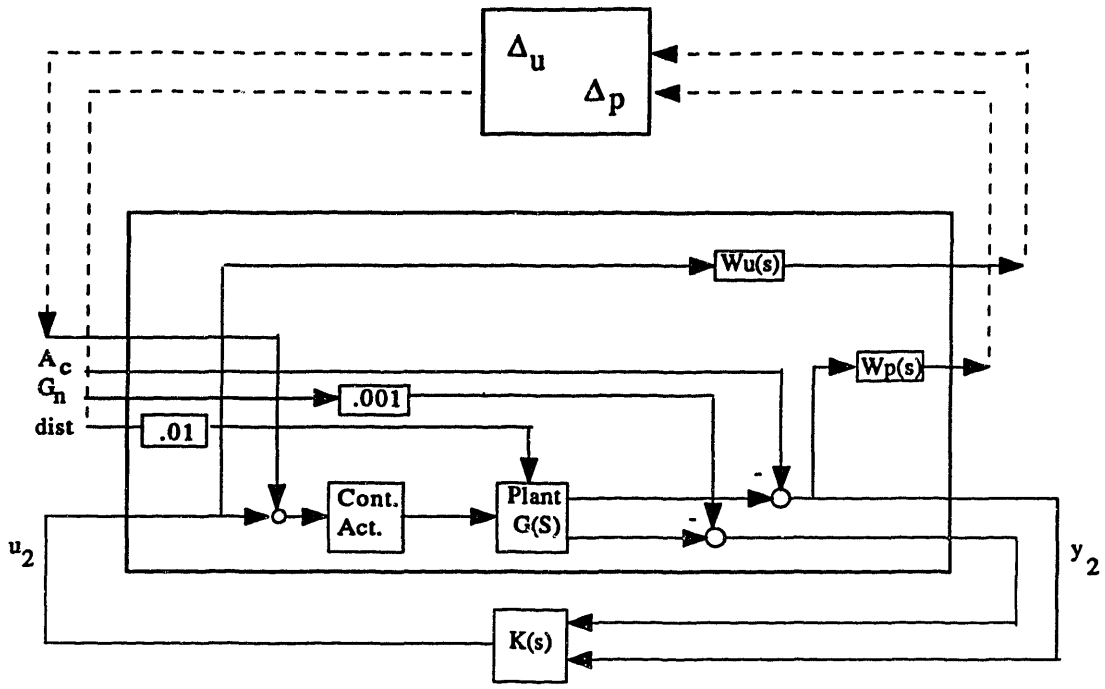

Figure 4.17 H_∞ Problem Formulation Design I

optimal scaling procedure (μ synthesis) to reduce the conservatism of the H_∞ solution. The improvement in performance of the optimal scaling procedure will then be evaluated against the increase is state order.

Figure 4.17 shows the block diagram of the H_∞ problem. The minimum γ achievable using normal H_∞ techniques was .8340. This value of γ satisfies the performance and robustness requirements. Figure 4.18 shows the plot of the maximum singular value along with the structured singular value. In this case, there is not a significant difference between the maximum singular value and μ at low frequencies. There is however, a slight difference between the maximum singular value and μ for high frequencies. For this reason, the μ-synthesis algorithm was used to reduce the difference between the two norms.

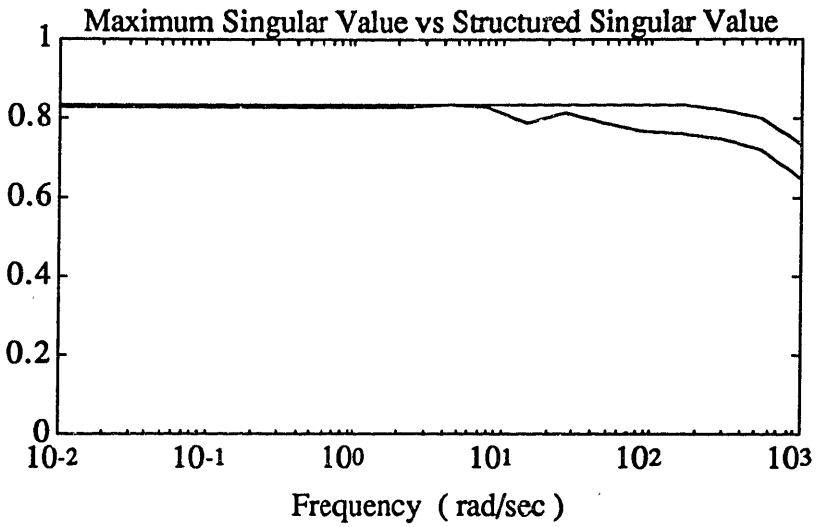

Figure 4.18

Figure 4.19 shows the reduction of the μ-bounds for three D-K iterations. The D-scale was approximated using a 3rd order stable transfer function.

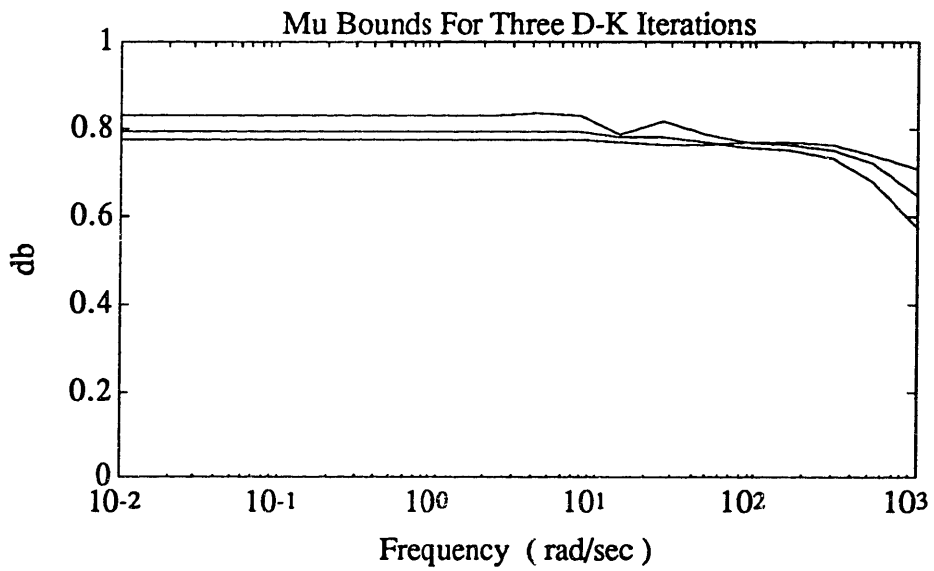

Figure 4.19 μ Plots for Three D-K Iterations

The values for each successive γ and maximum μ value are listed in Table 4.3.

Iterations	γ_0	μ
1	.8340	.8328
2	.7922	.7916
3	.7740	.7739

Table 4.3 D-K Iterations (Design I)

In the H_∞ problem, robust performance is measured by the $\|\bullet\|_\infty$ norm of the closed loop system. In any problem, the $\|\bullet\|_\infty$ norm is guaranteed to be less than γ. In the limit as γ goes to γ_0, γ is identically the $\|\bullet\|_\infty$ norm. Considering the first iteration, the minimum γ achievable is .8340. Using the optimal scaling procedure to reduce the conservatism of $\|\bullet\|_\infty$, the μ robust performance index is .8328. Since the system is fairly well scaled, and the $\|\bullet\|_\infty$ is not much larger than the μ robust performance index.

By applying the optimal scaling procedure, the μ robust performance index was reduced to .7739. This represents a 7.1% improvement over the original value of μ. Of course, the increase in robust performance came about by increasing the order of the controller from 7 states to 13 states; an addition of 6 new states.

The singular value plot of the final controller is shown in Figure 4.20. According to Figure 4.20, the controller is attempting to invert the lightly damped poles of the short period mode. This can also be seen by examining the poles and zeros of the compensator listed in Appendix B.

Figures 4.21 through 4.23 show the singular value plots of the complementary sensitivity, the sensitivity, and the open loop pitch actuator branch respectively. As Figure 4.23 indicates the open loop pitch actuator branch has the required -20 db of attenuation and at least a two pole off. According to Figure 4.23, the crossover

frequency is 26.83 rad/sec. At the crossover frequency, there is 113° of phase margin and at the phase crossover, there is a downward gain margin of .0016. These are excellent margins for robustness to unmodelled gain and phase.

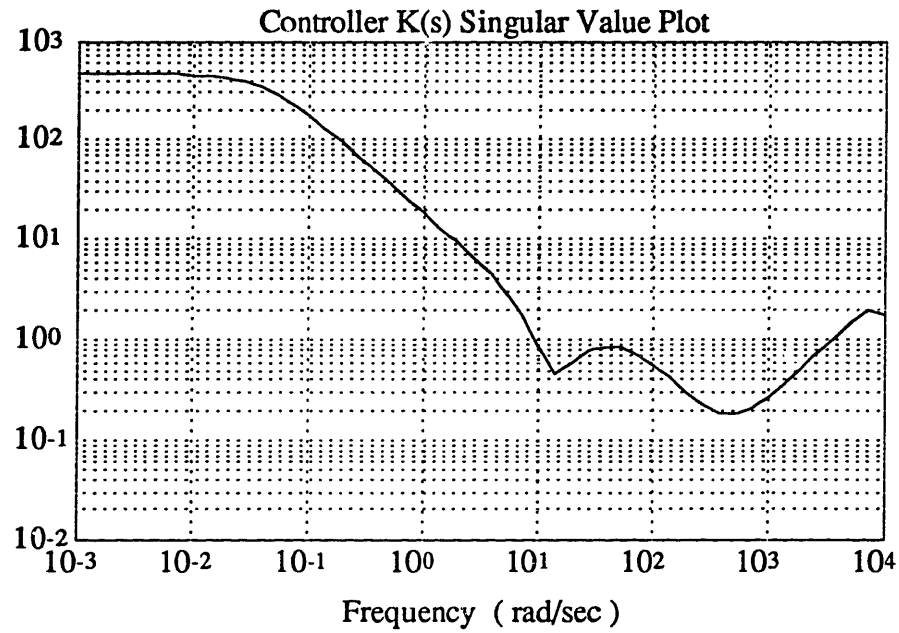

Figure 4.20 Maximum Singular Value of K(s)

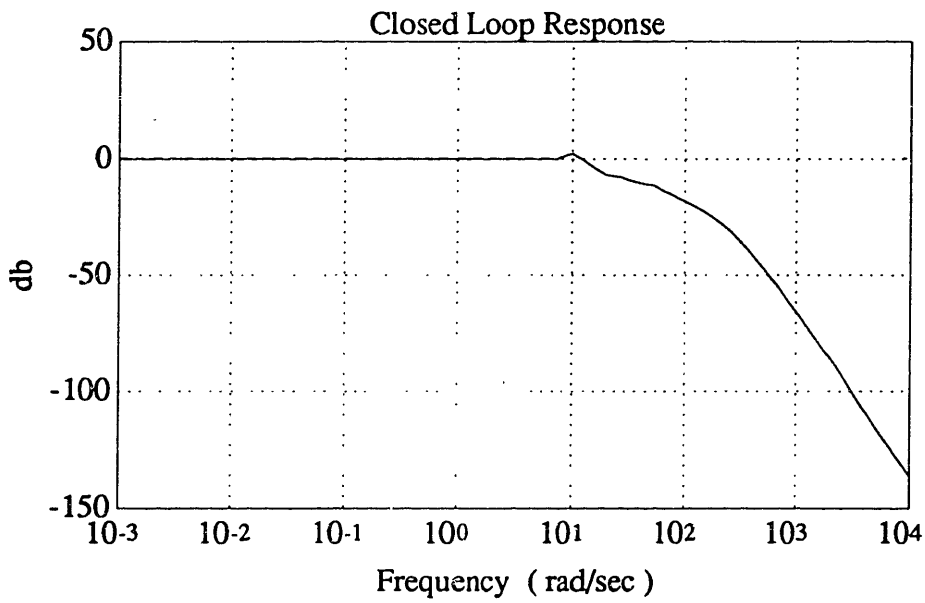

Figure 4.21 Complementary Sensitivity (Design I)

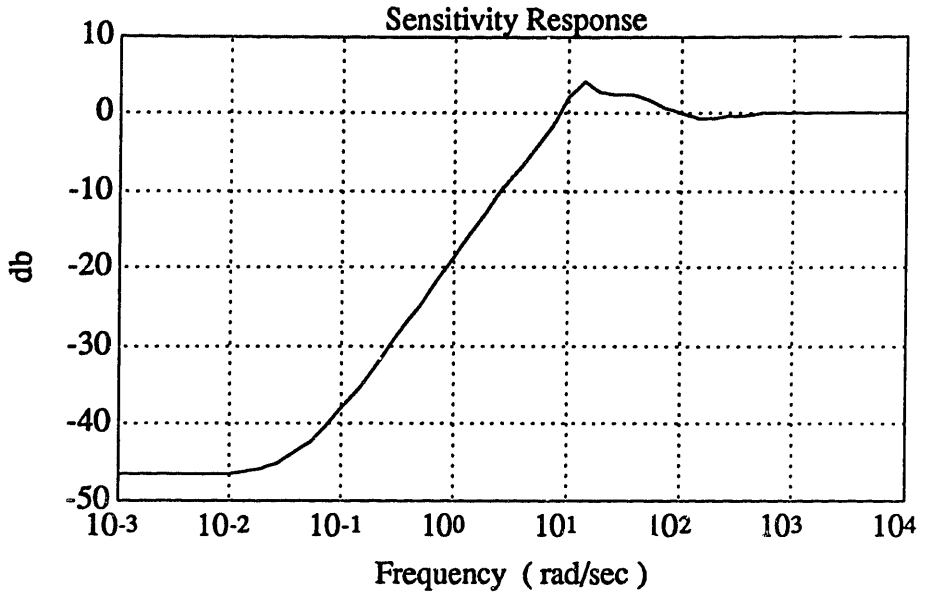

Figure 4.22 Sensitivity (Design I)

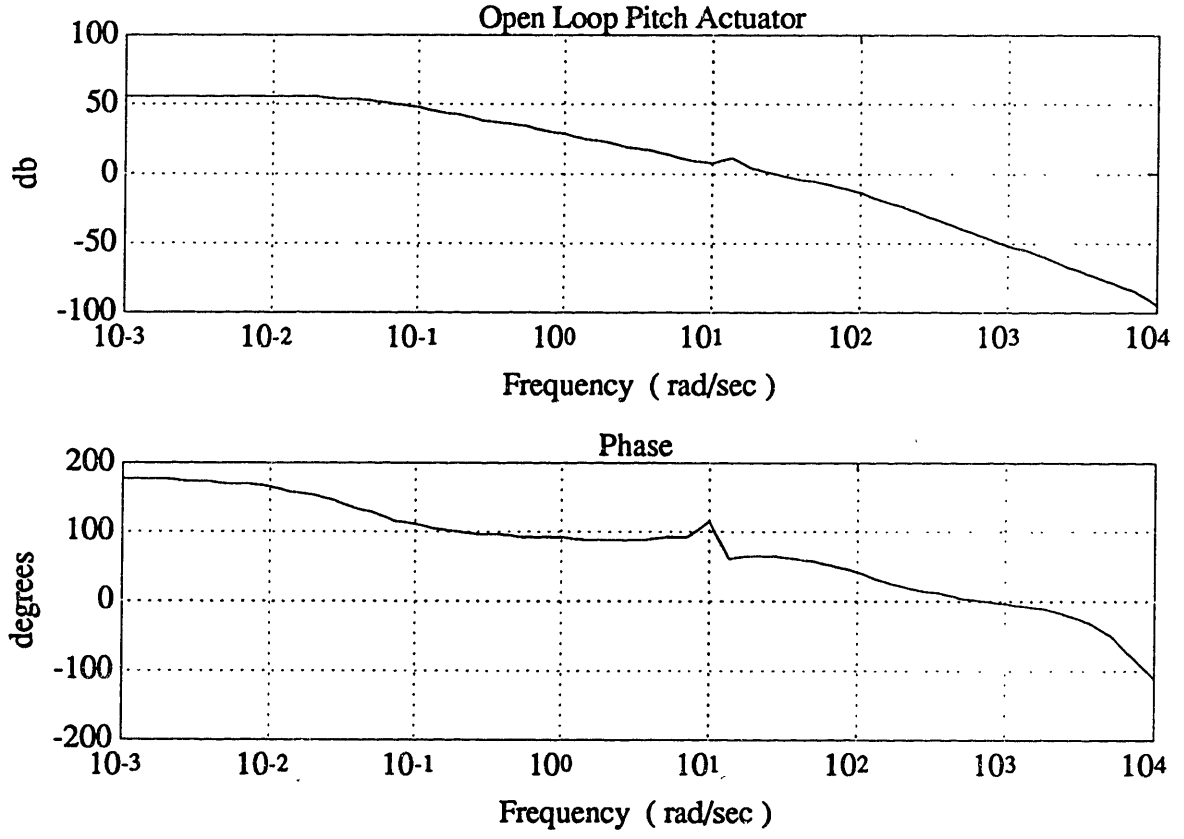

Figure 4.23 Open Loop K(s)G(s) (Design I)

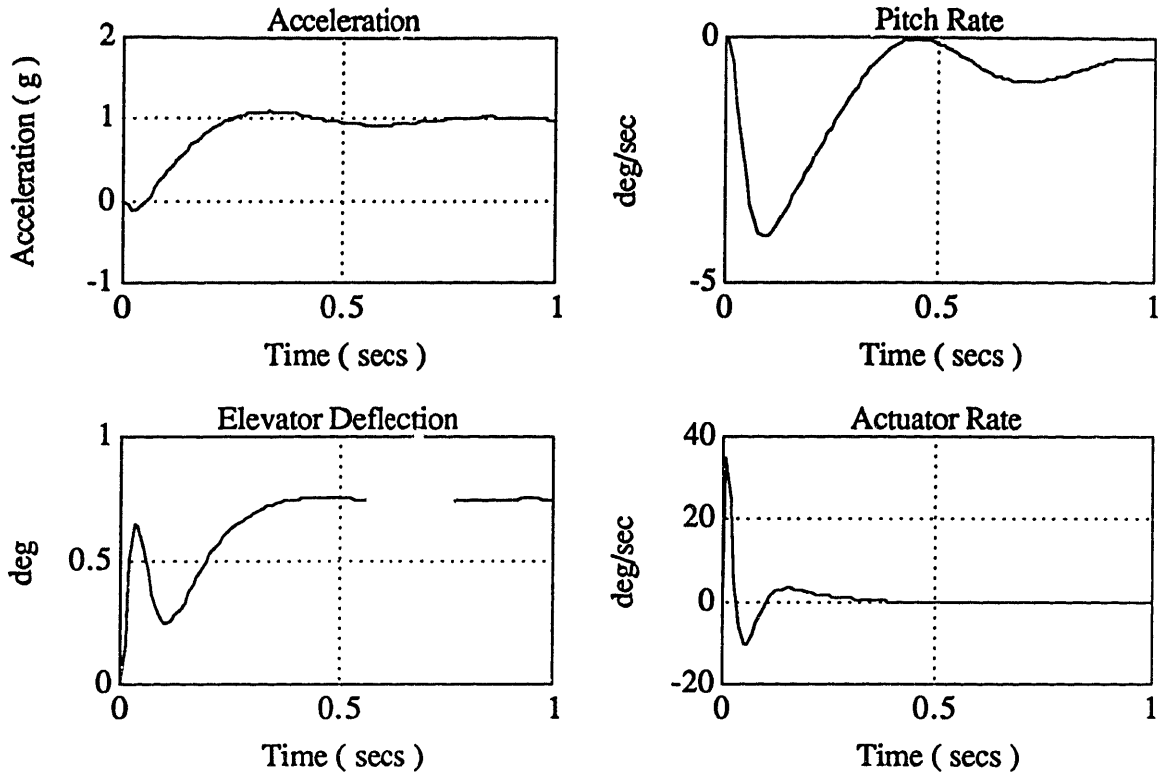

Figure 4.24 Acceleration Step Response Design I

Figure 4.24 shows the step response of the nominal design. The missile achieves a 1g acceleration in approximately .3 secs, with a maximum deflection rate of about 35 deg/sec. This response meets all the necessary time domain performance specifications.

Figure 4.25 plots the step response of the closed loop system for three different values of angle of attack: 0°, 10°, and 20°. The closed loop system responds fairly well for 10° and 20° angle of attack, but the system becomes unstable at 0°. Figure 4.26 shows a plot of the low frequency closed loop poles for the range of 0° to 20° angle of attack. At about 3° the system becomes unstable.

Although the closed loop system has excellent nominal performance, it is not stable in the presence of parametric variation. The system becomes unstable for small angles of

attack. This is not surprising since [14] showed that H_∞ designs are sensitive to parametric variations which affect the location of lightly damped pole pairs.

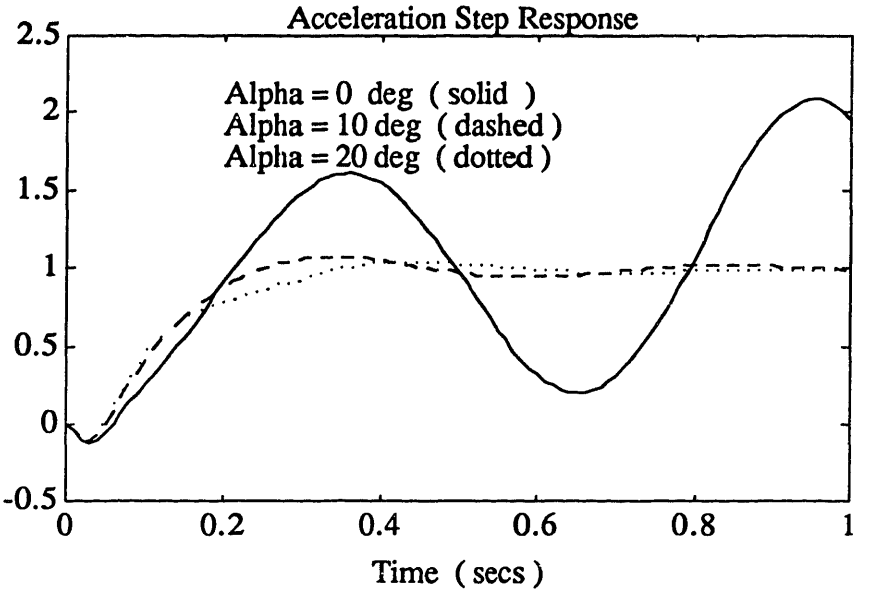

Figure 4.25 Step Variation with Angle of Attack (Design I)

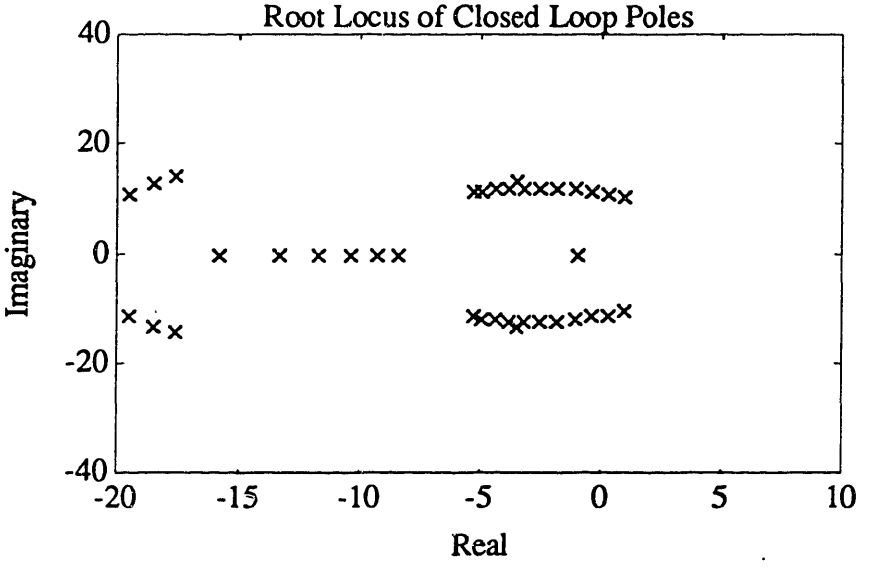

Figure 4.26 Variation of Poles with Angle of Attack (Design I)

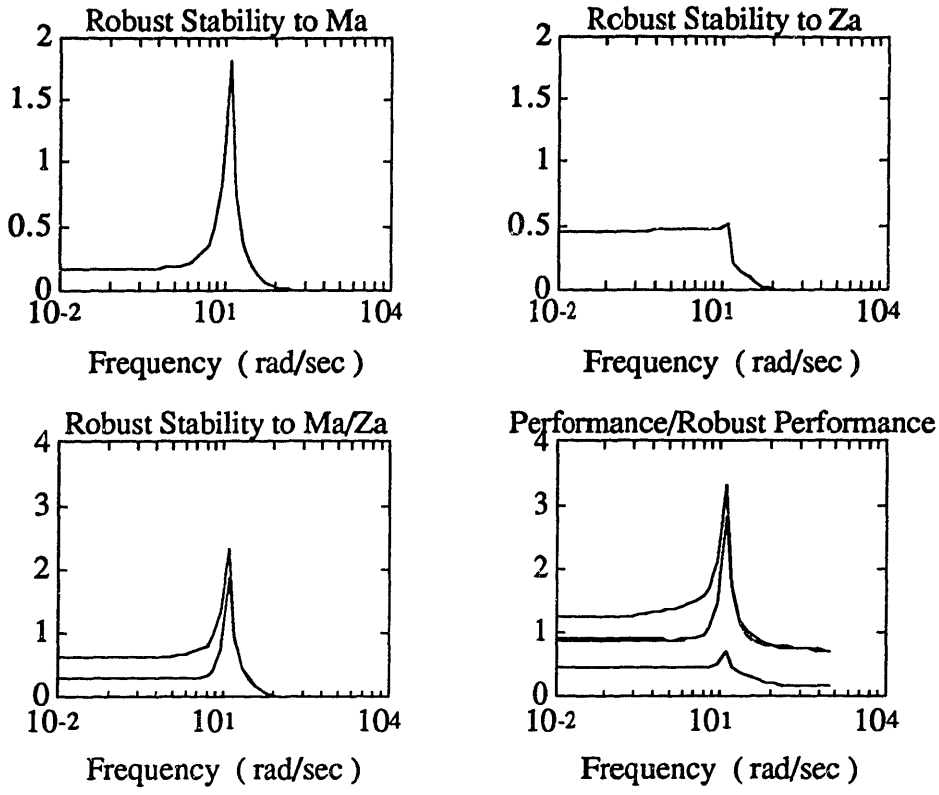

Figure 4.27 Robustness Analysis (Design I)

The graphs of Figure 4.27 provide an analysis of the robustness properties of the closed loop system to various perturbation structures. As it was mentioned in section 2.1, there are three specific problems of interest in the analysis of the closed loop system: nominal performance, robust stability, and robust performance. There are two forms of uncertainty which are accounted for in this analysis: parameter uncertainty, and multiplicative input uncertainty. As Appendix A indicates, of the four parameters that make up the state space of eqs 3.25 and 3.26, the stability derivatives M_α and Z_α have the most significant variation throughout the range of angle of attack from 0° to 20°. The parameter M_α varies by as much as 124%, while Z_α varies by 40%. Therefore, in determining the stability of the system to variations in angle of attack, the analysis will be restricted to the variations of M_α and Z_α.

The first graph in Figure 4.27 provides a measure of how robust the closed loop system is to variations in the parameter M_α. This measure is obtained by applying the small gain theorem to the closed loop system with the uncertainty structure of equation 4.5.

$$M_\alpha = (1+1.24\Delta)M_\alpha \tag{4.5}$$

In equation 4.5, Δ represents the possible phase characteristics of the M_α variation. For real parameter uncertainty this represents the sign of the parameter variation. The value of 1.24 was chosen to normalize the perturbation to cover the entire range of angle of attack under consideration. In this case, since M_α varies by as much as 124%, the normalizing weight is chosen to be 1.24. Variations in the uncertainty of M_α are discussed as fractions of the total variation throughout the flight regime.

The transfer function between the input and output of Δ is analyzed using the small gain theorem. Since this analysis is formulated with uncertainty in M_α alone, there is one input and one output in the transfer function; because of this, the *ssv* is identically the maximum singular value. If the maximum singular value of the transfer function between Δ is exactly one, then the system will be guaranteed stable for a 124% variation in M_α. If the maximum singular value is less than one, then the system can withstand a perturbation, Δ, greater than one before an instability will result. The maximum possible perturbation for the system before an instability will result is $1/\mu$. Therefore, if μ is equal to 2, the system remains stable for perturbations less than .5. A perturbation of less than .5 is equivalent to a 62% (.5x1.24=.62) variation in M_α

The maximum singular value for the first graph is approximately 1.8, so the closed loop system is stable for 55.6% (1/1.8) of the total variation of M_α or a 69% (.556x1.24) variation in M_α. The closed loop system is most sensitive to M_α

variations at around 13 rad/sec. It should not be surprising that the nominal location of the lightly damped poles are at 12.65 rad/sec. This result indicates that the lightly damped poles may be the reason why the closed loop system is sensitive to variations in angle of attack. This phenomena was predicted by [14].

The second graph provides a measure of how robust the system is to variations in Z_α alone. The uncertainty structure for Z_α is represented by equation 4.6.

$$Z_\alpha = (1+.40\Delta)Z_\alpha \tag{4.6}$$

where .4 represents the total variation of Z_α over the range of angle of attack from 0° to 20°. The second graph represents the transfer function around Δ. Similar to that of M_α variations, the transfer function is represented by a single input and a single output. As the second graph indicates, the maximum singular value is .5. Therefore, the system can handle perturbations in Δ up to 1/.5 or 2. This represents twice the total variation of Z_α or 80% of Z_α.

Based on the results of the first two graphs, it is obvious that the system is more sensitive to variations in M_α than variations in Z_α. This result is not surprising since it is known in the field of flight dynamics that the short period mode is most sensitive to M_α variations [27], [28].

The third graph of Figure 4.27 provides a measure of how robust the closed loop system is to simultaneous variations of M_α and Z_α assuming dependant and independent variations. The parameters M_α and Z_α vary nonlinearly with angle of attack. To make the assumption that their variation is independent of one another would be overly conservative, however, to assume that they vary in a linearly related fashion would be a mistake as well. Therefore, both plots are provided to serve as an upper and lower bound for the stability margins to variations in angle of attack.

The uncertainty structure for the dependant variation can be represented as

$$\begin{pmatrix} M_\alpha & 0 \\ 0 & Z_\alpha \end{pmatrix} = \left(I_2 + \Delta_2 \begin{bmatrix} 1.24 & 0 \\ 0 & .40 \end{bmatrix} \right) \begin{bmatrix} M_\alpha & 0 \\ 0 & Z_\alpha \end{bmatrix} \tag{4.7}$$

where 1.24 and .40 represent the total variations of M_α and Z_α respectively. Δ_2 is represented as a two dimensional repeated scalar block. Since this repeated scalar block is the only uncertainty present for this particular analysis, the *ssv* is again equivalent to the maximum singular value.

The robustness of the closed loop system to the dependant variation of M_α and Z_α can be seen by the lower plot in the third graph of Figure 4.27. According to Figure 4.27, the graph is very similar to the stability of the M_α variation represented in the first plot. This is not surprising since it has already been shown that the system is much more sensitive to variations in M_α than variations in Z_α. Like the first plot, the closed loop system can withstand up to 1/1.86 or .54 times the total variation of eq 4.7.

The uncertainty structure for the independent variations can be represented as

$$\begin{pmatrix} M_\alpha & 0 \\ 0 & Z_\alpha \end{pmatrix} = \left(I_2 + \begin{bmatrix} 1.24\Delta_{m\alpha} & 0 \\ 0 & .40\Delta_{z\alpha} \end{bmatrix} \right) \begin{bmatrix} M_\alpha & 0 \\ 0 & Z_\alpha \end{bmatrix}. \tag{4.8}$$

Equation 4.8 represents a two block uncertainty structure since both parameters are assumed to be varying independently. In this case the structured singular value is used to measure the stability margins for this uncertainty structure. The larger plot in the third graph represents the robustness of the closed loop system to independent variations of M_α and Z_α. Again, the instability occurs at the frequency of the short period mode eigenvalues. According to this plot the system can withstand 1/2.33 or

.43 times the uncertainty structure of eq. 4.8. As expected this plot is slightly larger than that of the dependant variations.

It is expected that the stability of the system to angle of attack variations lies somewhere within the bounds of these two graphs. Since both uncertainty structures, 4.7 and 4.8, have values of μ greater than one the system will definitely become unstable at some point in the range of angle of attack under consideration. This was indeed evidenced in Figures 25 and 26.

The final graph in Figure 4.27 provides a measure for the performance and robust performance of the closed loop system to two different uncertainty structures. The smallest plot is a measure of the nominal system's performance. Since this plot is well below one, the system has exceeded the nominal performance requirements. The middle plot represents the robust performance (μ) of the system to the simultaneous effect of the unstructured multiplicative uncertainty as well as a dependant variations of M_α and Z_α. Since there are three blocks under consideration: performance, multiplicative input uncertainty, and dependant parametric variation, the problem is represented as a three block uncertainty, Δ. The measure provided by this μ-analysis is the robust performance of the system with all three blocks occurring simultaneously. As the figure shows, the system does not satisfy the robust performance requirements; the largest degradation again being exhibited at the location of the lightly damped pole pair. The largest plot in the last graph represents the robust performance (μ) to the simultaneous effect of the unstructured uncertainty and independent variations of M_α and Z_α. This problem is represented by a four block uncertainty since M_α and Z_α are considered independent. As the figure shows, the system does not satisfy this uncertainty structure as well. Again, the greatest degradation in performance is experienced at the frequency of the short period poles.

The above robustness analysis of Figure 4.27 clearly shows that the system is quite sensitive to parameter variations which affect the location of the short period mode. The next design will attempt to desensitize the H_∞ controller to variations in M_α by explicitly modelling uncertainty in this parameter.

4.3.2 H_∞ Optimization with Parameter Uncertainty

The results of section 4.3.1 indicate that the nominal H_∞ controller is extremely sensitive to variations of M_α when considering robustness to changes in angle of attack. The following design is similar to the nominal H_∞ design, however this time, uncertainty in M_α will be modelled explicitly in the problem formulation. This will hopefully reduce the sensitivity of the controller to variations of M_α, thereby producing a control system which will maintain stability over the prescribed range of angle of attack. This will be done by expressing the coefficient M_α as

$$M_\alpha = (1 + k\Delta)M_\alpha \tag{4.9}$$

where k represents the maximum variation of M_α. After modelling the uncertainty in M_α, the H_∞ problem is formulated as the three block uncertainty problem of Figure 4.28; where Δ_p represents the performance requirement, Δ_u represents the unstructured uncertainty, and $\Delta_{m\alpha}$ represents the variation of M_α. The weights Wq and Wu are the same as those of design I.

This new H_∞ problem was initially formulated with k=1.24; this represents a 124% variation in M_α. The solution to this problem could not produce a μ of less than 1 even with high order dynamic scaling. Therefore, it is impossible to achieve robust performance with that significant a variation in the parameter M_α.

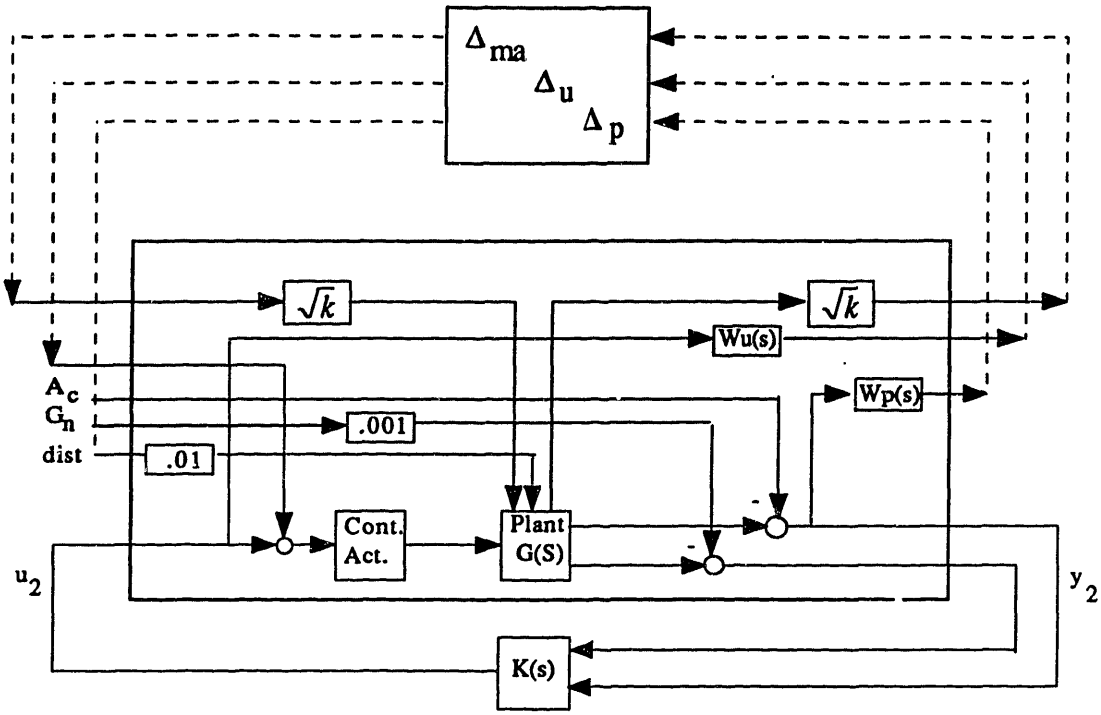

Figure 4.28 H_∞ Problem Formulation Design II

The value of k was reduced until a solution could be found that had a μ of less than one. The final choice of k was chosen such that a third order D scale could reduce the value of μ to less than one in three iterations. This value was 57% of M_α (k=.57). Since the final value of μ was less than one, the robust performance of the system is guaranteed for up to 57% of the variation in M_α as well as a simultaneous variation in the dynamics of the model as represented by the multiplicative input error. This represents a variation in angle attack of about 12°, or from 3° angle of attack to 15° angle of attack.

Figure 4.29 shows a graph of the maximum singular value for the first design iteration along with subsequent μ bounds for each of the three iterations of μ synthesis.

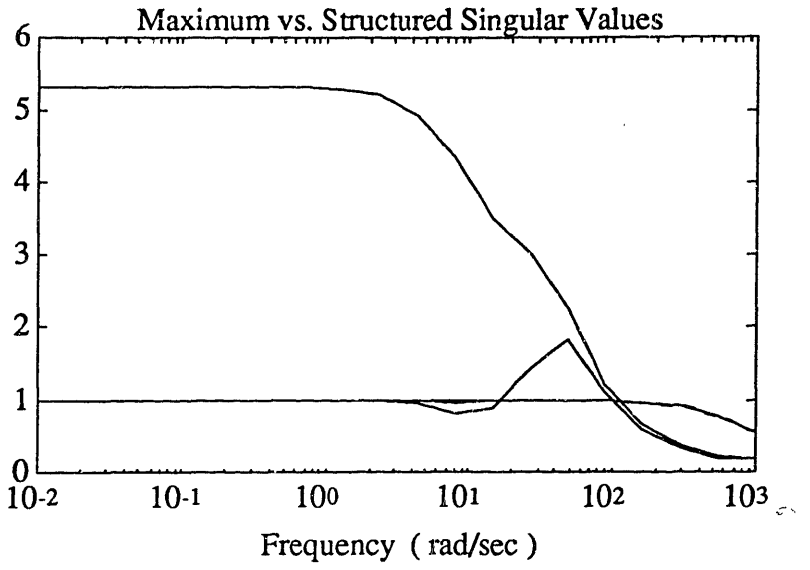

Figure 4.29 Maximum vs. Structured Singular Values (Design II)

Without the reduction in the conservatism provided by the optimal dynamic scaling, it would have been impossible to achieve robust performance for the 57% variation of M_α. The values of γ_o along with their associated structured singular values are listed in Table 4.4

Iteration	γ	μ
1	5.3242	1.840
2	1.0088	1.005
3	.9929	.9929

Table 4.4

Since there are three uncertainty blocks, it was necessary to build two separate D-scale transfer functions. These scales were fit using third order filters. Use of these D-scales increased the final order of the controller from 13 states in Design I to 19 states for the method considered in this section. The use of the 12 states for dynamic scaling improved the robust performance measure (μ) by 53.96% over the first H_∞ iteration.

For this case, the use of dynamic scaling has had a remarkable improvement in the robust performance as measured by μ.

The maximum singular value plot of the final controller is shown in Figure 4.30. As the plot shows, the valley which was present in Design I is no longer present in this design. This shows that the controller is no longer trying to invert the lightly damped poles of the short period mode. Appendix C has a list of the poles and zeros of the controller.

Figures 4.31 through 4.33 show the singular value plots for the complementary sensitivity, the sensitivity and the open loop pitch actuator plant respectively. As Figure 4.33 shows, the open loop pitch actuator branch has the required -20 db attenuation and two pole roll off. According to Figure 4.33, the crossover frequency is 34.3 rad/sec. This provides 123° of phase margin at crossover, and a gain margin of .0018 at the phase crossover.

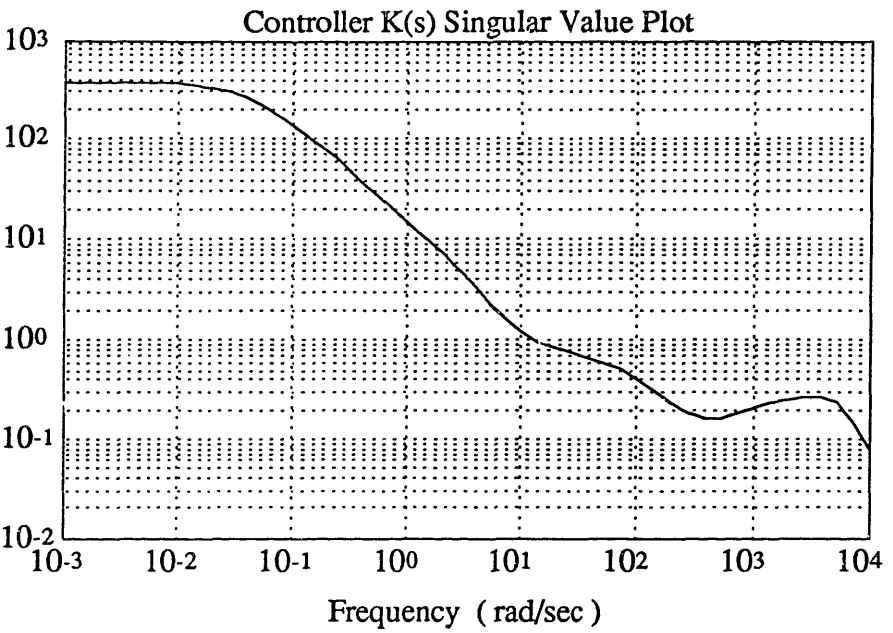

Figure 4.30 Maximum Singular Value of K(s) (Design II)

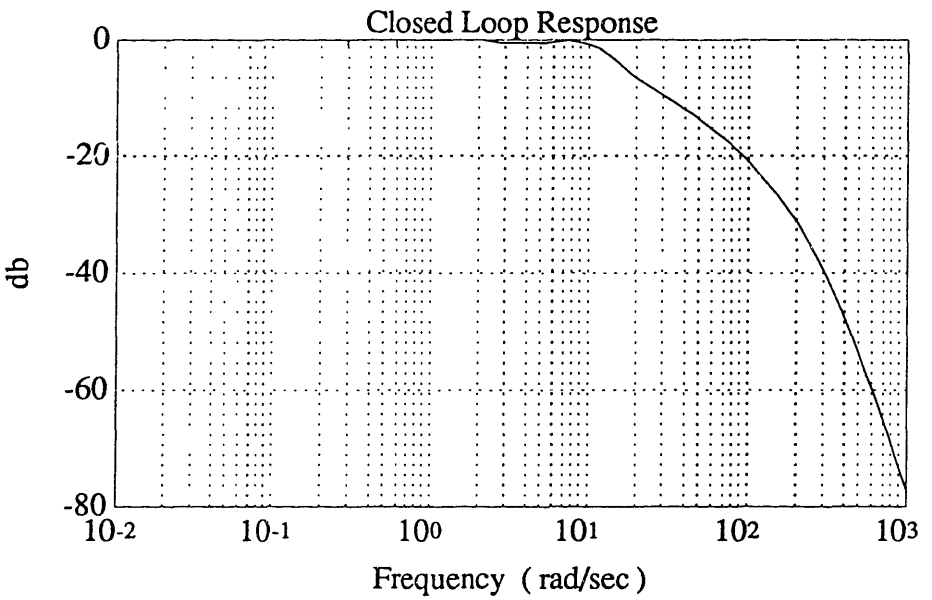

Figure 4.31 Complementary Sensitivity (Design II)

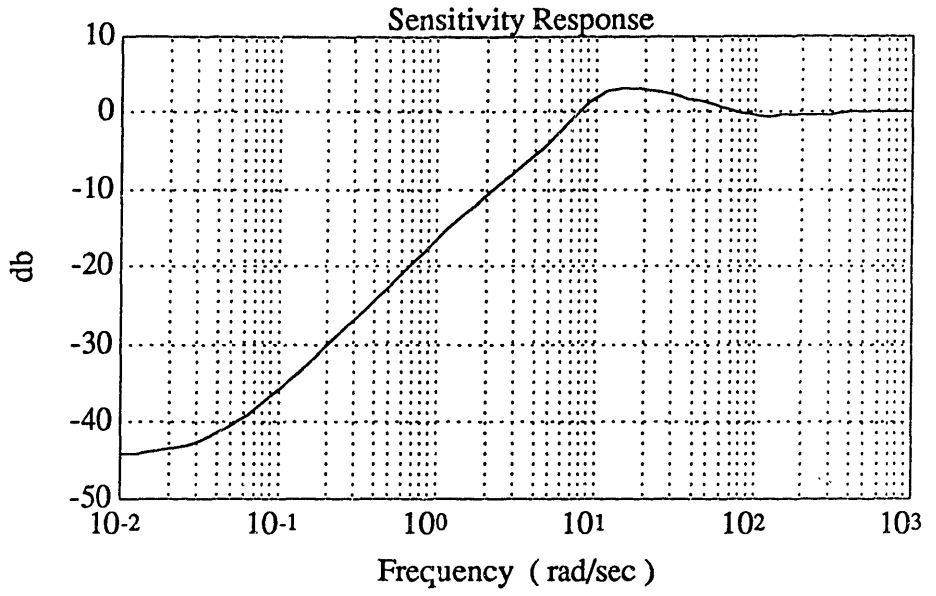

Figure 4.32 Sensitivity (Design II)

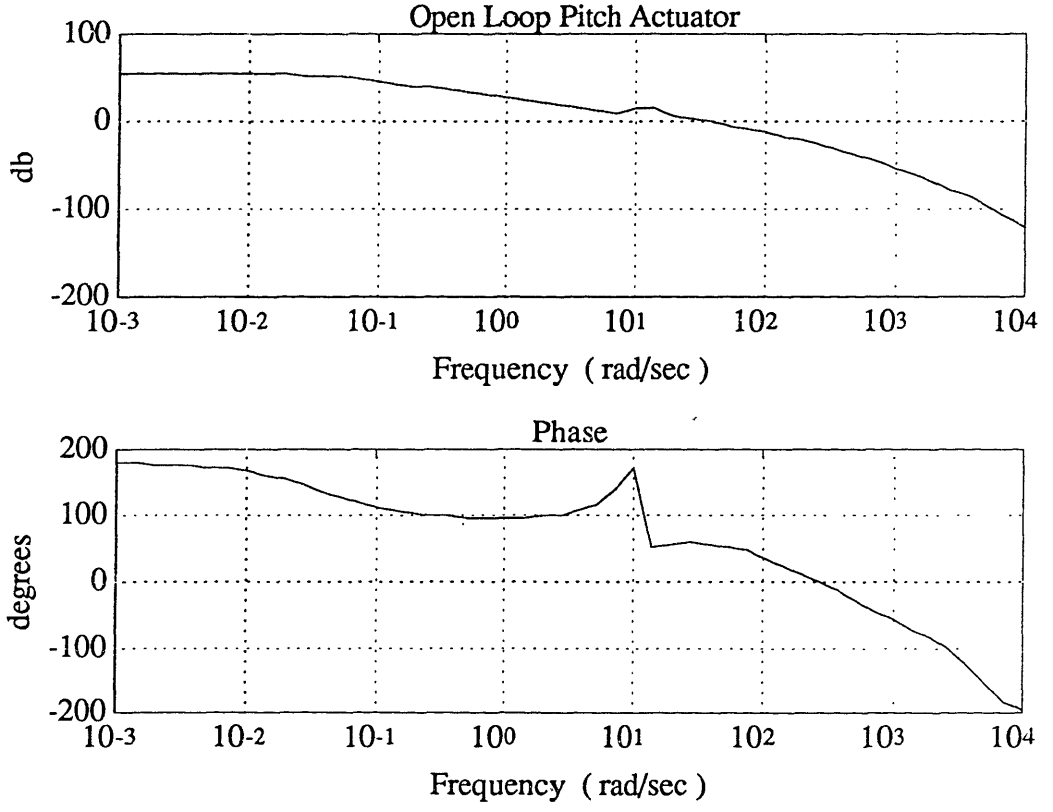

Figure 4.33 Open Loop K(s)G(s) for Design II

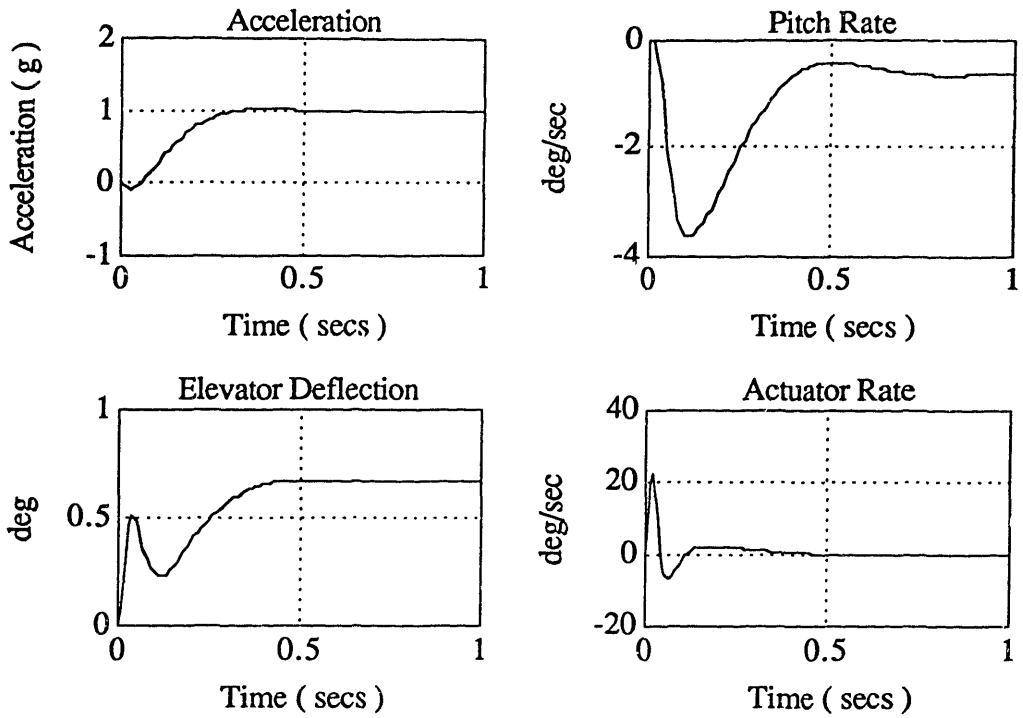

Figure 4.34 Acceleration Step Response Design II

Figure 4.34 shows the step response of the nominal model. The missile achieves a one g acceleration in about .3 secs, with a maximum deflection rate of about 21 deg/sec. It is obvious that the addition of M_α uncertainty has added more damping into the system from the slightly less oscillatory nature of the system as well as from the slight reduction in the actuator rate. The above time response clearly meets all time domain performance specifications.

Figure 4.35 plots the step response of the closed loop system for three different values of angle of attack: 0°, 10°, and 20°. The closed loop system responds extremely well for 10° and 20° angle of attack. The instability of the closed loop system at low angles of attack has been eliminated, although there is a slight degradation in performance. This degradation is represented by the oscillatory nature of the response. The response however, is fairly well damped and will settle quickly. The inclusion of parametric

uncertainty directly into the design process has eliminated the inversion problem inherent in the H_∞ optimization. The variation of the lightly damped poles has less of a destabilizing effect on the closed loop system as can be seen by the root locus of Figure 4.36.

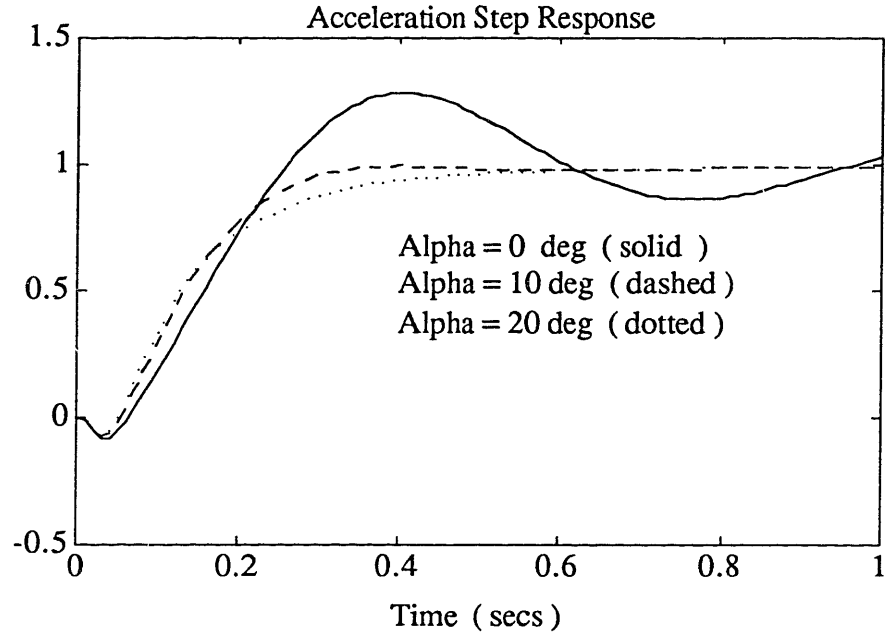

Figure 4.35 Step Variation with Angle of Attack (Design II)

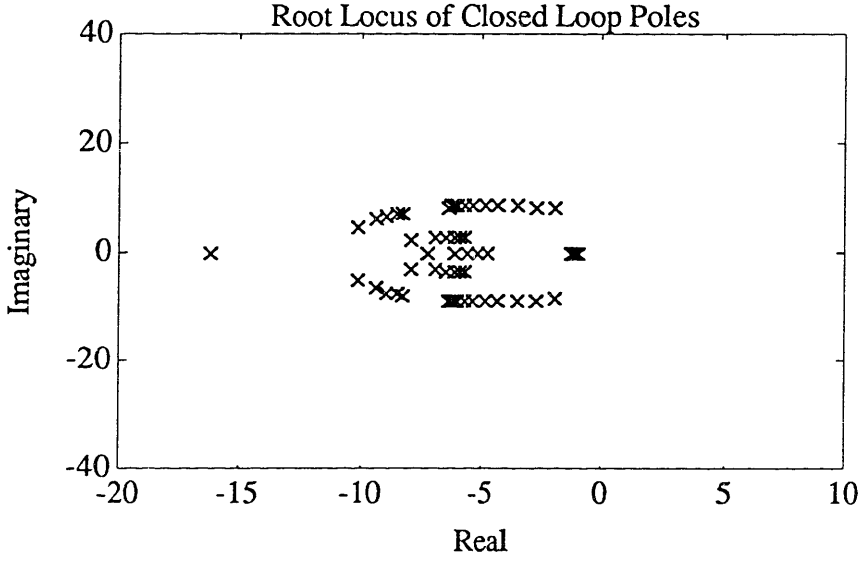

Figure 4.36 Variation of Poles with Angle of Attack (Design II)

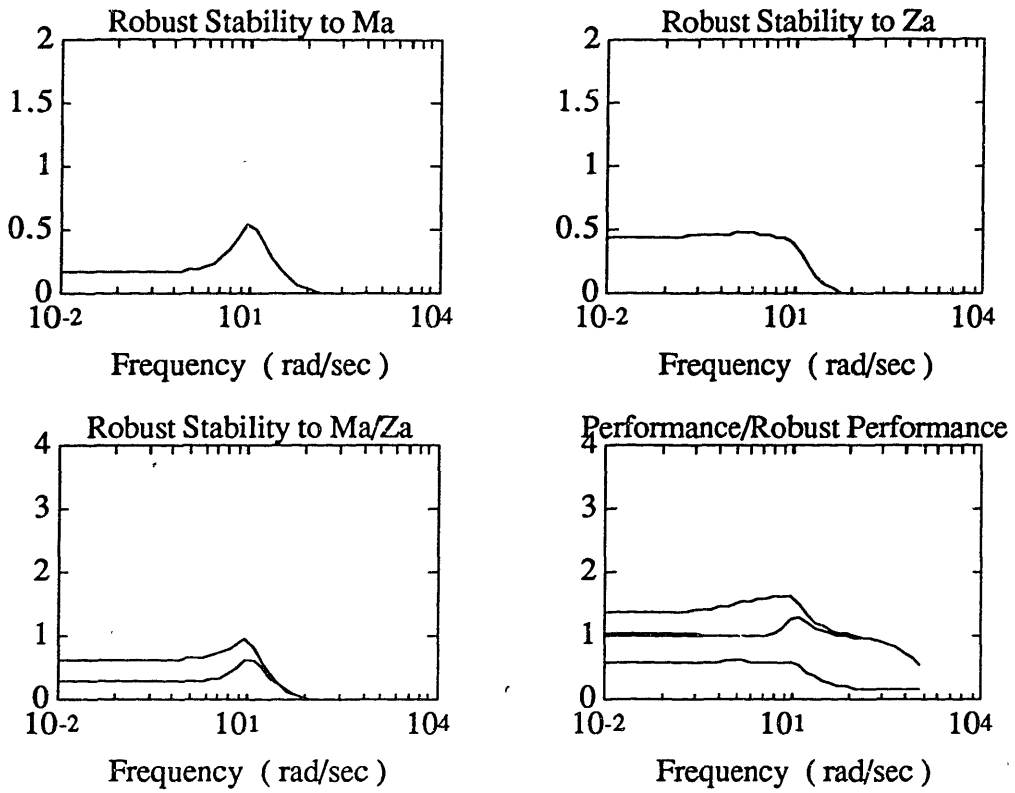

Figure 4.37 Robustness Analysis of Design II

The robustness analysis of Design II as illustrated in Figure 4.37 shows the excellent benefits of modelling parameter uncertainty in the H_∞ design process. As the first graph indicates, the system is stable to 185% of the total variation of M_α. This amounts to M_α varying by 229%. The previous H_∞ design was stable for variations of 69%. The increase in the order of the controller by 6 states has resulted in a system which has 3.3 times as much stability to variations in M_α.

The second graph reveals only slight improvement in robustness to Z_α. This is as expected since uncertainty to Z_α was not taken into account in the design process. The system is robust to approximately two times the total variation, or 80% of the variation of Z_α.

The improved parametric robustness is again evidenced in the third plot of independent and dependant variations of M_α and Z_α. Both these plots indicate that the system is stable for the entire range of angle attack for both uncertainty structures. This was evidenced as well in the stable responses of the unit step command for the three angles of attack.

The last plot shows the performance and robust performance. As expected, the nominal performance is similar to that of the previous design. The robust performance, on the other hand, shows a substantial improvement. The plot of robust performance for the dependant uncertainty structure with unmodelled dynamics indicates that the system has almost complete robust performance for the entire variation of angle of attack with only a slight degradation in performance.

The independent variation is remarkably improved, however, it still does not indicate satisfactory robust performance. This is, however, a conservative estimate since the variations of M_α and Z_α are coupled.

In general, the inclusion of the parametric variation has shown significant improvements in the robust performance of the H_∞ design with only a slight penalty in the increase of the number of states (6 states). It should be remembered that achieving high performance over such a significant variation of open loop poles is truly a challenging problem.

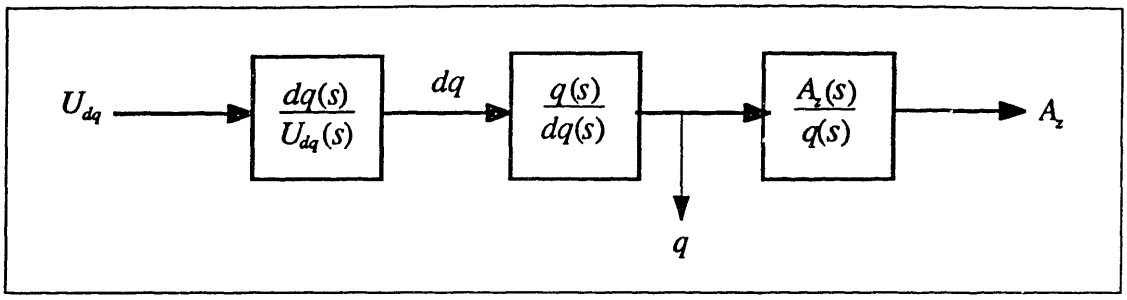

Figure 4.38 Classical Block Diagram

4.3.3 Classical Design

In the following section, a control system is developed using classical design techniques. This design will serve as a comparison for the modern control techniques. The design of a longitudinal autopilot using classical methods is not a complicated task since the missile is considered to be a single input multi-output design problem. If the missile problem were a true multi-input multi-output system, the synthesis of a controller using classical methods would be extremely difficult.

Figure 4.38 shows the block diagram of the missile formulated as a classical design problem. The desired classical control architecture is shown in the block diagram of Figure 39.

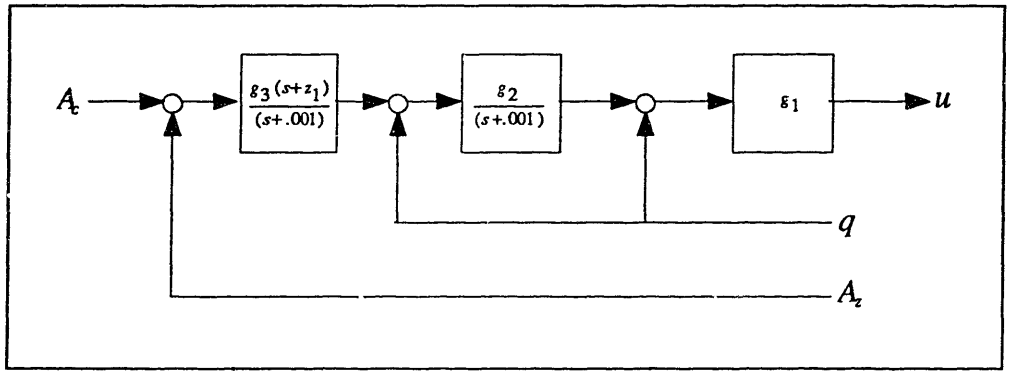

Figure 4.39 Desired Classical Architecture

The inner loop is considered to be the transfer function between the deflection dq and the pitch rate q. The transfer function of the inner loop is

$$\frac{q(s)}{dq(s)} = \frac{(s+.9591)}{(s^2+1.103s+160.1)} \tag{4.10}$$

The lightly damped poles of the short period mode appear in the transfer function of the inner loop. In the following classical design, a high bandwidth inner loop is developed to reject the parameter uncertainty associated with variations in angle of attack. The sensitivity transfer function of the loop is a measure of the closed loop system's ability to reject parameter variations. Therefore, it is desired to develop a classical design that has a small sensitivity gain at low frequencies.

The inner loop will be designed using a proportional plus integral feedback architecture. The choice of gains for the proportional and integral feedback will be based on root locus techniques.

The first loop to be closed will be a proportional gain feedback. The lightly damped poles are located at -.5516±12.653i. Figure 4.40 shows the roots locus of the low frequency poles as the feedback gain g1 is decreased from zero to -.4. As Figure 4.40 shows, one of the poles is migrating towards the zero located at -.95913, while the other increases in frequency towards infinity.

The feedback gain, g1, is chosen based on the fact that it is known that when the integrator pole is closed in the loop, the two poles of the inner loop will begin to approach each other and break away from the real axis somewhere in between their locations of Figure 4.40. The integrator pole in the mean time will approach the zero located at -.95913. The gain g1 is therefore chosen to sufficiently move the point where the breakaway will occur. This will determine the bandwidth of the inner loop.

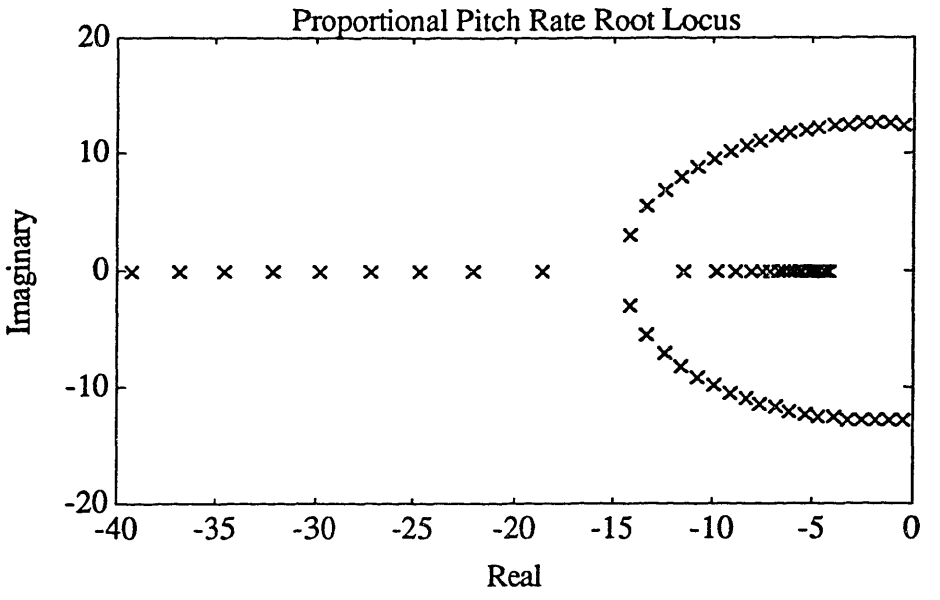

Figure 4.40 Root Locus of Proportional Inner Rate Loop

After choosing the gain g1, the next step is to include an integrator in the loop to decrease the sensitivity gain at low frequencies. Figure 4.41 shows the root locus for the integral feedback around the inner loop.

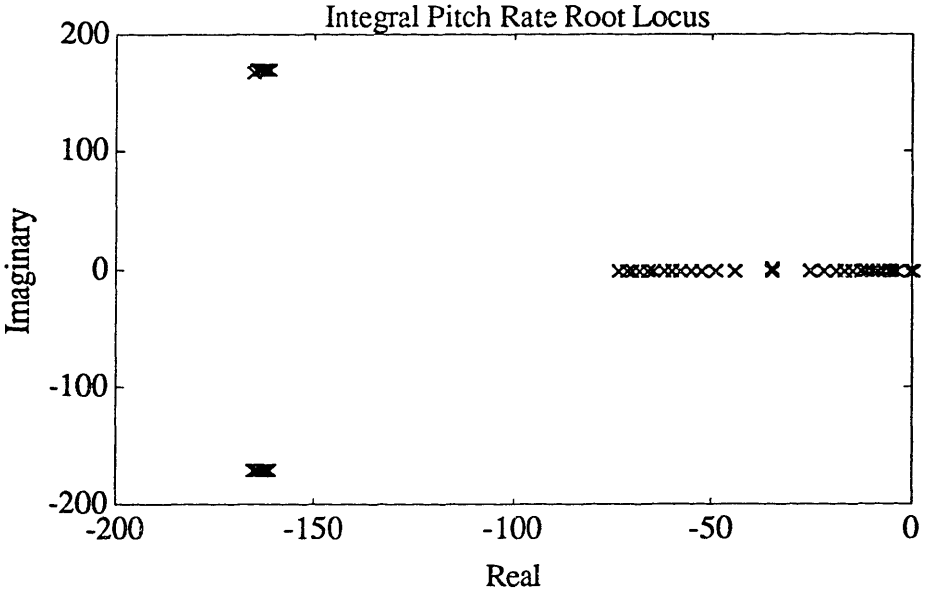

Figure 4.41 Integral Inner Loop Root Locus

The feedback gain, g2, was varied from 0 to 12.9. The gain was chosen to provide the maximum inner loop bandwidth without excessive use of control energy. It should be remembered that there is the requirement that the open loop pitch actuator have -20 db attenuation at 200 rad/sec. The gain g2 was selected to be 12.9 because this brought the poles together, but was not sufficiently large enough to have them breakaway from the real axis.

At this point, Figure 4.42 shows the closed loop bode plot of the inner loop while Figure 4.43 shows the inner rate loop sensitivity function. As Figure 4.42 and 4.43 show, the sensitivity function has a very small gain at low frequencies. This should provide the necessary sensitivity to reject parameter variations.

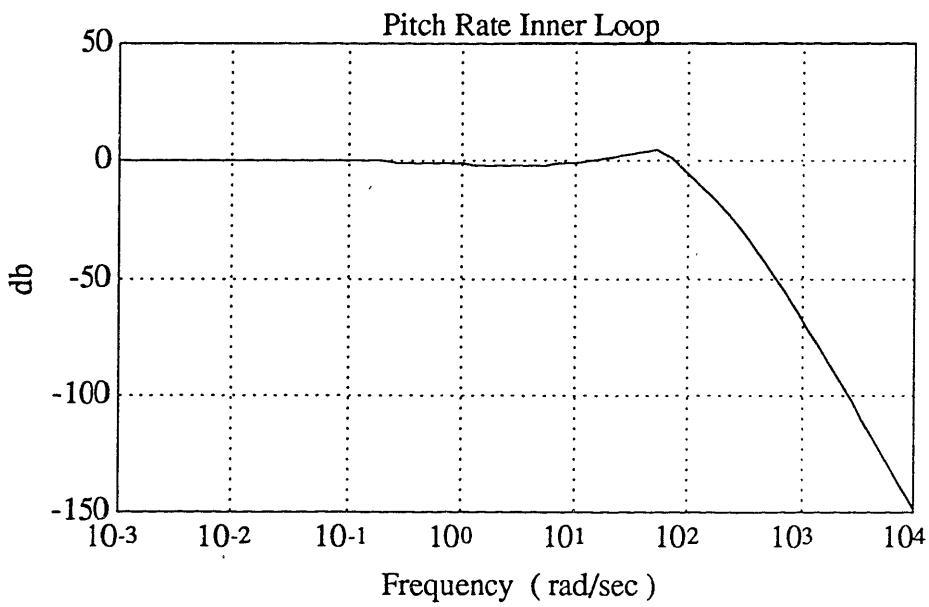

Figure 4.42 Inner Loop Complementary Sensitivity

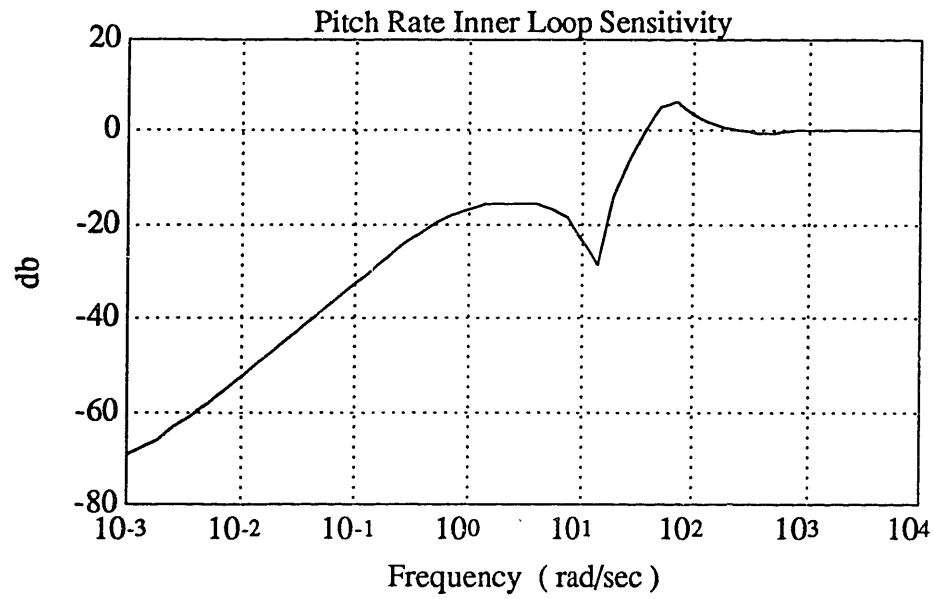

Figure 4.43 Inner Loop Sensitivity

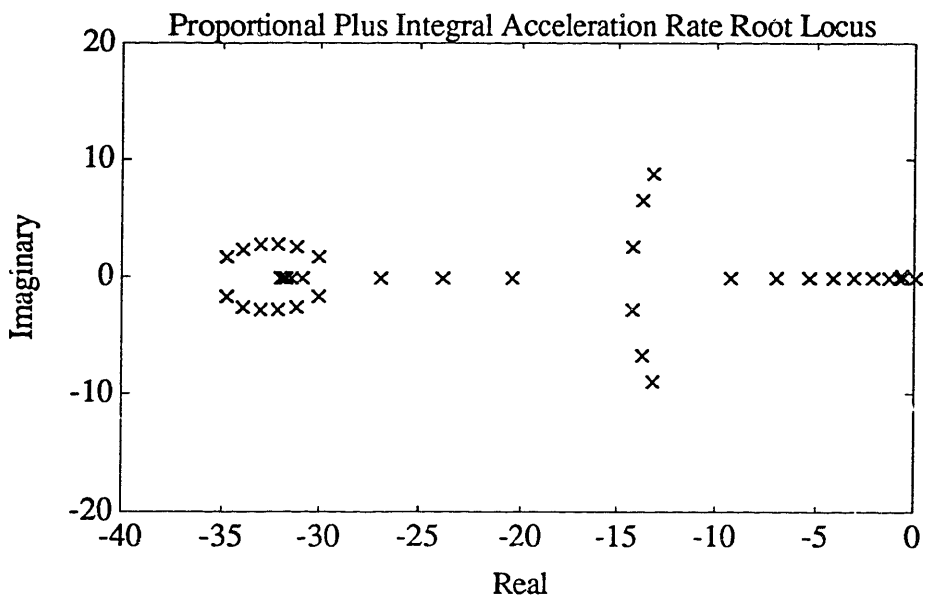

Figure 4.44 Proportional Plus Integral Root Locus

The final part of the classical design synthesis is the development of the compensator to be placed in the outer loop; this is designed to provide the necessary performance requirements. For this case, a proportional plus integral compensator is designed to provide the required performance. The integrator was placed at -.001 (as an

approximation to an integrator) while the zero was placed at -.8 rad/sec. Figure 4.44 shows the root locus for the feedback gain , g3, from 0 to 5.5. The feedback gain g3 was chosen to provide the required amount of sensitivity in the outer performance loop. This value was 5.5.

After choosing this feedback design, evaluation of the resulting Bode plots revealed that the -20 db requirement was not satisfied at 200 rad/sec. An additional 10 db attenuation was required. This was accomplished by placing a low pass filter at the actuator input to provide the required attenuation.

$$W_f = \frac{90}{(s+90)} \tag{4.11}$$

The locations of the poles for the closed loop system are listed in Table 4.5.

real	imaginary	frequency	damping
-.80362	0	.80362	1
-11.225	-7.8699i	13.709	.8188
-11.225	+7.8699i	13.709	.8188
-21.902	-47.565i	52.365	.4182
-21.902	+47.565i	52.365	.4182
-212.10	-198.50i	290.50	.7301
-212.10	+198.50i	290.50	.7301

Table 4.5 Closed Loop Poles (Design III)

The classical feedback architecture for this design is shown in Figure 4.45, and the maximum singular value plot of the controller is shown in Figure 4.46. The high gain at low frequency is indicative of the two low frequency poles.

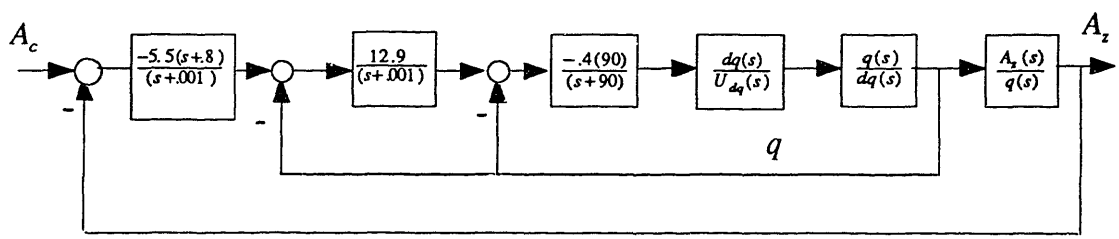

Figure 4.45 Classical Feedback Architecture

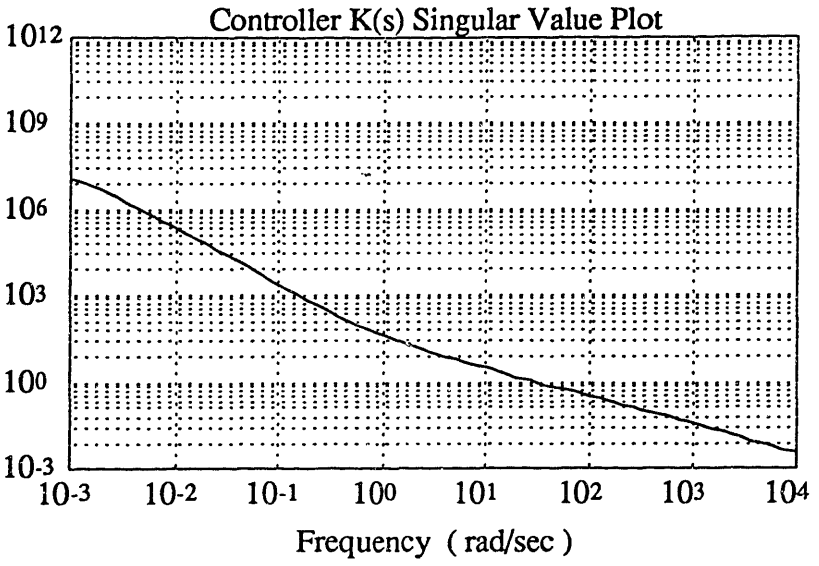

Figure 4.46 Maximum Singular Value K(s) (Design III)

The closed loop bode plot for this design is shown in Figure 4.47, while the sensitivity and loop transfer functions are shown in figures 4.48 and 4.49. As Figure 4.48 shows, the sensitivity transfer function satisfies the performance specifications established in section 4.1.

According to Figure 4.49, the open loop pitch actuator branch has the required -20 db attenuation at 200 rad/sec along with the required two pole roll off. The system also has 147.66° of phase margin at a crossover frequency of 43.29 rad/sec and a significant amount of gain margin.

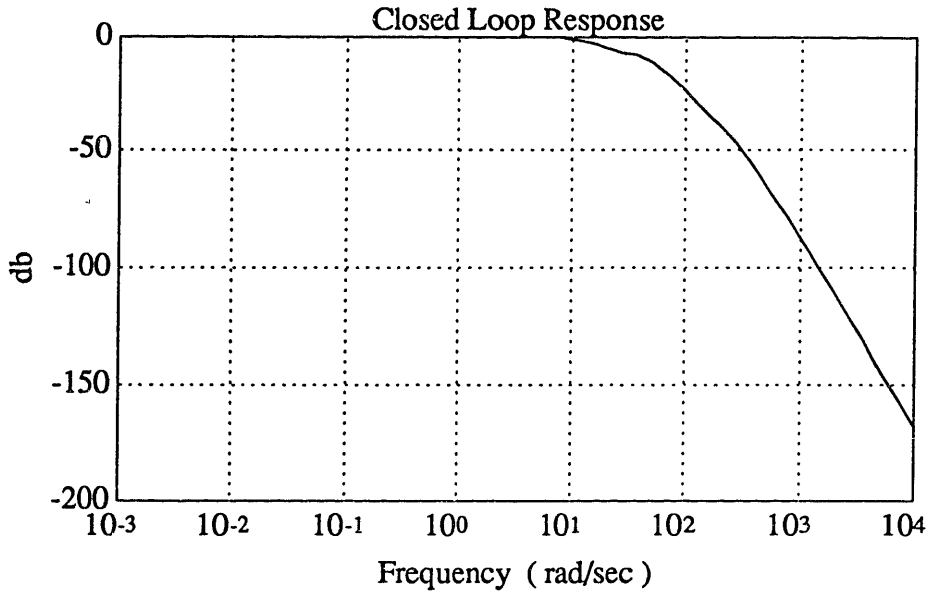

Figure 4.47 Complementary Sensitivity (Design III)

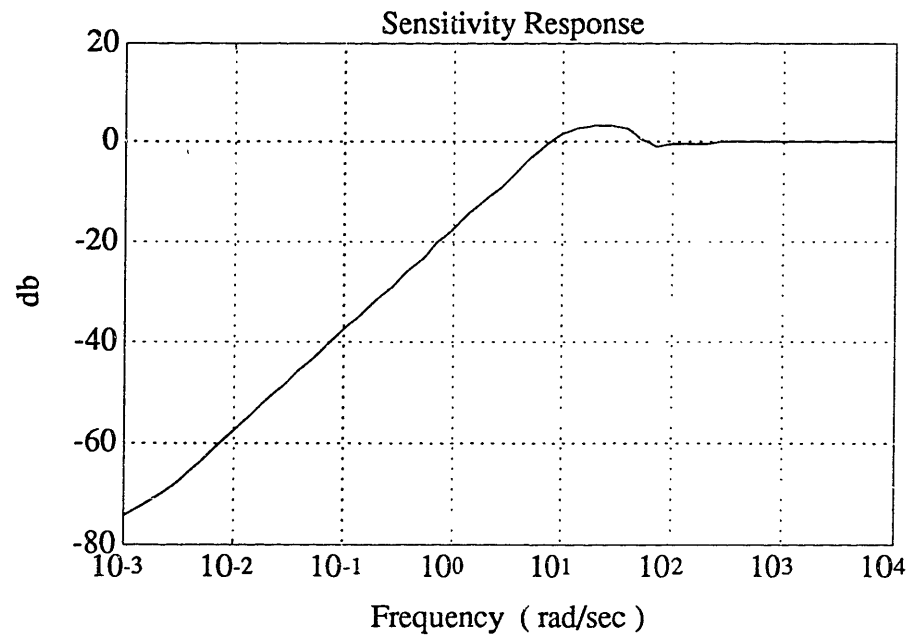

Figure 4.48 Sensitivity (Design III)

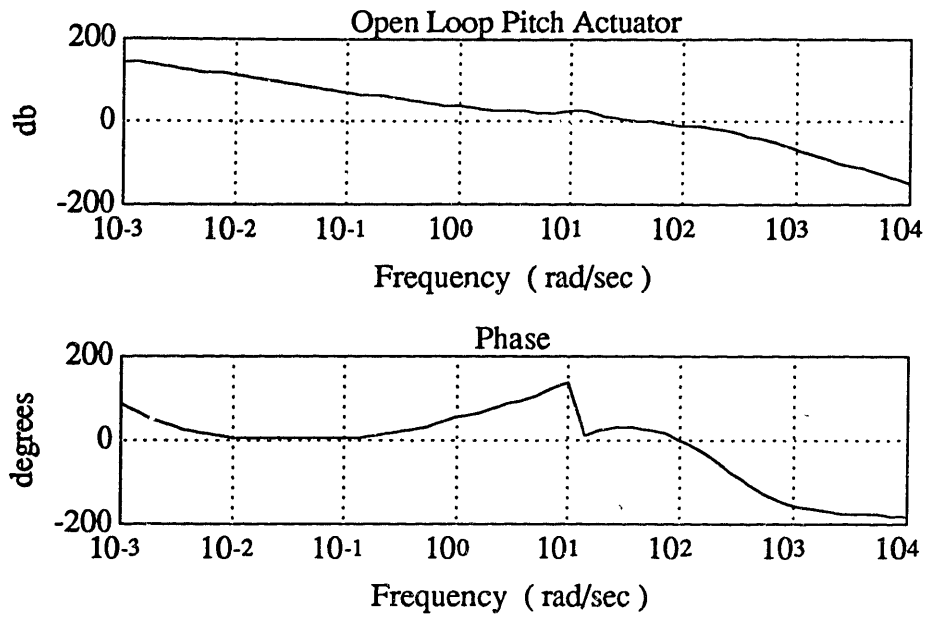

Figure 4.49 Open Loop K(s)G(s) (Design III)

Figure 4.50 shows the step response of the nominal design. The missile achieves a 1g acceleration in about .3 secs, with a maximum deflection rate of about 20 deg/sec. This response has excellent transient response as well as satisfaction of all the necessary time domain performance criterion.

The above classical design has provided an excellent nominal controller. The favorable results of this classical design should be balanced with the realization that this problem was a simple formulation of a single input single output system. In cases where the system is a true multi input multi output system, such an efficient classical design formulations may not be possible.

Figure 4.51 plots the step response of the closed loop system for the variation in angle of attack. As Figure 4.51 shows, the system performs exceptionally well for all angles of attack. The worst case is at 0°; but even this response is outstanding. The inner loop pitch rate design has provided a system which has excellent robust performance to variations in angle of attack.

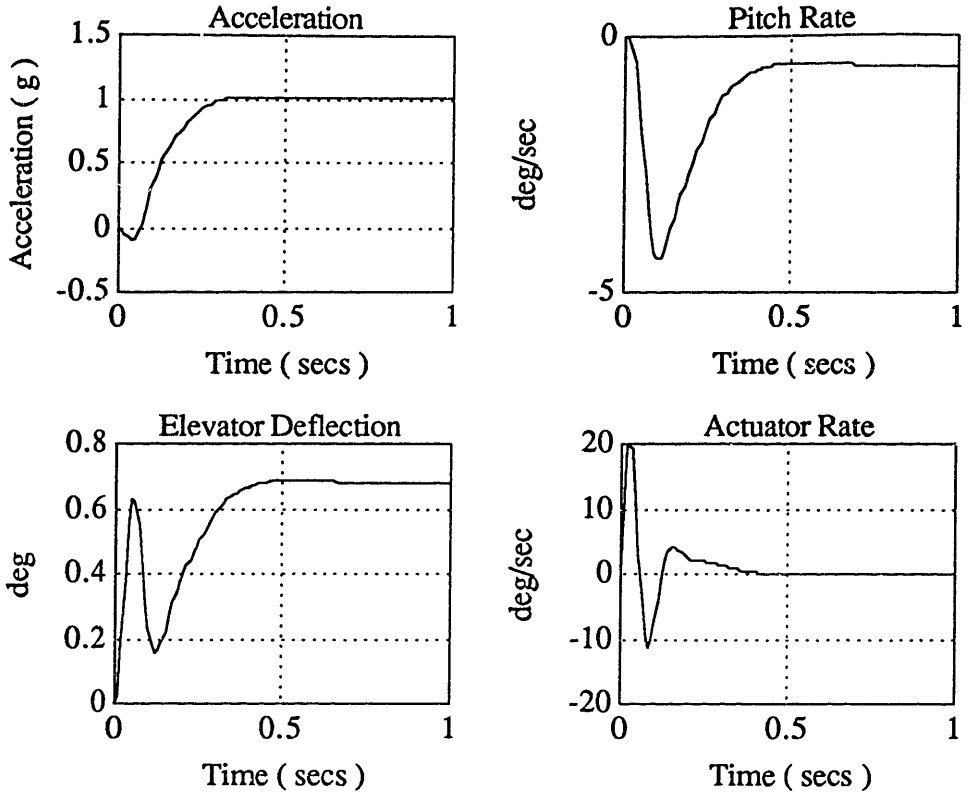

Figure 4.50 Acceleration Step Response (Design III)

The plot of Figure 4.52 shows the low frequency closed loop poles as the angle of attack is varied form 0° to 20° angle of attack. As the plot indicates, the closed loop pole variation is significantly far enough from the imaginary axis to prevent instabilities from resulting over this range of angle of attack. In fact, it is their distance from the imaginary axis that also provides the exceptional performance demonstrated in Figure 4.51.

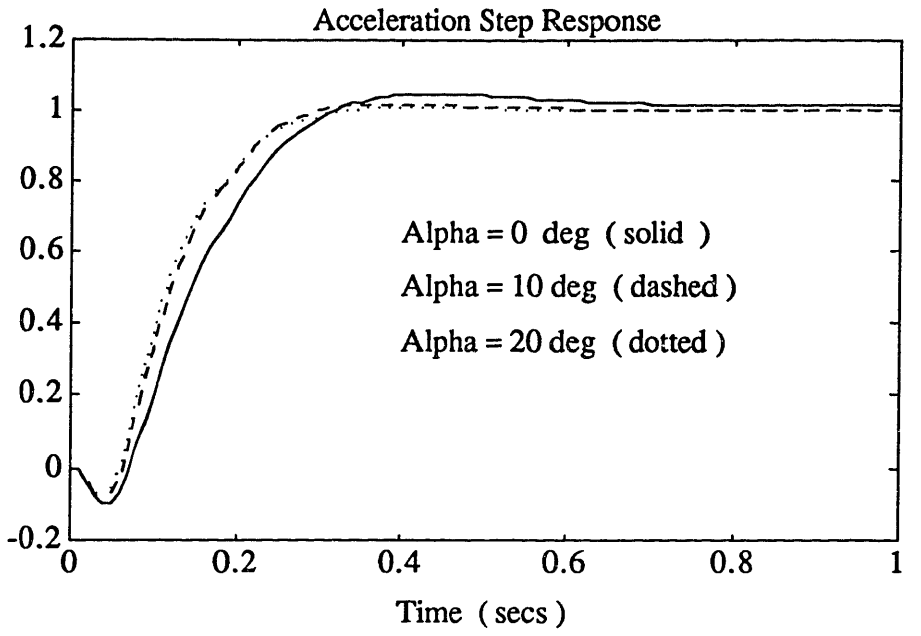

Figure 4.51 Step Variation with Angle of Attack (Design III)

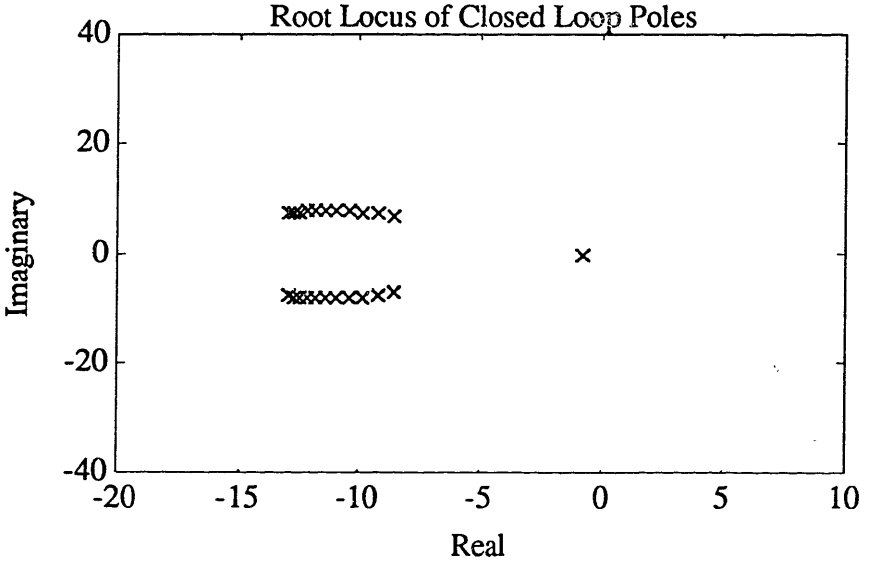

Figure 4.52 Variation of Poles with Angle of Attack (Design III)

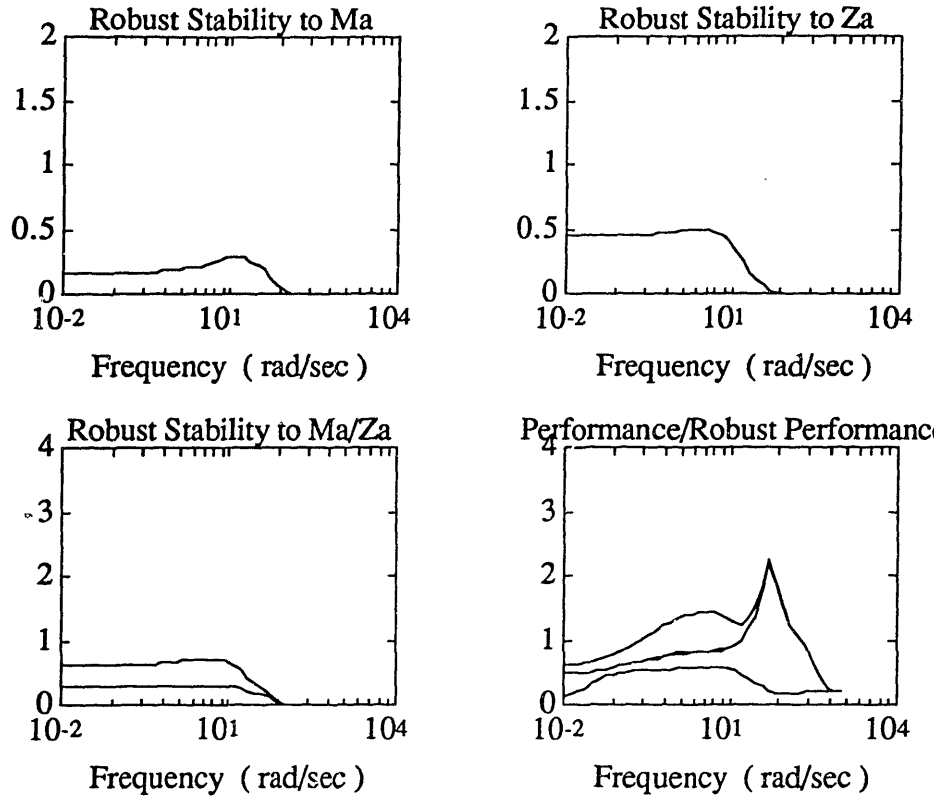

Figure 4.53 Robustness Analysis (Design III)

The outstanding stability of Figure 4.52 can be seen in the robustness analysis of Figure 4.53. The first graph shows the robustness of the classical design to variations in M_α. The system is extremely robust to M_α variations. The controller can handle up to approximately 3.3 times the total variation of M_α before instability may occur, or 409.2% variation in M_α. This result is extremely satisfying. The result of the inner loop design has been almost a total desensitization of the system to parametric variations of M_α.

The second plot shows the robustness to variations of Z_α. This result is exactly the same as previous results. There has been no significant improvement in the robustness of the system to Z_α.

The third plot demonstrates that the closed loop system has excellent stability margins due to independent and dependant variations of Z_α and M_α simultaneously. These results are a simple extension of those seen in the two previous plots.

The final plot shows the measure of performance and robust performance for the closed loop system. These results are not quite as favorable as those of the previous three plots. The smallest plot indicates that the nominal performance has been satisfactorily met. The two larger plots, however, show that the robust performance of the system is not satisfactorily met at high frequencies.

There is a simple explanation for these poor results. Actually, the system has satisfactory robust performance when one considers the performance in the presence of parametric uncertainty without the addition of unmodelled dynamics. This robust performance measure is illustrated in the graph of Figure 4.54. As the graph indicates, the system has excellent robust performance when the uncertainty is modelled as a dependant variation, and only a slight degradation below desired levels when the uncertainty is modelled as an independent variation (the upper plot).

The decrease in robust performance of the system as indicated by the fourth graph of Figure 4.53 is a consequence of the fact that the system does not satisfy the unmodelled dynamic uncertainty requirement at the crossover point of the control transfer function R(s). The system, despite this violation, is considered stable to unmodelled dynamics because it has the required -20 db of attenuation at 200 rad/sec with a two pole roll off.

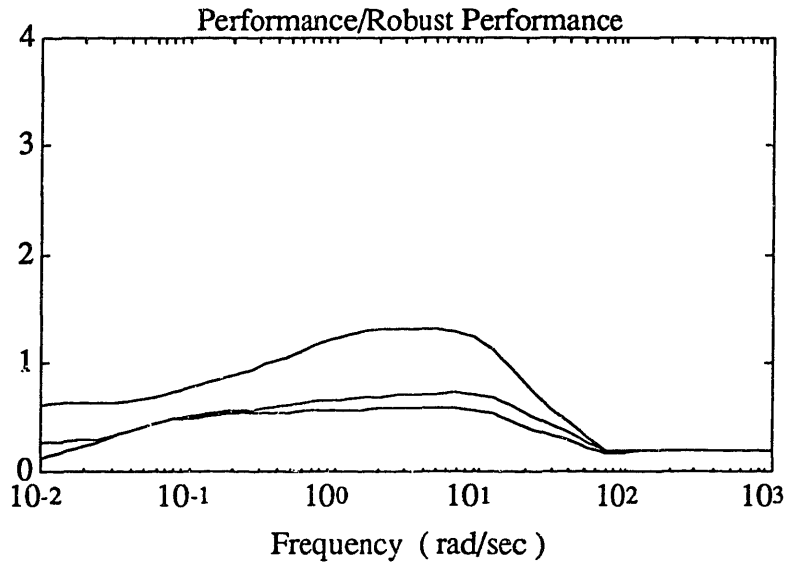

Figure 4.54 Robust Performance due to M_α/Z_α (Design III)

The error model chosen to quantify the stability robustness requirements in this case turn out to be excessively conservative. This model was chosen to reflect uncertainties at high frequencies, while the violation of stability due to this model error is in the mid frequency range.

It is questionable as to whether or not this degradation in performance is an important problem. The violation occurs when one considers the simultaneous satisfaction of model uncertainty and performance. It is not certain if the results of Figure 4.53 are significant in terms of robust performance since the performance criterion is meant to be applicable primarily at the lower tracking frequencies. The violation of robust performance occurs above the 10 rad/sec bandwidth of the system. Therefore, the tracking performance of the system does not degrade in the presence of this uncertainty structure.

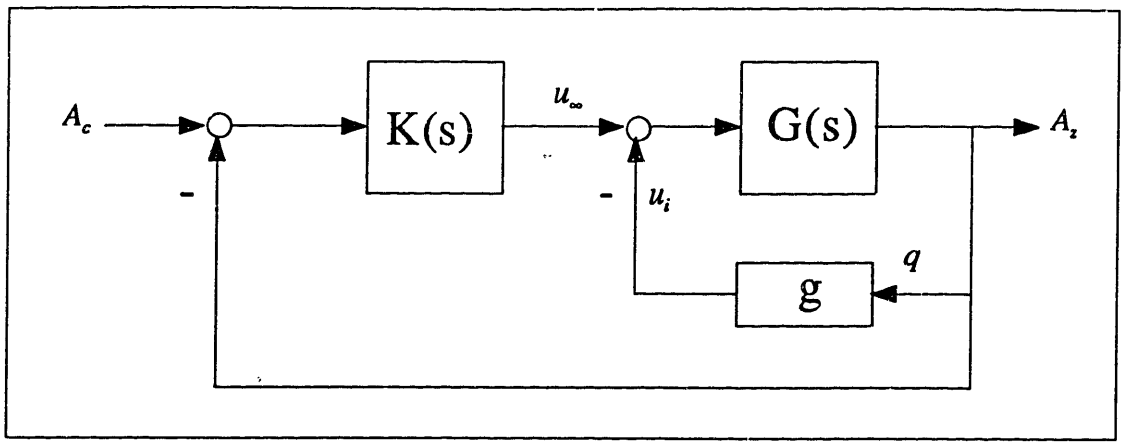

Figure 4.55 H_∞ Inner Loop Design

4.3.4 H_∞ Inner Loop Design

The final design to be considered is the H_∞ inner loop design methodology. This design was proven to provide excellent robustness to parametric variations by [14],[15], and [16]. The design procedure combines the results of H_∞ theory with that of classical and full state feedback theory. As Craig demonstrated, by providing an inner rate feedback loop, the damping of the lightly damped open loop poles can be increased to provide the extra parametric robustness. An H_∞ outer loop can then be designed to provide the additional controller structure necessary to satisfy the performance and stability robustness criteria.

Based on the results of [14] and [16], an inner pitch rate loop using constant gain feedback will be designed using the classical results of section 4.3.3. The problem formulation is similar to that shown in Figure 4.55. The feedback gain, g, was chosen using the root locus technique of Figure 4.40. It was desired to use just enough gain in the inner loop feedback path to move the lightly damped poles from their open loop location to the real axis. The gain g, was therefore chosen to be -.19.

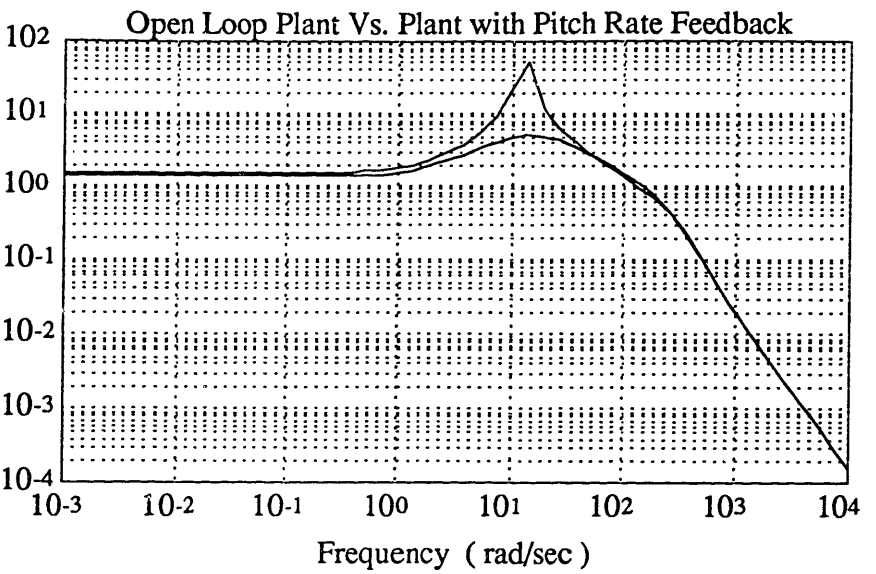

Figure 4.56 Maximum Singular Value Plot

The plot of the maximum singular values of the new plant obtained by closing the inner loop, along with the singular values of the original open loop plant are shown in Figure 4.56. As Figure 4.56 indicates, the plants are similar except that the damping of the short period mode has been substantially increased. For frequencies above 200 rad/sec, the two plots are exactly equivalent.

Two H_∞ designs were investigated. The first design is formulated to include the rate feedback architecture directly into the H_∞ problem formulation. The second problem is formulated similar to [14]: the feedback gain is provided to the nominal plant and all uncertainty and performance requirements are placed on the new plant. The subtle difference between the two formulations is the location of the unstructured uncertainty. In the first case, the unstructured uncertainty is placed inside the inner loop; thereby placing the constraint on the "old " plant and the surrounding controller architecture, whereas in the second case, the unstructured uncertainty requirement is placed as a constraint on the "new plant".

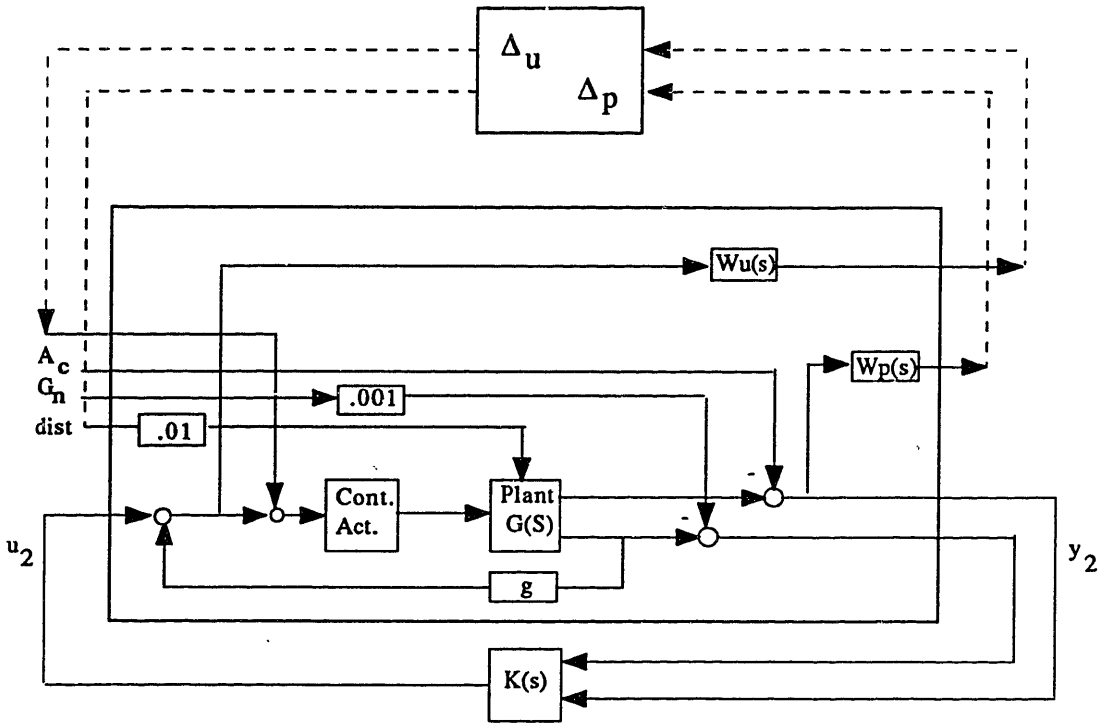

Figure 5.57 H_∞ Inner Loop Design IVa

Figure 5.57 shows the block diagram for the first design. The results of the first design are similar to that of the nominal H_∞ design (I) of section 4.3.1. Figure 4.58 shows the singular value plot of the controller K(s). As Figure 4.58 indicates, the controller is attempting to invert the poles of the open loop plant. This can also be seen by the poles and zeros of the compensator in Appendix D. Despite the addition of the inner rate loop, the H_∞ process is still attempting to invert the lightly damped pole pair. The inner rate loop can be seen in Appendix D as the feedthrough term in Dc. Careful observation of the compensator gains shows that despite the dramatic difference in gains between Design I and Design IVa, the resulting controllers have very similar pole/zero locations.

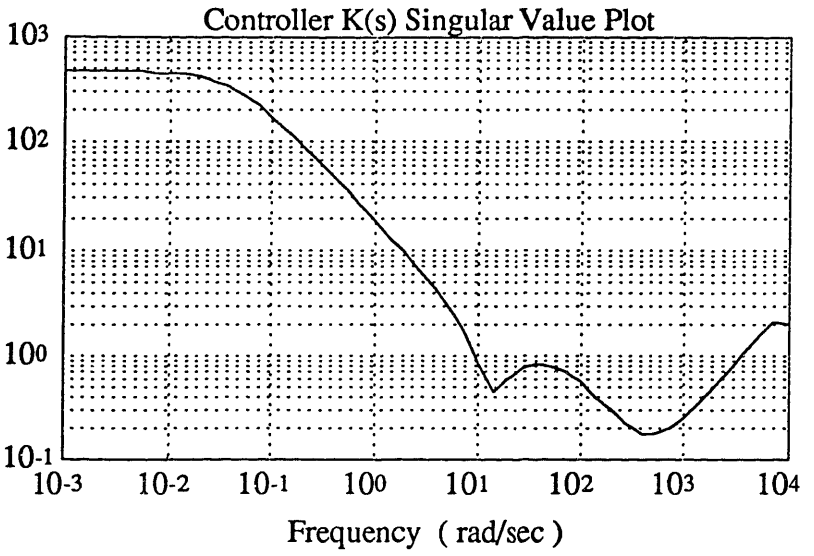

Figure 4.58 Maximum Singular Value of K(s)

The plot of the closed loop transfer function, sensitivity transfer function, and open loop pitch actuator transfer function is shown in Figure 4.59 though 4.61. Figures 4.59 through 4.61 also verify that this design is similar to the first H_∞ mixed sensitivity problem.

Figure 4.62 shows the step response of the nominal closed loop plant, while Figure 4.63 shows the step response at various angles of attack. Like design I, the closed loop system becomes unstable at low angles of attack. This can also be verified by Figure 4.64 which shows the measures of robustness to the various perturbation structures. The use of the inner loop has done nothing to improve the robustness characteristics of this H_∞ design.

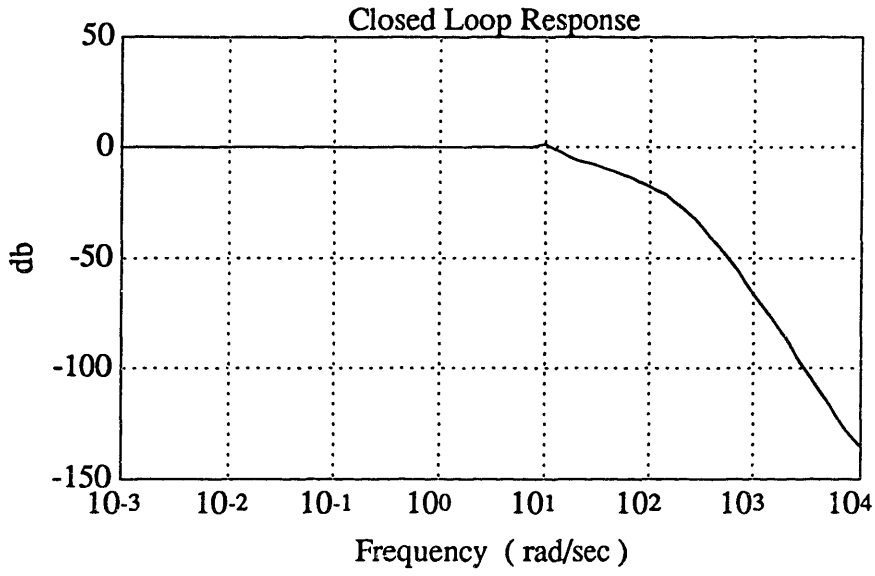

Figure 4.59 Complementary Sensitivity (Design IVa)

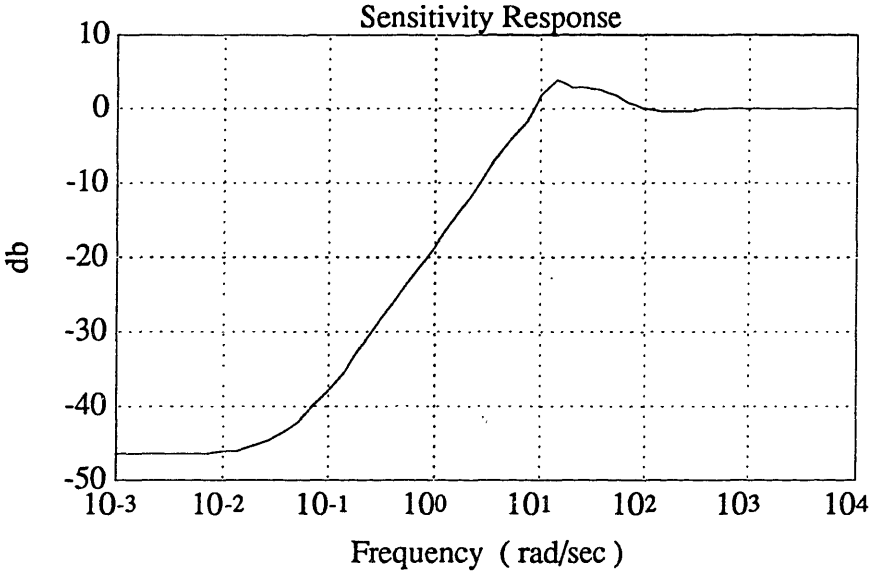

Figure 4.60 Sensitivity (Design IVa)

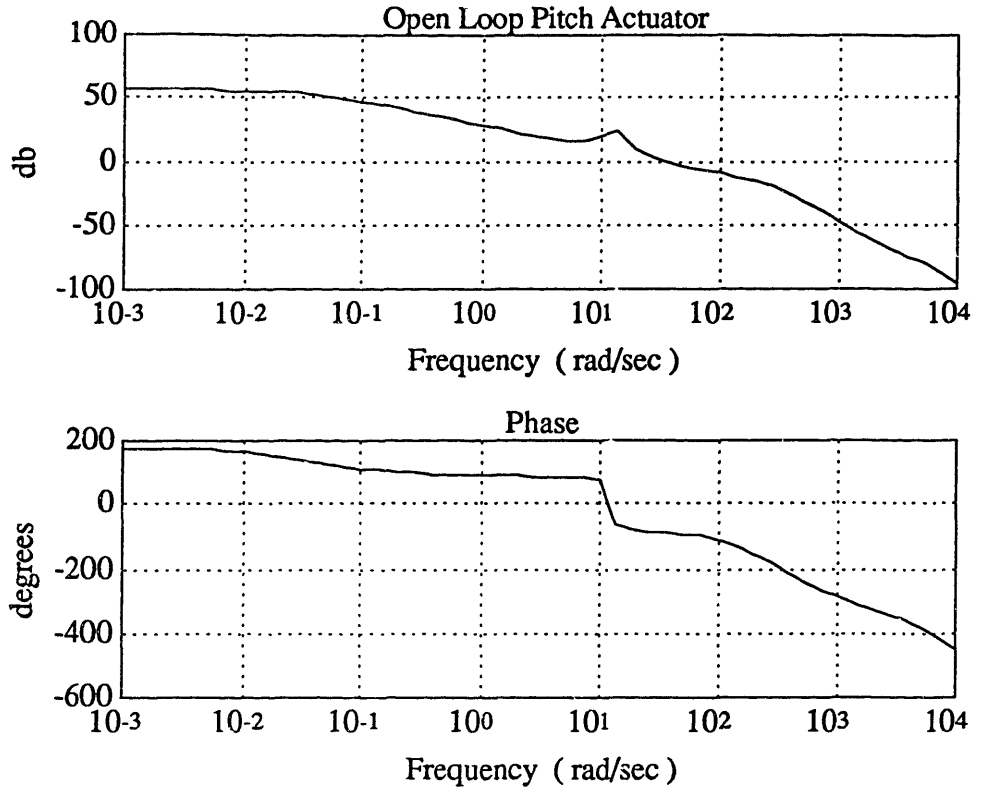

Figure 4.61 Open Loop K(s)G(s) (Design IVa)

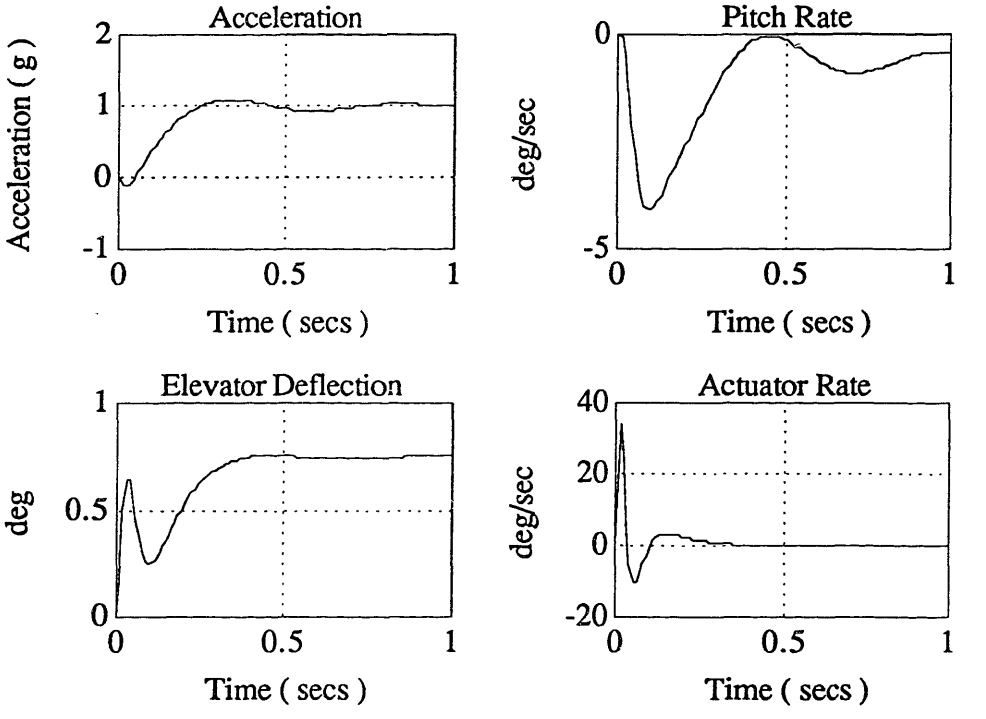

Figure 4.62 Acceleration Step Response (Design IVa)

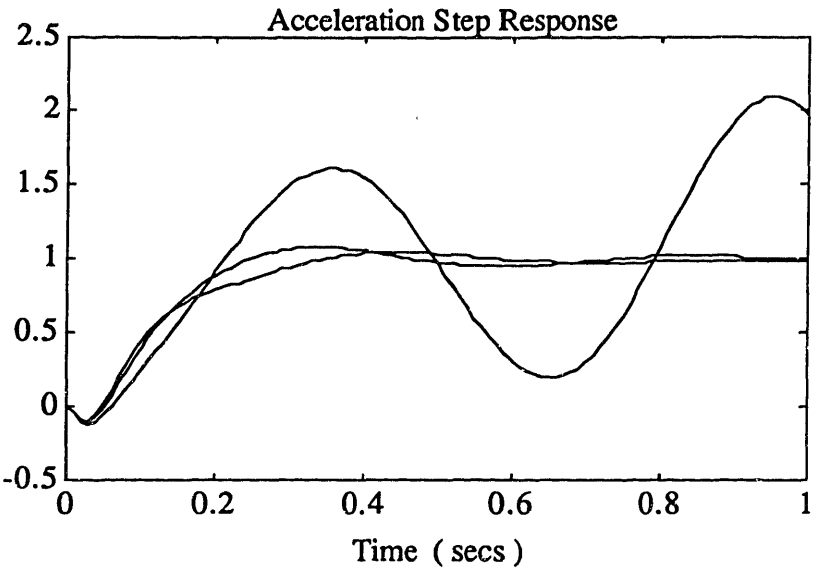

Figure 4.63 Step Variation with Angle of Attack (Design IVa)

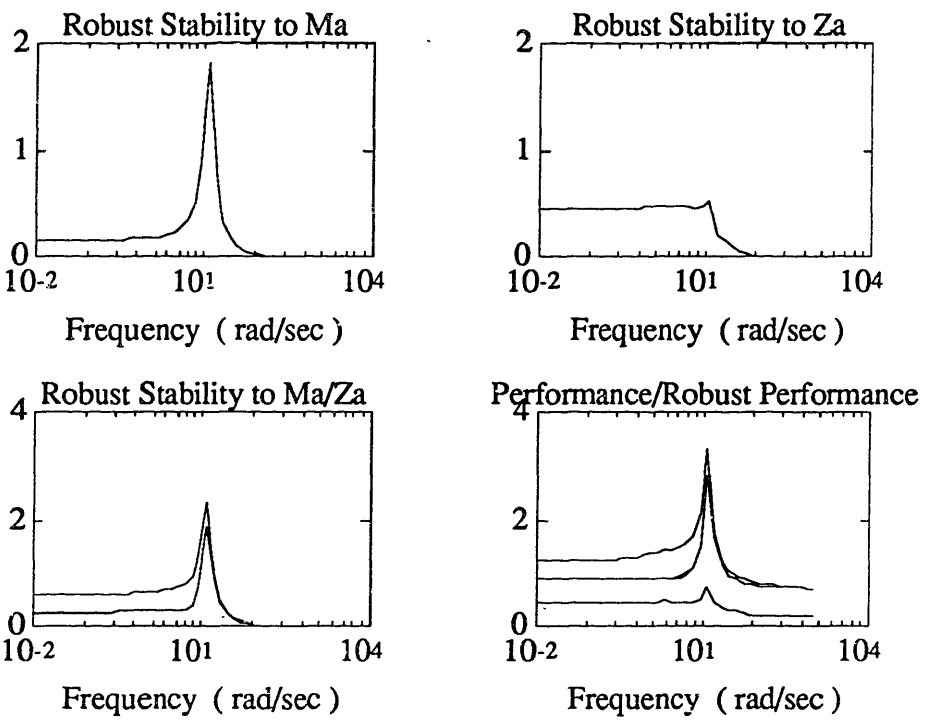

Figure 4.64 Robustness Analysis (Design IVa)

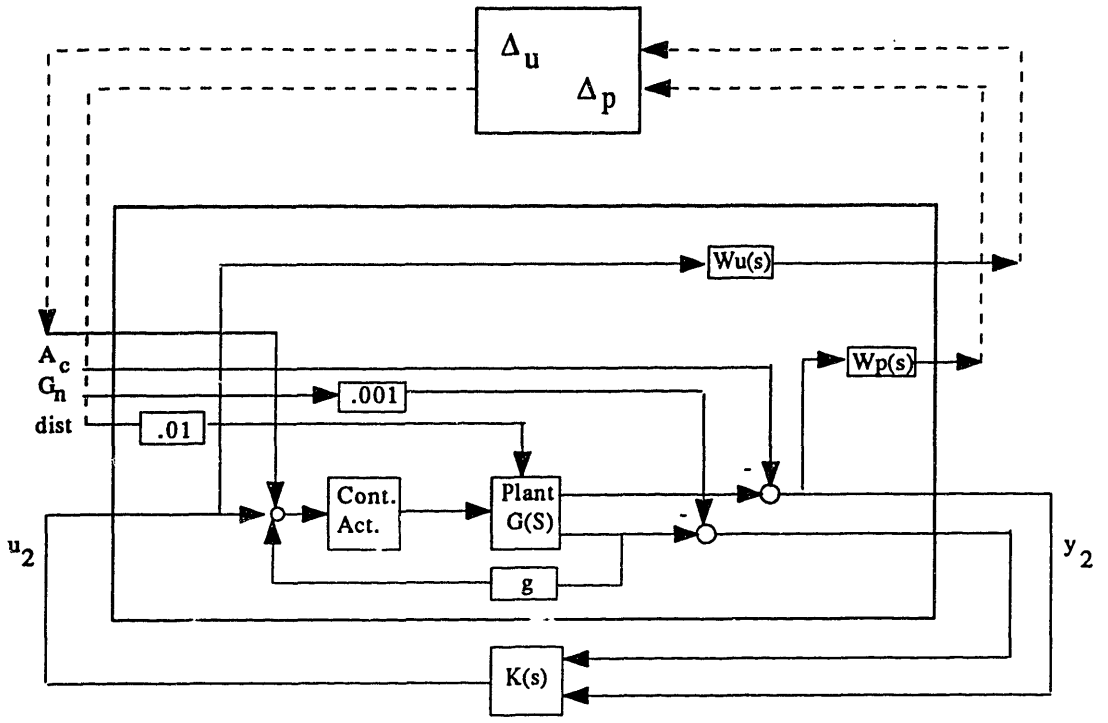

Figure 4.65 H_∞ Inner Loop Design IVb

Figure 4.65 shows the block diagram structure for the second H_∞ inner loop design. In this problem, an H_∞ controller is designed around a "new" plant model. The "new" plant model is simply the "old" plant with the pitch rate feedback loop closed around it. The performance specifications and stability robustness requirements are applied to this new plant directly.

Using this architecture, the minimum γ achievable utilizing normal H_∞ techniques was .8340. This value of γ satisfied the necessary performance and robustness requirements. Despite the fact that the robust performance requirement was satisfied, the optimal scaling procedure was used to see what improvements in performance could be achieved. Figure 4.66 shows a plot of the maximum and structured singular values for three D-K iterations.

The D-scale used in the synthesis procedure was approximated using a 3rd order stable transfer function. The values for each successive γ and maximum μ for each iteration are listed in Table 4.6.

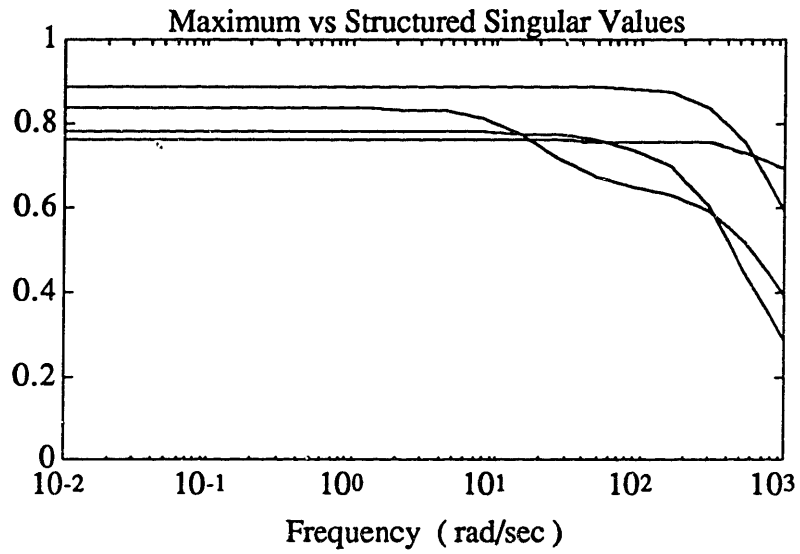

Figure 4.66 Maximum vs. Structured Singular Value (Design IVb)

Iteration	γ	μ
1	.8876	.8360
2	.7780	.7778
3	.7606	.7604

Table 4.6 D-K Iteration (Design IVb)

The use of dynamic scales improved the performance of the system by 9.04% with an increase of six new states in the controller. With the addition of the six new states, the final controller has thirteen states. The singular value plot of the controller is shown in Figure 4.67. According to Figure 4.67, the valley which was present in the first H_∞ design is no longer present in this H_∞ inner loop design. This indicates that no pole zero cancellation of the lightly damped mode is occurring. This can also be evidenced by the location of the poles and zeros of the compensator in Appendix E.

Figure 4.68 through 4.70 show the singular value plots for the complementary sensitivity, the sensitivity, and the open loop pitch actuator branch respectively. As Figure 4.70 shows, the open loop pitch actuator branch has the required -20 db attenuation and two pole roll off. According to Figure 4.70, the crossover frequency is 31.81 rad/sec. There is 148.88° of phase margin at the crossover point. The system has upward gain margin of 24.3 and a lower gain margin of .0011. Just as in the previous designs, these margins are excellent for robustness to unmodelled gain and phase characteristics.

Figure 4.71 shows the step response of the H_∞ inner loop design. The missile achieves a 1g acceleration in approximately .3 sec, with a maximum deflection rate of about 38 deg/sec. The addition of the inner loop feedback has resulted in a system with better transient response since the rate loop added damping to the system. This increase in damping is offset by the fact that the actuator rate is slightly larger than desired magnitudes. Except for the slightly larger control rates, the step response of the closed loop system meets all time domain performance specifications.

Figure 4.72 plots the step response of the closed loop system for variations in angle of attack. The closed loop system responds extremely well for 10° and 20° angle of attack. The instability of the closed loop system at low angles of attack has been eliminated; although there is a slight degradation in performance. This degradation can be seen as a small overshoot in the step response of the system. The inclusion of the inner loop pitch rate feedback has eliminated the inversion problem experienced in normal H_∞ problem formulations. The variation of the lightly damped poles has less of a destabilizing effect on the system as verified by the root locus of Figure 4.73.

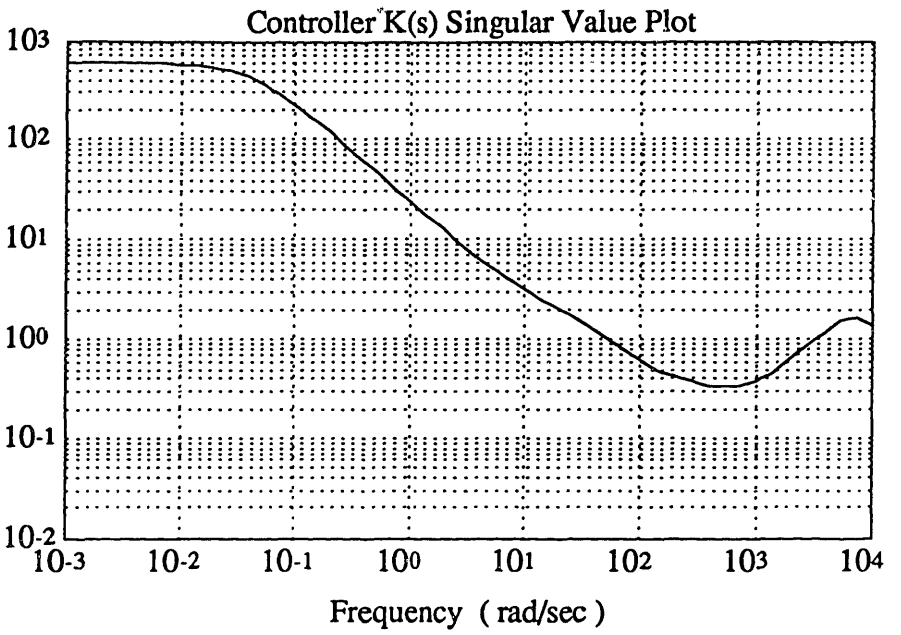

Figure 4.67 Maximum Singular Value of K(s) (Design IV)

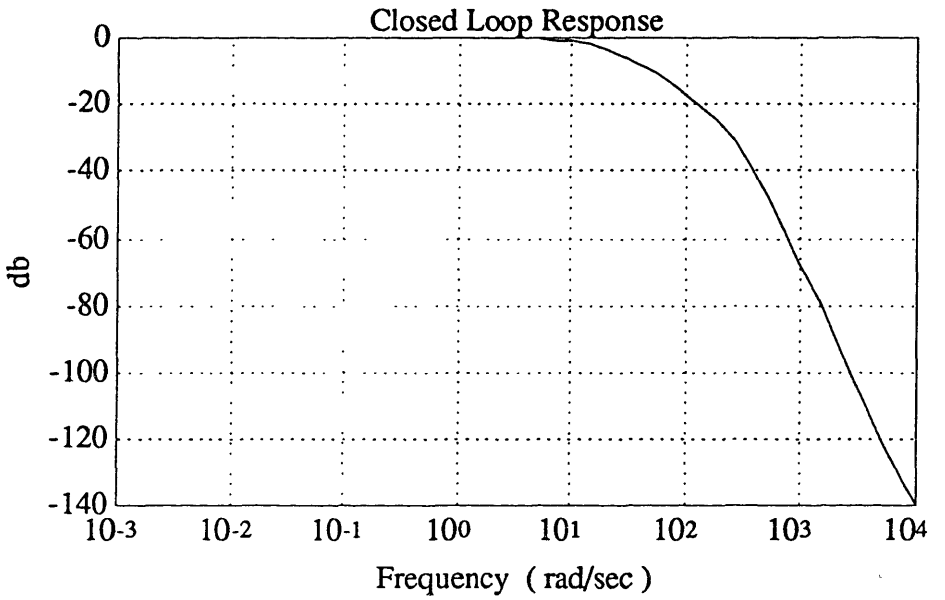

Figure 4.68 Complementary Sensitivity (Design IVb)

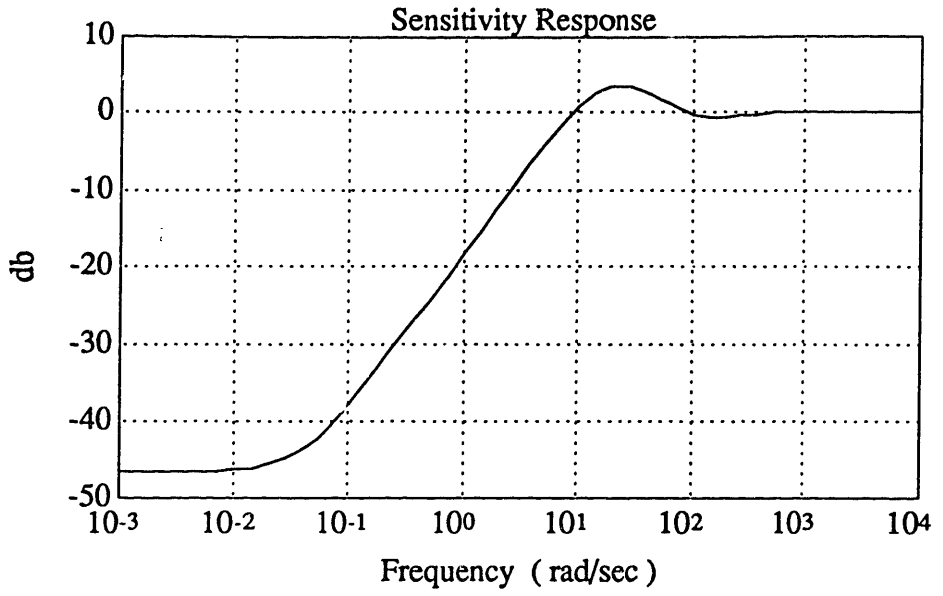

Figure 4.69 Sensitivity (Design IVb)

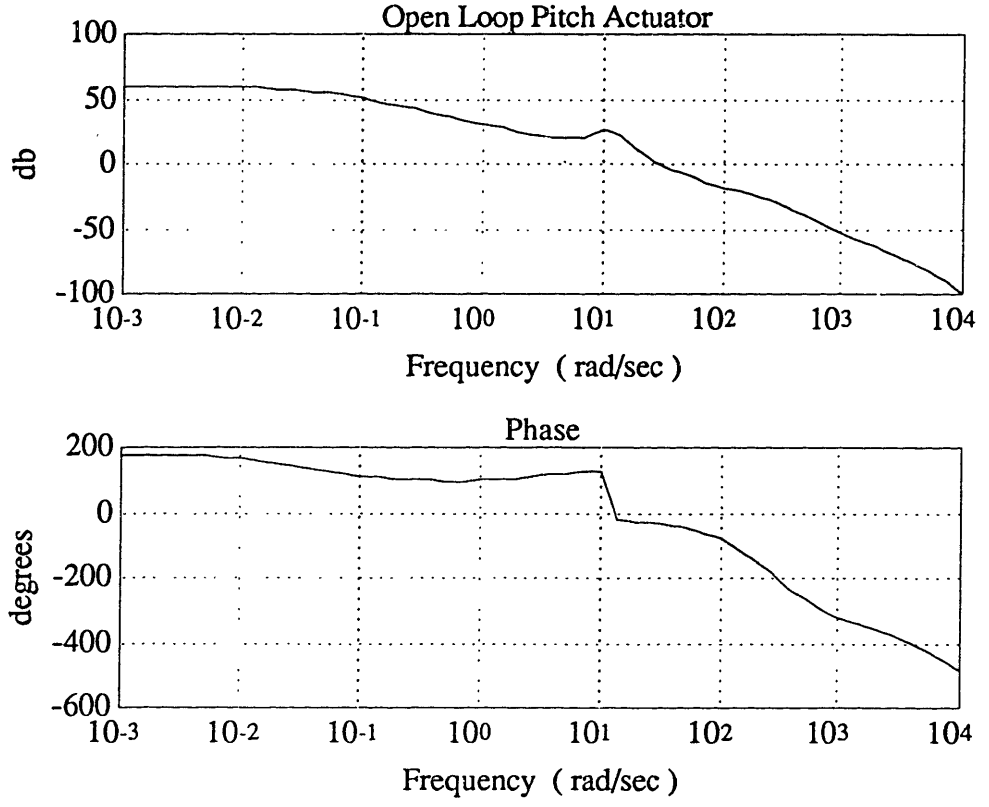

Figure 4.70 Open Loop K(s)G(s) (Design IVb)

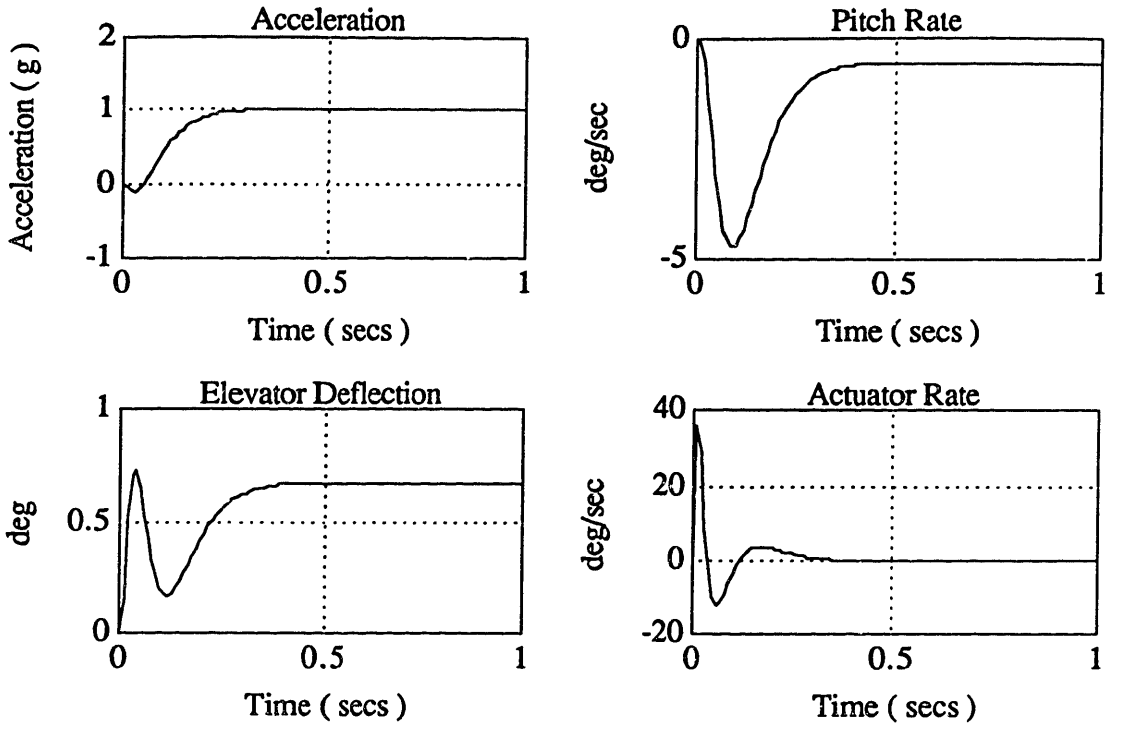

Figure 4.71 Acceleration Step Response (Design IV)

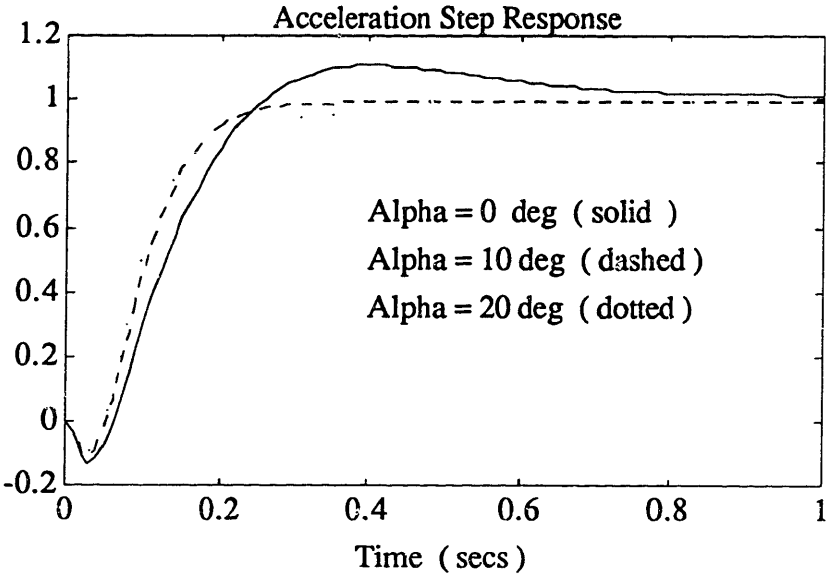

Figure 4.72 Step Variation with Angle of Attack (Design IV)

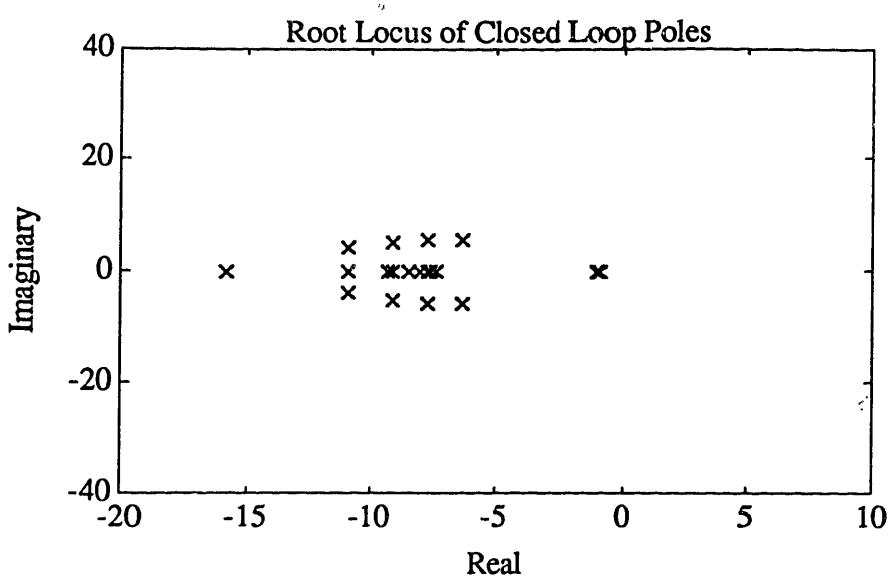

Figure 4.73 Variation of Poles with Angle of Attack (Design IV)

Figure 4.74 shows the robustness analysis of the H_∞ inner loop design. The first plot shows the stability robustness of the closed loop system to variations in M_α. This design procedure has produced the best results in terms of robustness to variations in M_α. The system will remain stable to approximately 4.54 times the total variation of M_α, or 563% variation in M_α. These results are quite substantial. The addition of the inner rate loop has done an exceptional job of reducing the sensitivity of the closed loop systems to variations of M_α.

The robustness to variations in Z_α are similar to subsequent results. The system can handle a 200% change in the total variation of Z_α or 80% variation in Z_α.

As expected, the robustness to simultaneous variations of M_α and Z_α have also improved substantially. The system is stable for up to a 1.5 times the total variation of M_α and Z_α simultaneously.

The final plots shows the measure of performance and robust performance for the H_∞ inner loop design. The nominal performance of the system satisfies the performance requirements, but like design III, the robust performance degrades substantially at high frequencies. The cause of the degradation in performance is almost identical to design III. The unstructured uncertainty and performance criterion violate the small gain theorem for high frequencies.

It should be commented that this violation is the result of the fact that the inner rate loop was not included in the uncertainty weight during the H_∞ synthesis process. The inclusion of the inner rate loop in the uncertainty weight produced the results of design IVa. The test of stability here, however, places the uncertainty directly at the actuator input.

Like the third design, it is uncertain as to whether or not this degradation in performance at high frequencies is an important problem. The system is nominally stable to the unstructured uncertainty as represented by Figure 4.70 where it was shown that the system had the required -20 db attenuation and two pole roll off, and the robust performance is satisfied over the tracking bandwidth of the system.

Like design III, the H_∞ inner loop design has excellent robust performance when one considers the variations of M_α and Z_α alone - without the inclusion of the unmodelled dynamic weight. The plot of robust performance to parameter variations can be seen in Figure 4.75.

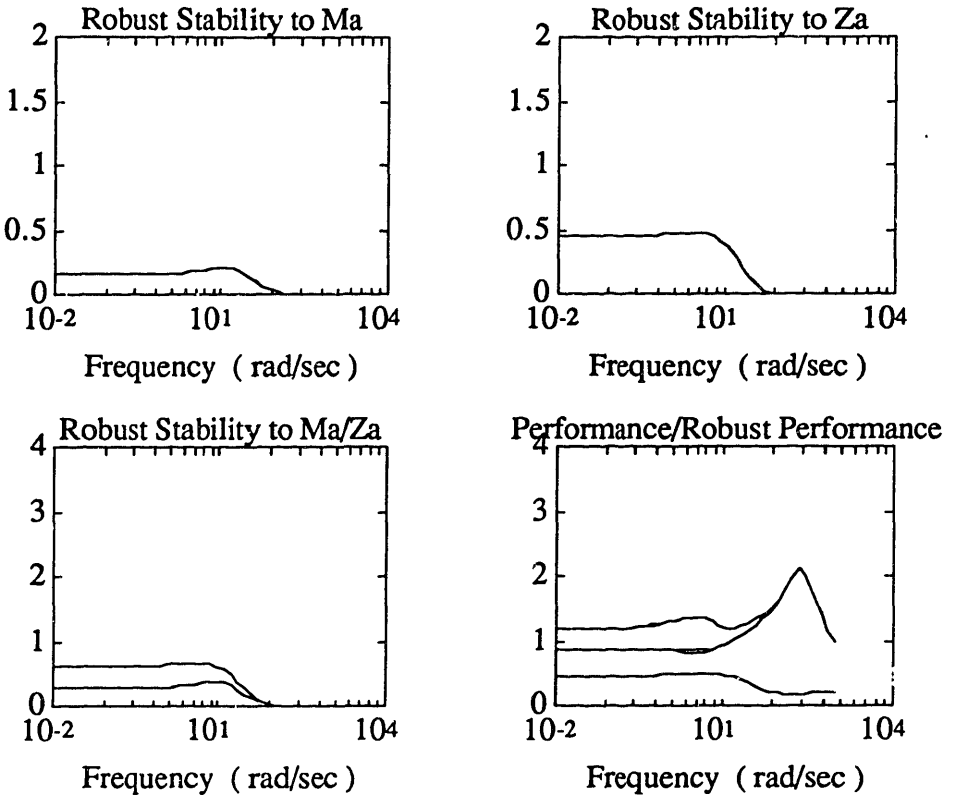

Figure 4.74 Robustness Analysis (Design IV)

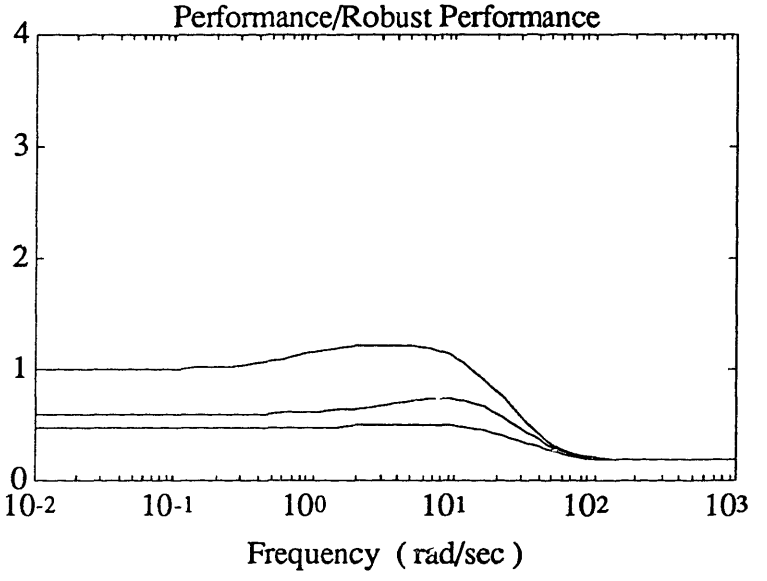

Figure 4.75 Robust Performance M_α/Z_α (Design IV)

4.3.5 Discussion

A comparison of the four design examples should provide some interesting results about the robust stability/performance of H_∞ designs in the presence of parametric variations. In analyzing the structure of the compensator for the nominal H_∞ design (I) it is obvious that the H_∞ methodology is inverting the dynamics of the open loop plant. Since the lightly damped poles of the open loop vary substantially with changes in angle of attack (Figure 3.3), the pole/zero cancellation of the first design becomes ineffective; in fact, for small angles of attack, the closed loop system becomes unstable.

The addition of parametric uncertainty into the design process has effectively eliminated the pole/zero cancellation problem. Examination of the maximum singular value plot for the compensator, K(s), (Figure 4.30) verifies the absence of the lightly damped mode. Although the stability of the system to variations in M_α has been substantially improved, the system does not have the desired robust performance capabilities.

The H_∞ inner loop design (IVb) provided even more interesting results. The addition of the inner rate loop to the controller architecture provided a closed loop system which exhibited outstanding robustness to parametric variations. The inner rate loop has effectively eliminated the system's sensitivity to variations in M_α. This is not a surprising fact when one considers what the inner rate loop does to the design plant. By feeding back the proportional rate, the inner rate loop increases the damping of the system thereby producing a "new" plant model which is significantly less sensitivity to parameter variations. This make the job of the H_∞ controller easier.

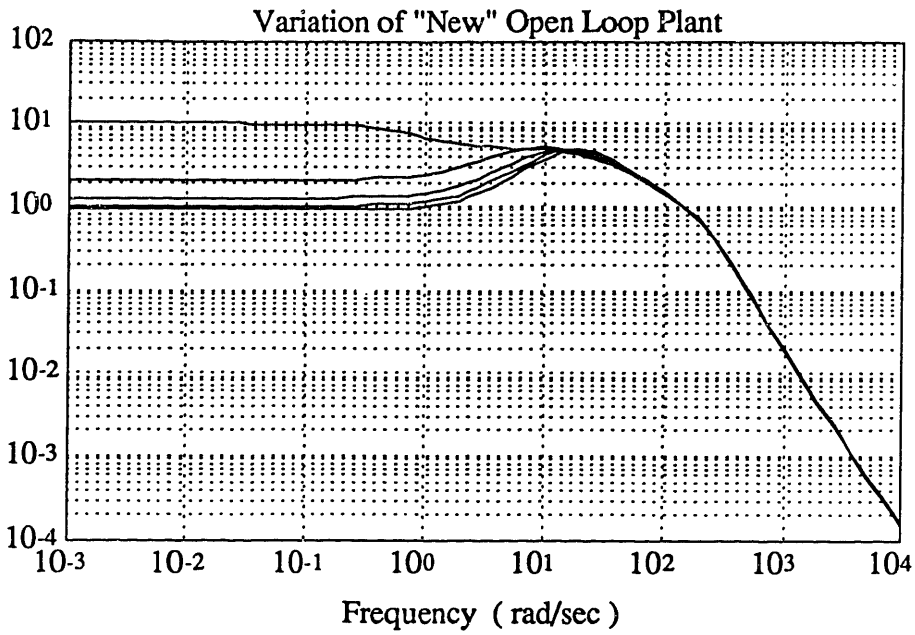

Figure 4.76 Variation of "New Plant"

Figure 4.76 shows the variation of the frequency response for the "new plant" as angle of attack varies from 0° to 20°. According to the figure, the variation of the new plant's poles are substantially less than the actual design plant model. Because the new plant model is less sensitive to parameter variations, the pole/zero cancellation of the resulting H_∞ controller is more effective.

The control signal generated by the nominal H_∞ controller of design I is developed using a state feedback matrix in combination with a state estimator. In thinking about the estimation problem, when the open loop poles of the plant vary significantly, it is difficult to provide an accurate estimation of the plant's dynamics. When the plant is provided with direct feedback of the rate loop, the estimation problem becomes considerably easier since the rate loop eliminates much of the plant's variation. Therefore, the direct feedback of the rate loop would probably work equally as well for a variety of design problems.

There is a fundamental difference between the H_∞ design with parameter variation and the H_∞ inner rate loop design. In the first case, the H_∞ algorithm develops a controller that acknowledges the potential variation of the plant poles and optimally places the poles and zeros of the controller to account for this potential variation. This optimization takes into account all the disturbance rejection and stability robustness requirements placed on the "old" plant model. In the second case, the inner loop is used to reduce the variation of the plant poles. The H_∞ controller is developed for the "new" plant, so the pole zero cancellation becomes more effective. The algorithm does not find the optimal solution taking into account the disturbance rejection and stability robustness requirements of the "old" plant; to do so would produce the results of design IVa.

It is important to intuitively try to understand what is being done to to the controller architecture in order to provide the better robustness properties. One of the leading indicators of robustness to parametric variations as well as rejection of external disturbances is the sensitivity plot of the closed loop system. Since the parameter variation is most predominant in the inner loop, it would be interesting to see what the inner loop sensitivity is for each design. The sensitivity function for the inner loop is defined as the transfer function from the gyro measurement to pitch rate output with the acceleration loop broken.

It is a widely known fact that increasing the loop gain reduces the closed loop sensitivity to plant parameter uncertainty [29]. Therefore, it is desired to have small sensitivities wherever there is significant parameter uncertainty. This desire, of course, is constrained by the fact that the complementary sensitivity must be small in regions where there exist significant high frequency unmodelled dynamics and noisy

measurements. As stated earlier, this is the fundamental tradeoff between performance and stability robustness.

This particular problem is an inherently difficult one since the location of the lightly damped poles is right around the required crossover frequency of the closed loop system. Because of this, it is difficult to achieve small sensitivities at and around the frequency of the lightly damped poles.

Upon examination of the inner loop sensitivity function (see Figure 4.77), the results of the parameter robustness become more obvious. The nominal H_∞ controller of Design I has the largest sensitivity at the location of the lightly damped poles. The nominal design has a slight valley near the frequency of the short period mode. This valley provides a small increase in the sensitivity near the critical region.

The addition of uncertainty in M_α in the second design has resulted in an increase in the width and depth of this valley as shown by Figure 4.77. This decrease in the sensitivity around the critical frequencies results in the improvement of the robust stability of the closed loop system to parameter variations as demonstrated by figure 4.37. The decrease in sensitivity around the critical frequency is important because it allows the frequency of the lightly damped mode to vary, yet still remain in a region that has some small sensitivities.

The improvements in the stability of the closed loop systems of Designs III and IVb may be manifested by the substantial increase in the depth and width of the valley of the sensitivity plot as indicated in Figure 4.77. This decrease in sensitivity is what produced the complete desensitization of the system to variations in M_α. It is interesting to note that while the sensitivity of the classical design in significantly smaller at low frequencies, the H_∞ inner loop design actually has greater robustness to

variations in M_α. This result seems to indicate that for this problem, the inner rate loop integrator may not have been necessary.

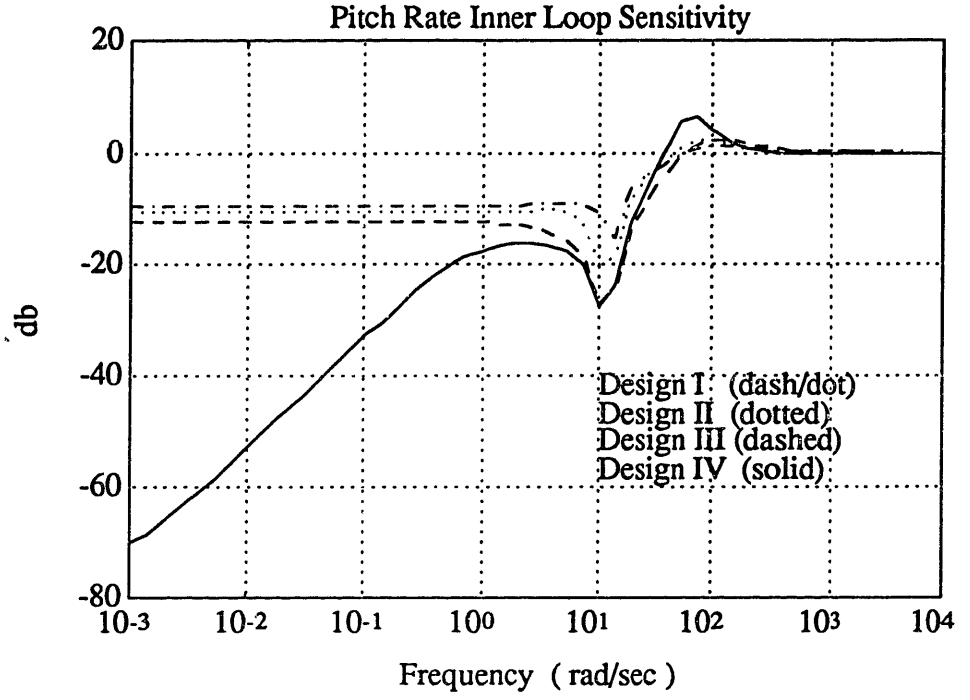

Figure 4.77 Inner Loop Sensitivities

The final question that remains unanswered is which design, II or IVb, provides the best robust performance for the given problem. This is a difficult comparison since the two designs have different strengths and weaknesses. The H_∞ design with modelled parametric variation has excellent performance and robust performance in the presence of the unstructured multiplicative input error, but only marginal robust performance to presence of parametric variations. The H_∞ inner loop design, on the other hand, has poor robust performance in the presence of the multiplicative error but excellent robustness to the parametric variations.

In trying to answer this question, the role and importance of the multiplicative input model must be addressed. The procedure of Design II was such that the satisfaction of

robustness to unstructured uncertainty was more important than the requirement for robust stability/performance in the presence of parameter variations. The resulting controller was therefore limited by the constraints of the uncertainty model. The development of the H_∞ inner loop was such that it ignored the robust performance constraints of the error model at certain frequencies. If the error model was not conservative, and the stability robustness criterion was a necessary and sufficient condition for stability, then there would be no doubt that Design II was the better design. If, however, the error model was conservative, then there may be a strong argument for the H_∞ inner loop. The H_∞ inner loop satisfies the nominal requirement for robust stability, — it does not satisfy the requirement placed on the robust performance of the closed loop to variations modelled by the input uncertainty error. Even then, the violation of robust performance occurs at frequencies well above the tracking bandwidth of the system where the importance of the performance weight is not significant.

The above results may lead one to believe that perhaps the H_∞ inner loop provides the best robust performance. It is difficult to say since the H_∞ inner loop explicitly ignored requirements that the $H_\infty/M\alpha$ design tried to satisfy; the robust stability in the presence of unmodelled dynamics. Figure 4.78 may actually shed some light on this difficult comparison. The H_∞ inner loop controller amplifies high frequency signals much more than that of the $H_\infty/M\alpha$ controller. It is this high frequency response that is responsible for the improved robustness to parametric variations. By satisfying the robust performance constraints of the unstructured uncertainty model, the second design formulation produced a controller with a slightly smaller bandwidth. It is the increase in bandwidth that is responsible for the improvement is parameter robustness.

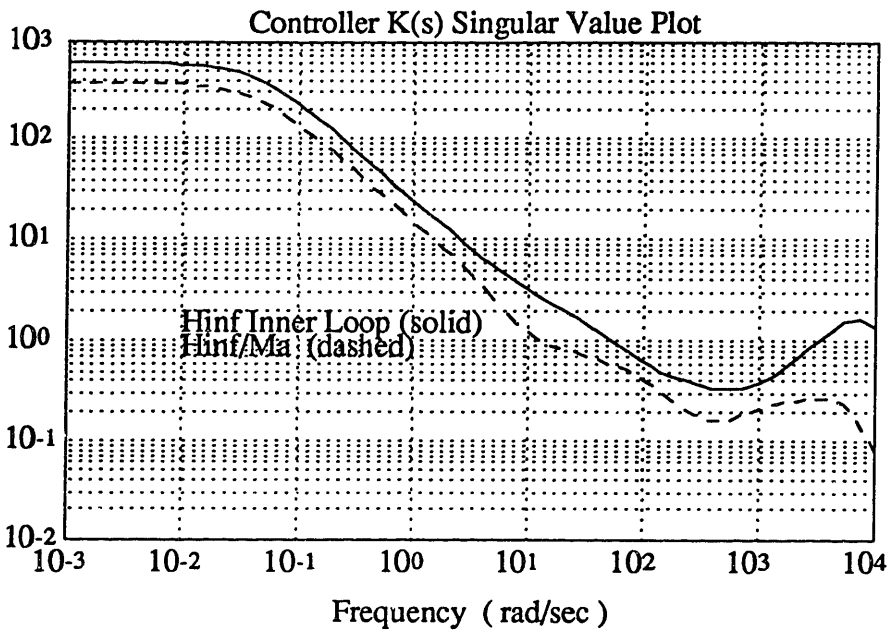

Figure 4.78 Comparison of K(s) for Designs II and IV

It seems that the fairest conclusion that can be made is that while the H_∞ inner loop design provides excellent robustness to parametric variations with no significant increase in the order of the compensator, the H_∞ μ– synthesis procedure provides the best framework for the simultaneous satisfaction of multiple uncertainty requirements. This procedure, however, results in an increase in the number of states in the compensator.

Chapter Five:

Conclusion

As the previous examples have shown, the application of the structured singular value (μ) to the analysis of linear systems with block diagonal perturbation structures results in stability margins that are less conservative than those obtained by strictly applying the $\|\bullet\|_\infty$ norm. The degree to which conservatism can be reduced is a function of how poorly the original problem is scaled.

When the H_∞ problem is formulated with input/output sets that are unrelated, the relative scaling difference between sets may result in a solution that is also conservative. By applying the optimal scaling technique used in the evaluation of the structured singular value, the conservatism of the H_∞ problem is reduced. This reduction in conservatism is approached in a stepwise manner by iterating on the solution of the optimal H_∞ controller and the optimal dynamic scaling. This is the celebrated D-K iteration.

Although the optimal scaling procedure produced results which increased the order of the compensator, the benefits of utilizing the structured information compensated for

the increase in state order. In one case, the μ-synthesis procedure increased the performance measure by 54% while only increasing the order of the compensator by six states. In certain cases it was essential to apply the scaling procedure, while in others, no significant improvement could be realized.

One example was produced where the optimal D-scale inverted the uncertainty weight. This effectively moved the uncertainty weight from the input to the output of the system. It was shown that when this rearrangement of the uncertainty weight ocurred, the problem could be better formulated if the designer changed the location of the uncertainty weight in the original problem formulation. Such a restructuring may result in similar improvements in performance as those realized using μ-Synthesis techniques without the excessive increases in state order.

The development of a control system robust to variations in angle of attack proved to be a difficult problem. Conflicting requirements between sensitivity optimization and stability robustness impeded the synthesis of controllers which exhibited robust performance in the presence of structured and unstructured uncertainties. The minimization of the sensitivity function around the frequencies of the lightly damped poles of the open loop appeared to be a salient feature of controllers robust to parametric variations which affect the location of the lightly damped pole pair.

The H_∞ optimization with modelled parametric uncertainty provided the best framework for the simultaneous satisfaction of multiple uncertainty and performance objectives. In the case where it was desired to provide robust performance in the presence of structured and unstructured uncertainties, the design was iterated on the magnitude of the expected parameter variation until a value of $\mu \approx 1$ was achieved. This iterative technique provided the largest allowable parameter variation capable of satisfying robust performance constraints on the nominal plant.

The H_∞ inner loop demonstrated the best robustness to parameter variations, but exhibited poor robust performance in the presence of unmodelled dynamics. This result was due to the fact that the uncertainty was not specified inside the pitch rate feedback loop. When the problem was formulated as such, the solution was similar to the nominal H_∞ mixed sensitivity formulation of Design I.

The extension of μ-analysis to the synthesis of robust control systems is one in many steps towards mechanizing the development of complex control systems. Although the benefits of utilizing such a technique are great, overly conservative and/or unnecessarily high order systems may result if the method is applied blindly. As always, the best control systems are developed when the control engineer makes use of all his/her resources and applies them intelligently to the problem at hand.

5.1 Directions For Future Research

The H_∞/μ-Synthesis theory proved to be an excellent tool for simultaneously satisfying multiple uncertainty requirements. By explicitly modelling parameter uncertainties, H_∞ controllers that are robust to structured parametric variations were synthesized. It should be possible, however, to obtain the results of the robust design by formulating the H_∞ problem with performance specifications on both the inner and outer loops, rather than by modelling parameter uncertainties. At present, most H_∞ designs place performance specifications only on the outer loops.

By explicitly formulating an inner loop performance requirement, robustness to parameter uncertainty may be achieved without directly modelling parameter uncertainty. This particular problem is important because it is in the formulation of additional performance requirements that controllers with more sophisticated

architectures are developed. For example, if it was necessary to have an integrator in the inner loop, as was done in the classical design, the modelling of parametric variations will not produce the additional architecture necessary for providing the integrator. Therefore, utilizing parameter uncertainty as the only method for achieving robustness may produce controllers with limited capabilities.

Appendix A: Aerodynamic Data

The Table below is a listing of the variations of the stability derivatives used in this design example. These values are based on the following parameters:

Altitude	6 kilometers
Velocity (V)	947.7 m/s
Mach (M)	3
Speed of Sound	315.9 m/s
Density (ρ)	.6601 kg/m^3
S_{ref}	.040876 m^2
d_{ref}	.2286 m
Mass (m)	203.968 Kg
Moment of Inertia (I_{yy})	247.36 Kg-m^2

Alpha	Z_α	$Z_{\dot{\alpha}}$	M_α	$M_{\dot{\alpha}}$
0	-577.27	-115.05	+32.721	-132.04
2	-701.24	-114.98	-15.784	-132.04
4	-815.67	-114.77	-60.975	-132.04
6	-920.19	-114.42	-102.85	-132.04
8	-1014.5	-113.93	-141.41	-132.04
10	-1098.3	-113.30	-176.66	-132.04
12	-1171.4	-112.53	-208.60	-132.04
14	-1233.8	-111.63	-237.21	-132.04
16	-1285.4	-110.59	-262.52	-132.04
18	-1326.1	-109.41	-284.51	-132.04
20	-1356.1	-108.11	-303.19	-132.04
mean values	-1045.5	-112.61	-160.09	-132.04
% variation	+45%	-2%	+120%	0%
	-30%	+4%	-89.0%	0%
center values	-966.685	-111.58	-135.23	-132.04
% variation	40%	3%	124%	0%

Appendix B: Design I Data

Ac=

Columns 1 through 6

5.7942e+05	1.6875e+05	2.9341e+04	-2.6668e+06	2.6226e+06	-9.1104e+05
1.5006e+05	4.3703e+04	7.6090e+03	-6.9070e+05	6.7925e+05	-2.3596e+05
6.2152e+05	1.8100e+05	3.1247e+04	-2.8606e+06	2.8132e+06	-9.7726e+05
1.2574e+05	3.6619e+04	6.3706e+03	-5.7526e+05	5.6562e+05	-1.9771e+05
-2.1574e+04	-6.2826e+03	-1.0930e+03	1.0281e+05	-1.0121e+05	3.3916e+04
1.0335e+01	3.0098e+00	5.2362e-01	-4.8140e+01	4.0058e+01	-7.5163e+03
-5.3485e+01	-1.5576e+01	-2.7098e+00	2.4912e+02	-2.0728e+02	3.8914e+04
7.7832e+00	2.2666e+00	3.9433e-01	-3.6250e+01	3.0112e+01	-5.7021e+03
-5.6810e+01	-1.6544e+01	-2.8782e+00	2.6457e+02	-2.1959e+02	4.1775e+04
2.3800e+01	6.9310e+00	1.2058e+00	-1.1078e+02	9.0933e+01	-1.8312e+04
1.9477e-08	5.6591e-09	1.0107e-09	-1.2300e+00	2.2259e+01	1.6955e+04
5.0215e-09	1.4590e-09	2.6057e-10	-3.1760e-01	5.7474e+00	4.3779e+03
1.9375e-08	5.6296e-09	1.0054e-09	-1.2210e+00	2.2095e+01	1.6830e+04

Columns 7 through 12

7.3368e+04	8.8380e+04	1.3382e+03	-4.9271e+02	-4.5731e+05	-1.8205e+05
1.9002e+04	2.2890e+04	3.4658e+02	-1.2761e+02	-1.1844e+05	-4.7152e+04
7.8700e+04	9.4803e+04	1.4354e+03	-5.2852e+02	-4.9054e+05	-1.9528e+05
1.5935e+04	1.9180e+04	2.7634e+02	-1.1113e+02	-9.9243e+04	-3.9508e+04
-2.2794e+03	-3.2885e+03	-5.3408e+02	-1.2666e+02	1.7027e+04	6.7783e+03
6.7397e+05	3.1252e+03	-7.2096e+05	-2.1590e+05	2.9742e+02	-8.2393e+01
-3.4893e+06	-1.6178e+04	3.7326e+06	1.1177e+06	-1.5415e+03	4.2698e+02
5.1132e+05	2.3689e+03	-5.4695e+05	-1.6378e+05	2.3265e+02	-6.4293e+01
-3.7461e+06	-1.7354e+04	4.0071e+06	1.1998e+06	-1.7153e+03	4.7373e+02
1.6422e+06	7.6074e+03	-1.7565e+06	-5.2625e+05	9.0815e+02	-2.4756e+02
-1.5237e+06	-7.0553e+03	1.6299e+06	4.8807e+05	-7.0369e+02	1.9370e+02
-3.9342e+05	-1.8217e+03	4.2085e+05	1.2602e+05	-1.9370e+02	4.6048e+01
-1.5125e+06	-7.0033e+03	1.6179e+06	4.8448e+05	-7.6206e+02	1.8765e+02

Column 13

-1.9847e+04
-5.1404e+03
-2.1290e+04
-4.3071e+03
7.3918e+02
3.2744e+02
-1.6969e+03
2.5588e+02
-1.8861e+03
9.9349e+02
-7.6206e+02
-1.8765e+02
-1.0433e+03

Appendix B: Design I Data

Bc =

```
-5.1229e-13 -3.8763e-08
-1.2859e-13 -1.0046e-08
-5.5228e-13 -4.1047e-08
 1.7982e-04  8.5701e+00
 6.1941e-03  2.9522e+02
-2.2731e+00  4.3953e+05
-5.0526e+01 -2.2755e+06
 6.5437e+00  3.3344e+05
-5.4709e+01 -2.4430e+06
 2.5412e+01  1.0710e+06
-2.2045e+01 -9.9365e+05
-5.6982e+00 -2.5657e+05
-2.2410e+01 -9.8635e+05
```

Cc =

Columns 1 through 6

```
 6.3472e-01  1.8484e-01  3.2157e-02 -2.8177e+00  2.8906e+00 -9.9798e-01
```

Columns 7 through 12

```
 8.0372e-02  9.6813e-02  1.4659e-03 -5.3973e-04 -5.0095e-01 -1.9943e-01
```

Column 13

```
-2.1741e-02
```

Dc =

```
 0     0
```

Poles of the Compensator

real	imaginary	frequency	damping
-4.0000e-02	0.0000e+00	4.0000e-02	1.0000e+00
-9.5913e-01	0.0000e+00	9.5913e-01	1.0000e+00
-1.1572e+01	0.0000e+00	1.1572e+01	1.0000e+00
-3.5192e+00	-1.3382e+01	1.3837e+01	2.5432e-01
-3.5192e+00	1.3382e+01	1.3837e+01	2.5432e-01
-7.8313e+01	0.0000e+00	7.8313e+01	1.0000e+00
-9.9503e+01	0.0000e+00	9.9503e+01	1.0000e+00
-2.4275e+02	0.0000e+00	2.4275e+02	1.0000e+00
-1.6111e+03	0.0000e+00	1.6111e+03	1.0000e+00
-3.7652e+03	-6.4243e+03	7.4464e+03	5.0565e-01
-3.7652e+03	6.4243e+03	7.4464e+03	5.0565e-01
-7.5323e+03	0.0000e+00	7.5323e+03	1.0000e+00
-2.0328e+04	0.0000e+00	2.0328e+04	1.0000e+00

Appendix B: Design I Data

Zeroes of the Compensator

real	imaginary	frequency	damping
-3.5192e+00	-1.3382e+01	1.3837e+01	2.5432e-01
-3.5192e+00	1.3382e+01	1.3837e+01	2.5432e-01
-2.4275e+02	-9.0436e-14	2.4275e+02	1.0000e+00

Poles of the Closed Loop System

real	imaginary	frequency	damping
-9.4544e-01	0.0000e+00	9.4544e-01	1.0000e+00
-5.3813e+00	-1.1363e+01	1.2573e+01	4.2801e-01
-5.3813e+00	1.1363e+01	1.2573e+01	4.2801e-01
-3.5191e+00	-1.3382e+01	1.3837e+01	2.5432e-01
-3.5191e+00	1.3382e+01	1.3837e+01	2.5432e-01
-1.7714e+01	-1.4292e+01	2.2761e+01	7.7828e-01
-1.7714e+01	1.4292e+01	2.2761e+01	7.7828e-01
-7.2135e+01	-1.6279e+01	7.3949e+01	9.7547e-01
-7.2135e+01	1.6279e+01	7.3949e+01	9.7547e-01
-2.4275e+02	0.0000e+00	2.4275e+02	1.0000e+00
-2.0013e+02	-1.9996e+02	2.8291e+02	7.0741e-01
-2.0013e+02	1.9996e+02	2.8291e+02	7.0741e-01
-1.6110e+03	0.0000e+00	1.6110e+03	1.0000e+00
-3.7654e+03	-6.4242e+03	7.4463e+03	5.0567e-01
-3.7654e+03	6.4242e+03	7.4463e+03	5.0567e-01
-7.5324e+03	0.0000e+00	7.5324e+03	1.0000e+00
-2.0327e+04	0.0000e+00	2.0327e+04	1.0000e+00

Appendix C: Design II Data

Ac =

Columns 1 through 6

-2.5771e+02 9.1962e+02 1.7514e+00 2.1591e-12 1.6127e-13 -4.3442e-14
-9.1957e+02 -4.8925e+02 -3.5432e+00 -9.7250e-13 -7.2636e-14 1.9567e-14
1.7884e+00 3.5081e+00 -1.3382e+00 2.4943e-13 1.8630e-14 -5.0185e-15
1.2381e+01 -2.4513e+00 -1.4772e+02 5.5647e+03 4.8787e+02 3.2235e+02
1.2100e+00 -2.3957e-01 -1.4436e+01 5.3784e+02 4.6436e+01 1.4686e+01
-1.3593e+01 2.6912e+00 1.6217e+02 -6.0892e+03 -5.1420e+02 -5.9470e+02
2.3551e+00 -4.6628e-01 -2.8098e+01 1.0627e+03 9.1251e+01 5.2878e+01
-4.0403e-01 7.9979e-02 4.8207e+00 -1.8232e+02 -1.5656e+01 -9.0722e+00
3.4264e-02 -3.2207e-02 -2.8976e-03 1.0521e-01 9.0338e-03 5.2350e-03
-1.3880e-01 1.3053e-01 1.0783e-02 -3.9004e-01 -3.3492e-02 -1.9408e-02
1.3563e-02 -1.2273e-02 -8.7502e-03 3.2928e-01 2.8275e-02 1.6385e-02
-9.8959e-02 9.2725e-02 1.3050e-02 -4.8093e-01 -4.1297e-02 -2.3931e-02
-1.9140e-02 1.8422e-02 -5.2535e-03 2.0121e-01 1.7278e-02 1.0012e-02
-1.2249e+00 1.1576e+00 4.1720e-03 -3.8176e-11 -2.8513e-12 7.6810e-13
6.0031e-01 -5.6732e-01 -2.0446e-03 3.0616e-11 2.2867e-12 -6.1598e-13
1.0543e+00 -9.9641e-01 -3.5910e-03 8.2286e-12 6.1459e-13 -1.6556e-13
-2.0205e-01 1.9095e-01 6.8816e-04 9.9478e-10 7.4299e-11 -2.0015e-11
2.9621e-01 -2.7994e-01 -1.0089e-03 1.0425e-10 7.7867e-12 -2.0976e-12
2.6621e-02 -2.5158e-02 -9.0668e-05 -1.0973e-09 -8.1960e-11 2.2079e-11

Columns 7 through 12

1.3248e-04 -2.7880e-03 -4.4175e+01 3.1470e+02 1.8564e+02 -1.6160e+02
-6.2344e-05 1.3672e-03 -3.5249e+01 1.1841e+02 2.8690e+02 9.9864e+01
-6.4764e-06 1.3929e-04 3.5950e-01 -6.7726e+00 2.8931e+00 8.5710e+00
-3.0827e+04 3.0259e+04 -1.2422e+04 1.2529e+03 9.3676e+02 1.3269e+01
-3.0127e+03 2.9572e+03 -1.2140e+03 1.2245e+02 9.1549e+01 1.2967e+00
3.3844e+04 -3.3220e+04 1.3638e+04 -1.3755e+03 -1.0284e+03 -1.4567e+01
-2.3890e+03 2.2360e+03 -2.3630e+03 2.4470e+02 1.7430e+02 -7.1110e+00
4.5257e+03 -4.5522e+03 3.9699e+02 1.9392e+02 -1.7675e+02 -3.3245e+02
-1.6423e+00 -1.7226e+00 -9.8227e+03 2.7073e+05 -1.6863e+05 -3.8206e+05
6.0863e+00 6.3899e+00 3.6420e+04 -1.0038e+06 6.2525e+05 1.4166e+06
-5.1378e+00 -5.3946e+00 -3.0748e+04 8.4748e+05 -5.2789e+05 -1.1960e+06
7.4960e+00 7.8504e+00 4.4891e+04 -1.2373e+06 7.7071e+05 1.7459e+06
-3.1447e+00 -3.1038e+00 -1.8488e+04 5.0958e+05 -3.1742e+05 -7.1891e+05
4.0410e-02 -8.6130e-01 -1.4016e+03 3.8620e+04 -2.4052e+04 -5.4503e+04
-1.2609e-02 2.6862e-01 4.3765e+02 -1.2058e+04 7.5087e+03 1.7017e+04
-4.5085e-03 9.6204e-02 1.5621e+02 -4.3035e+03 2.6798e+03 6.0726e+03
-5.8736e-01 1.2535e+01 2.0336e+04 -5.6052e+05 3.4915e+05 7.9102e+05
-6.2013e-02 1.3234e+00 2.1471e+03 -5.9180e+04 3.6863e+04 8.3516e+04
5.8303e-01 -1.2442e+01 -2.0186e+04 5.5639e+05 -3.4658e+05 -7.8520e+05

Appendix C: Design II Data

Ac=[

Columns 13 through 18

-6.0148e+01 -3.6193e-13 -1.7522e-13 5.3117e-14 -2.1554e-12 -3.0941e-13
1.8703e+01 1.6302e-13 7.8919e-14 -2.3925e-14 9.7081e-13 1.3936e-13
2.5956e+00 -4.1811e-14 -2.0241e-14 6.1363e-15 -2.4900e-13 -3.5744e-14
-4.3916e+00 -9.9721e+02 -4.8276e+02 1.4635e+02 -5.9386e+03 -8.5251e+02
-4.2918e-01 -9.7457e+01 -4.7180e+01 1.4303e+01 -5.8038e+02 -8.3315e+01
4.8214e+00 1.0948e+03 5.3001e+02 -1.6068e+02 6.5199e+03 9.3595e+02
-3.7158e+00 -1.8968e+02 -9.1829e+01 2.7838e+01 -1.1296e+03 -1.6216e+02
-9.9156e+01 3.2545e+01 1.5753e+01 -4.7761e+00 1.9395e+02 2.7807e+01
-1.1427e+05 2.1908e+00 -2.0972e+00 -4.7696e-03 1.6740e+02 -1.6386e+01
4.2367e+05 -7.3975e+00 7.0905e+00 1.5215e-02 -6.2011e+02 6.0703e+01
-3.5769e+05 5.7410e+00 -5.5096e+00 -1.1128e-02 5.2859e+02 -5.1743e+01
5.2204e+05 1.6198e-01 -3.0391e-02 -1.2858e-02 -8.0342e+02 7.8641e+01
-2.1529e+05 -2.2991e-03 -4.9157e-02 5.1565e-03 4.2258e+02 -4.1350e+01
-1.6309e+04 2.1146e+02 4.7623e+02 1.5348e-01 3.8110e-11 5.4708e-12
5.0929e+03 -4.7623e+02 -9.0823e+02 -5.0532e+00 -3.0562e-11 -4.3873e-12
1.8163e+03 1.5348e-01 5.0532e+00 -1.3327e+00 -8.2143e-12 -1.1792e-12
2.3658e+05 -1.6675e-10 -8.0727e-11 2.4473e-11 -3.8429e+02 4.3551e+01
2.4978e+04 -1.7476e-11 -8.4603e-12 2.5648e-12 -4.3551e+01 3.0125e+00
-2.3484e+05 1.8395e-10 8.9050e-11 -2.6996e-11 4.4204e+02 -2.6384e+01

Column 19

-1.8532e-14
8.3469e-15
-2.1408e-15
-5.1060e+01
-4.9900e+00
5.6057e+01
-9.7170e+00
1.5060e+00
-1.8390e+02
6.8126e+02
-5.8071e+02
8.8262e+02
-4.6418e+02
3.2766e-13
-2.6277e-13
-7.0625e-14
4.4204e+02
2.6384e+01
-7.2610e+02

Appendix C: Design II Data

Bc =

-1.2131e-03 1.7498e+02
-9.7082e-04 -8.9712e+01
-2.8504e-02 -8.7020e+00
-1.9242e-12 -1.0442e-07
-1.9126e-13 -1.0780e-08
1.9295e-12 1.0097e-07
1.4945e-04 9.7271e+00
5.1513e-03 3.3529e+02
-1.1601e+01 3.8583e+05
-2.6599e+01 -1.4306e+06
1.9484e+01 1.2078e+06
-3.0828e+01 -1.7633e+06
1.2549e+01 7.2623e+05
-2.3776e+01 5.5036e+04
1.0545e+01 -1.7183e+04
1.1662e-01 -6.1325e+03
-1.5632e+01 -7.9883e+05
-1.7043e+00 -8.4341e+04
1.3841e+01 7.9295e+05

Cc =

Columns 1 through 6

7.1643e-06 -1.4185e-06 -8.5476e-05 3.2327e-03 2.7759e-04 1.6086e-04

Columns 7 through 12

4.4567e-02 2.8216e-02 -7.1885e-03 7.2665e-04 5.4071e-04 7.6887e-06

Columns 13 through 18

-2.5422e-06 -5.7703e-04 -2.7935e-04 8.4686e-05 -3.4364e-03 -4.9330e-04

Column 19

-2.9545e-05

Dc =

0 0

Appendix C: Design II Data

Poles of the Compensator

real	imaginary	frequency	damping
-4.0000e-02	0.0000e+00	4.0000e-02	1.0000e+00
-1.1051e+00	-1.3525e-01	1.1133e+00	9.9259e-01
-1.1051e+00	1.3525e-01	1.1133e+00	9.9259e-01
-1.3516e+00	0.0000e+00	1.3516e+00	1.0000e+00
-4.8619e+00	0.0000e+00	4.8619e+00	1.0000e+00
-7.3507e+00	-8.0862e+00	1.0928e+01	6.7265e-01
-7.3507e+00	8.0862e+00	1.0928e+01	6.7265e-01
-5.4267e+01	0.0000e+00	5.4267e+01	1.0000e+00
-7.5479e+01	0.0000e+00	7.5479e+01	1.0000e+00
-1.1678e+02	0.0000e+00	1.1678e+02	1.0000e+00
-2.9589e+02	0.0000e+00	2.9589e+02	1.0000e+00
-6.4304e+02	0.0000e+00	6.4304e+02	1.0000e+00
-7.0625e+02	0.0000e+00	7.0625e+02	1.0000e+00
-3.7345e+02	-9.1227e+02	9.8575e+02	3.7885e-01
-3.7345e+02	9.1227e+02	9.8575e+02	3.7885e-01
-1.0270e+03	0.0000e+00	1.0270e+03	1.0000e+00
-2.8862e+03	-4.4683e+03	5.3194e+03	5.4258e-01
-2.8862e+03	4.4683e+03	5.3194e+03	5.4258e-01
-5.8976e+03	0.0000e+00	5.8976e+03	1.0000e+00

Zeros of the Compensator

real	imaginary	frequency	damping
-1.2373e+00	5.8492e-17	1.2373e+00	1.0000e+00
-7.8744e+00	7.1854e+00	1.0660e+01	7.3868e-01
-7.8744e+00	-7.1854e+00	1.0660e+01	7.3868e-01
-2.9625e+02	-7.3722e-14	2.9625e+02	1.0000e+00
-1.0000e+04	4.8023e-03	1.0000e+04	1.0000e+00
-1.0000e+04	-4.8023e-03	1.0000e+04	1.0000e+00

Appendix C: Design II Data

Poles of Closed Loop System

real	imaginary	frequency	damping
-1.0082e+00	0.0000e+00	1.0082e+00	1.0000e+00
-1.2184e+00	0.0000e+00	1.2184e+00	1.0000e+00
-1.3411e+00	0.0000e+00	1.3411e+00	1.0000e+00
-8.8437e+00	0.0000e+00	8.8437e+00	1.0000e+00
-5.2012e+00	-8.8448e+00	1.0261e+01	5.0690e-01
-5.2012e+00	8.8448e+00	1.0261e+01	5.0690e-01
-1.0294e+01	-2.8488e+00	1.0681e+01	9.6377e-01
-1.0294e+01	2.8488e+00	1.0681e+01	9.6377e-01
-4.0430e+01	0.0000e+00	4.0430e+01	1.0000e+00
-5.2018e+01	0.0000e+00	5.2018e+01	1.0000e+00
-5.4142e+01	0.0000e+00	5.4142e+01	1.0000e+00
-7.3609e+01	0.0000e+00	7.3609e+01	1.0000e+00
-2.0012e+02	-2.0023e+02	2.8309e+02	7.0691e-01
-2.0012e+02	2.0023e+02	2.8309e+02	7.0691e-01
-2.9593e+02	0.0000e+00	2.9593e+02	1.0000e+00
-6.4300e+02	0.0000e+00	6.4300e+02	1.0000e+00
-7.1335e+02	0.0000e+00	7.1335e+02	1.0000e+00
-3.7345e+02	-9.1227e+02	9.8575e+02	3.7885e-01
-3.7345e+02	9.1227e+02	9.8575e+02	3.7885e-01
-1.0271e+03	0.0000e+00	1.0271e+03	1.0000e+00
-2.8862e+03	-4.4683e+03	5.3194e+03	5.4258e-01
-2.8862e+03	4.4683e+03	5.3194e+03	5.4258e-01
-5.8975e+03	0.0000e+00	5.8975e+03	1.0000e+00

Appendix D: Design IVa Data

Ac

2.8019e+06	8.3015e+05	1.4849e+05	-1.2991e+07	1.2776e+07	-4.1634e+06
7.0875e+05	2.0999e+05	3.7572e+04	-3.2863e+06	3.2319e+06	-1.0532e+06
3.0366e+06	8.9969e+05	1.6071e+05	-1.4080e+07	1.3847e+07	-4.5123e+06
6.0334e+05	1.7876e+05	3.1978e+04	-2.7939e+06	2.7477e+06	-8.9658e+05
-9.6367e+04	-2.8553e+04	-5.1060e+03	4.5034e+05	-4.4300e+05	1.4330e+05
-7.8451e+04	-2.3234e+04	-4.1763e+03	3.6366e+05	-3.5765e+05	1.1554e+05
4.0642e+05	1.2036e+05	2.1636e+04	-1.8840e+06	1.8529e+06	-5.9857e+05
-8.3885e+04	-2.4843e+04	-4.4656e+03	3.8885e+05	-3.8243e+05	1.2356e+05
8.0075e+05	2.3715e+05	4.2628e+04	-3.7119e+06	3.6506e+06	-1.1797e+06
-3.0286e+05	-8.9694e+04	-1.6123e+04	1.4039e+06	-1.3807e+06	4.4641e+05
1.9758e+05	5.8514e+04	1.0518e+04	-9.1588e+05	9.0076e+05	-2.9101e+05
4.9885e+04	1.4774e+04	2.6556e+03	-2.3124e+05	2.2743e+05	-7.3475e+04
2.0237e+05	5.9932e+04	1.0773e+04	-9.3808e+05	9.2259e+05	-2.9812e+05

Columns 7 through 12

-7.0824e+05	-5.4669e+05	6.6039e+04	-8.3068e+05	-2.2146e+06	-8.8608e+05
-1.7914e+05	-1.3829e+05	1.6695e+04	-2.1014e+05	-5.6021e+05	-2.2415e+05
-7.6563e+05	-5.9251e+05	7.0125e+04	-9.0149e+05	-2.4002e+06	-9.6032e+05
-1.2508e+05	-1.1793e+05	-6.1072e+03	-1.9586e+05	-4.7688e+05	-1.9080e+05
-2.6082e+04	1.9174e+04	3.5178e+04	5.9802e+04	7.6155e+04	3.0480e+04
5.1880e+05	1.1612e+04	-3.7192e+05	-2.8577e+05	6.2243e+04	2.4741e+04
-2.6979e+06	-6.0081e+04	1.9343e+06	1.4868e+06	-3.2245e+05	-1.2818e+05
5.4815e+05	1.2461e+04	-3.9277e+05	-3.0146e+05	6.6564e+04	2.6453e+04
-5.1540e+06	-1.1953e+05	3.6909e+06	2.8290e+06	-6.3550e+05	-2.5249e+05
1.8285e+06	4.6100e+04	-1.3061e+06	-9.9530e+05	2.4053e+05	9.5455e+04
-1.3031e+06	-2.9264e+04	9.3405e+05	7.1751e+05	-1.5677e+05	-6.2297e+04
-3.2870e+05	-7.3909e+03	2.3561e+05	1.8097e+05	-3.9594e+04	-1.5733e+04
-1.3061e+06	-3.0184e+04	9.3553e+05	7.1723e+05	-1.6062e+05	-6.3816e+04

Column 13

-9.7180e+04
-2.4583e+04
-1.0532e+05
-2.0927e+04
3.3254e+03
2.9908e+03
-1.5479e+04
3.2068e+03
-3.0722e+04
1.1799e+04
-7.5508e+03
-1.8970e+03
-7.9993e+03

Appendix D: Design IVa Data

Bc =

```
-5.5044e-01  -4.9978e+04
-1.3925e-01  -1.2635e+04
-5.9465e-01  -5.3091e+04
 7.5815e-02   4.3336e+03
-5.4157e-01  -2.6044e+04
-3.6902e+00   2.7603e+05
-3.0526e+01  -1.4356e+06
 6.0760e+00   2.9151e+05
-6.0207e+01  -2.7395e+06
 2.2861e+01   9.6966e+05
-1.4818e+01  -6.9324e+05
-3.7414e+00  -1.7486e+05
-1.5202e+01  -6.9434e+05
```

Cc =

Columns 1 through 6

```
 4.0336e+00   1.1951e+00   2.1379e-01  -1.8565e+01   1.8417e+01  -5.9940e+00
```

Columns 7 through 12

```
-8.8888e-01  -7.8799e-01  -2.0183e-03  -1.2768e+00  -3.1882e+00  -1.2756e+00
```

Column 13

```
-1.3990e-01
```

Dc =

```
         0  -1.9000e-01
```

Poles of the Compensator

real	imaginary	frequency	damping
-4.0000e-02	0.0000e+00	4.0000e-02	1.0000e+00
-9.5913e-01	0.0000e+00	9.5913e-01	1.0000e+00
-1.1368e+01	0.0000e+00	1.1368e+01	1.0000e+00
-3.5412e+00	-1.3285e+01	1.3749e+01	2.5757e-01
-3.5412e+00	1.3285e+01	1.3749e+01	2.5757e-01
-7.5939e+01	0.0000e+00	7.5939e+01	1.0000e+00
-9.9318e+01	0.0000e+00	9.9318e+01	1.0000e+00
-2.4146e+02	0.0000e+00	2.4146e+02	1.0000e+00
-1.4935e+03	0.0000e+00	1.4935e+03	1.0000e+00
-3.7425e+03	-6.3092e+03	7.3357e+03	5.1017e-01
-3.7425e+03	6.3092e+03	7.3357e+03	5.1017e-01
-7.4671e+03	0.0000e+00	7.4671e+03	1.0000e+00
-1.0236e+05	0.0000e+00	1.0236e+05	1.0000e+00

Appendix D: Design IVa Data

Zeros of the Compensator

real	imaginary	frequency	damping
-3.5412e+00	1.3285e+01	1.3749e+01	2.5757e-01
-3.5412e+00	-1.3285e+01	1.3749e+01	2.5757e-01
-2.4146e+02	6.6486e-14	2.4146e+02	1.0000e+00

Poles of the Closed Loop System

real	imaginary	frequency	damping
-9.5913e-01	0.0000e+00	9.5913e-01	1.0000e+00
-2.2226e+00	-1.2069e+01	1.2272e+01	1.8112e-01
-2.2226e+00	1.2069e+01	1.2272e+01	1.8112e-01
-3.5412e+00	-1.3285e+01	1.3749e+01	2.5757e-01
-3.5412e+00	1.3285e+01	1.3749e+01	2.5757e-01
-1.4003e+01	0.0000e+00	1.4003e+01	1.0000e+00
-3.8717e+01	0.0000e+00	3.8717e+01	1.0000e+00
-6.2068e+01	0.0000e+00	6.2068e+01	1.0000e+00
-6.8115e+01	0.0000e+00	6.8115e+01	1.0000e+00
-2.4146e+02	0.0000e+00	2.4146e+02	1.0000e+00
-2.0019e+02	-2.0018e+02	2.8311e+02	7.0712e-01
-2.0019e+02	2.0018e+02	2.8311e+02	7.0712e-01
-1.4935e+03	0.0000e+00	1.4935e+03	1.0000e+00
-3.7426e+03	-6.3091e+03	7.3356e+03	5.1019e-01
-3.7426e+03	6.3091e+03	7.3356e+03	5.1019e-01
-7.4671e+03	0.0000e+00	7.4671e+03	1.0000e+00
-1.0236e+05	0.0000e+00	1.0236e+05	1.0000e+00

Appendix E: Design IVb Data

Ac =

Columns 1 through 6

2.8060e+05	4.3163e+04	2.8532e+03	-1.1018e+06	1.0844e+06	-7.1616e+05
-2.7726e+05	-4.2757e+04	-3.3943e+03	1.0888e+06	-1.0716e+06	7.0773e+05
-7.8104e+05	-1.2078e+05	-1.4066e+04	3.0673e+06	-3.0189e+06	1.9937e+06
5.5399e+04	8.5054e+03	5.1277e+02	-2.1402e+05	2.1054e+05	-1.4137e+05
-9.5046e+03	-1.4593e+03	-8.7975e+01	4.0834e+04	-4.0290e+04	2.4254e+04
4.1071e+00	6.3057e-01	3.8015e-02	-1.6806e+01	1.4572e+01	-7.1826e+02
-2.1381e+01	-3.2826e+00	-1.9790e-01	8.7480e+01	-7.5848e+01	3.7411e+03
3.6717e+00	5.6372e-01	3.3986e-02	-1.5022e+01	1.3016e+01	-6.4411e+02
-2.3161e+01	-3.5559e+00	-2.1438e-01	9.4757e+01	-8.2082e+01	4.0665e+03
1.0857e+01	1.6669e+00	1.0049e-01	-4.4409e+01	3.8358e+01	-1.9266e+03
-4.5854e-08	-6.8636e-09	7.4108e-12	-7.8386e-01	9.9170e+00	1.7046e+03
4.0075e-08	5.9984e-09	-6.4767e-12	5.5322e-01	-6.9992e+00	-1.2031e+03
7.4350e-08	1.1129e-08	-1.2016e-11	-1.3711e-03	1.6825e-02	3.0446e+00

Columns 7 through 12

-3.6927e+04	-3.9921e+04	-6.4122e+03	2.6737e+03	-2.1160e+05	-3.5749e+04
3.6492e+04	3.9451e+04	6.3367e+03	-2.6422e+03	2.0911e+05	3.5328e+04
1.0280e+05	1.1114e+05	1.7851e+04	-7.4434e+03	5.8908e+05	9.9522e+04
-7.2888e+03	-7.8803e+03	-1.2664e+03	5.2756e+02	-4.1770e+04	-7.0568e+03
1.2705e+03	1.3521e+03	1.9539e+02	-9.8197e+01	7.1663e+03	1.2107e+03
3.5529e+05	1.4367e+03	-3.8953e+05	-1.3678e+05	3.3939e+02	-3.3898e+02
-1.8507e+06	-7.4812e+03	2.0291e+06	7.1247e+05	-1.7506e+03	1.7486e+03
3.1867e+05	1.2851e+03	-3.4936e+05	-1.2267e+05	3.1479e+02	-3.1429e+02
-2.0118e+06	-8.1088e+03	2.2055e+06	7.7430e+05	-2.0068e+03	2.0034e+03
9.5329e+05	3.8414e+03	-1.0449e+06	-3.6720e+05	1.1691e+03	-1.1648e+03
-8.5582e+05	-3.4547e+03	9.3829e+05	3.2946e+05	-9.9786e+02	1.0138e+03
6.0401e+05	2.4381e+03	-6.6221e+05	-2.3252e+05	1.0138e+03	-1.1042e+03
-1.5170e+03	-7.3053e+00	1.6648e+03	5.8712e+02	2.8988e+03	-3.4393e+03

Column 13

8.0246e+01
-7.9301e+01
-2.2340e+02
1.5839e+01
-2.7710e+00
-9.5345e+02
4.9184e+03
-8.8407e+02
5.6354e+03
-3.2774e+03
2.8988e+03
-3.4393e+03
-1.4193e+04

Appendix E: Design IVb Data

Bc =

1.7156e-12	9.6320e-08
-1.3814e-12	-7.3544e-08
-1.6063e-12	-5.2275e-08
-4.2504e-07	3.4426e-01
-1.4826e-05	1.1854e+01
-6.3468e+00	2.1207e+05
-2.1463e+01	-1.1047e+06
3.4960e+00	1.9020e+05
-2.3714e+01	-1.2008e+06
1.2004e+01	5.6900e+05
-1.0180e+01	-5.1083e+05
7.6355e+00	3.6053e+05
4.0937e+00	-9.0560e+02

Cc =

Columns 1 through 6

3.3812e-01 5.1912e-02 3.1297e-03 -1.2022e+00 1.3280e+00 -8.6284e-01

Columns 7 through 12

-4.4490e-02 -4.8097e-02 -7.7254e-03 3.2213e-03 -2.5494e-01 -4.3071e-02

Column 13

9.6682e-05

Dc =

0 -1.9000e-01

Poles of the Compensator

real	imaginary	frequency	damping
-4.0000e-02	0.0000e+00	4.0000e-02	1.0000e+00
-9.5913e-01	0.0000e+00	9.5913e-01	1.0000e+00
-9.3849e+00	0.0000e+00	9.3849e+00	1.0000e+00
-1.9649e+01	0.0000e+00	1.9649e+01	1.0000e+00
-9.9601e+01	0.0000e+00	9.9601e+01	1.0000e+00
-1.0478e+02	0.0000e+00	1.0478e+02	1.0000e+00
-5.9684e+02	0.0000e+00	5.9684e+02	1.0000e+00
-5.2606e+03	0.0000e+00	5.2606e+03	1.0000e+00
-3.4878e+03	-5.2225e+03	6.2800e+03	5.5538e-01
-3.4878e+03	5.2225e+03	6.2800e+03	5.5538e-01
-1.4150e+04	0.0000e+00	1.4150e+04	1.0000e+00
-1.5679e+04	0.0000e+00	1.5679e+04	1.0000e+00
-1.5771e+04	0.0000e+00	1.5771e+04	1.0000e+00

Appendix E: Design IVb Data

Zeros of the Compensator

real	imaginary	frequency	damping
-1.0478e+02	0.0000e+00	1.0478e+02	1.0000e+00
-9.3849e+00	0.0000e+00	9.3849e+00	1.0000e+00

Poles of the Closed Loop System

real	imaginary	frequency	damping
-9.4464e-01	0.0000e+00	9.4464e-01	1.0000e+00
-7.4894e+00	0.0000e+00	7.4894e+00	1.0000e+00
-9.3849e+00	0.0000e+00	9.3849e+00	1.0000e+00
-2.4022e+01	-1.6734e+01	2.9276e+01	8.2053e-01
-2.4022e+01	1.6734e+01	2.9276e+01	8.2053e-01
-4.6860e+01	-6.2883e+00	4.7280e+01	9.9112e-01
-4.6860e+01	6.2883e+00	4.7280e+01	9.9112e-01
-1.0478e+02	0.0000e+00	1.0478e+02	1.0000e+00
-1.8572e+02	-1.8643e+02	2.6315e+02	7.0576e-01
-1.8572e+02	1.8643e+02	2.6315e+02	7.0576e-01
-5.9661e+02	0.0000e+00	5.9661e+02	1.0000e+00
-5.2607e+03	0.0000e+00	5.2607e+03	1.0000e+00
-3.4880e+03	-5.2223e+03	6.2800e+03	5.5541e-01
-3.4880e+03	5.2223e+03	6.2800e+03	5.5541e-01
-1.4150e+04	0.0000e+00	1.4150e+04	1.0000e+00
-1.5679e+04	0.0000e+00	1.5679e+04	1.0000e+00
-1.5771e+04	0.0000e+00	1.5771e+04	1.0000e+00

References

[1] Doyle, J. and G. Stein, "Multivariable Feedback Design with Concepts for a Classical/Modern Synthesis," *IEEE Trans. on Automat. Contr.*, AC-26, pp. 4-16, Feb. 1981.

[2] Athans, M. and G. Stein, "The LQG/LTR Procedure for Multivariable Feedback Control Design," *IEEE Trans. on Automat. Contr.*, AC-32, pp. 105-114, Feb. 1987.

[3] Safonov, M. G., A.J. Laub, and G. Hartmann, "Feedback Properties of Multivariable Systems: The Role and Use of the Return Difference Matrix," *IEEE Trans. on Automat. Contr.*, AC-26, pp.47-65, Feb. 1981.

[4] Berstein, D. and W. Haddad, "LQG Control with an H_∞ Performance Bound: A Riccati Equation Approach," *IEEE Trans. on Automat. Contr.*, AC-34, pp.293-305, Mar. 1989.

[5] Madiwale, A.N., W. Haddad, and D. Bernstein, "Robust H_∞ Control Design for Systems with Structured Parameter Uncertainty," Systems and Control Letters, 12, pp. 393-407, 1989.

[6] Reichert, R.T., "Robust Autopilot Design Using μ-Synthesis," ACC, San Diego CA., pp. 2368-2373, May 1990.

[7] Wise, K. and Barry Mears, "Missile Autopilot Design Using H_∞ Optimal Control with μ-Synthesis," ACC, San Diego CA., pp. 2362-2367, May 1990.

[8] Foo, Y. K. and I. Postlethwaite, "An H_∞ minimax approach to the Design Of Robust Control Systems," Systems and Control Letters, 5, pp. 81-88, 1984.

[9] Safonov, M.G. and R. Chiang, "CACSD Using the State-Space L_∞ theory—A Design Example," *IEEE Trans. on Automat. Contr.*, AC-33, pp. 477-479, May 1988.

[10] Banda, S. and T. McQuade, "A Preliminary Investigation of H_∞ Optimization," *Proc. of the AIAA Guidance and Control Conference*, 1986, Paper No. 86-2197.

[11] Zames, G, " Feedback and Optimal Sensitivity: Model Reference Transformations, Multiplicative Seminorms and Approximate Inverses" *IEEE Trans. on Automat. Contr.*, Vol. AC-26, pp. 302-320, April 1981.

[12] Lehtomaki, N.A., "Pratical Robustness Measures in Multivariable Control System Analysis," Ph.D. Dissertation, MIT, Cambridge, Ma., 1981.

[13] Wise, K., "Singular Value Robustness Tests for Missile Autopilot Uncertainties," *Proc. of the AIAA Guidance and Control Conference*, 1989, Paper No.89-3552-CP.

[14] Craig, I.K., "Sensitivity of H_∞ controller Designs to Structured Uncertainty," SM Degree, MIT, Cambridge, Ma., 1989.

[15] Resnick, C.S., "A Method for Robust Control of Systems with Par. :tric Uncertainty Motivated by a Benchmark Example," SM Degree, MIT, Cambridge, Ma., 1991.

[16] Chiang, R.Y., M. Safonov, and J. Tekawy, " Flight Control Design with Large Parametric Robustness," ACC, San Diego CA., pp. 2496-2501, May 1990.

[17] Doyle, J.C., "Analysis of Feedback Systems with Structured Uncertainties," *IEE Proceedings*, vol. 129, Part D, no. 6, pp. 242-250, Nov. 1982.

[18] Safonov, M.G., "Optimal Diagonal Scaling for Infinity Norm Optimization," ACC, pp. 125-128, 1985.

[19] Doyle, J.C., "Structured Uncertainty in Control System Design," *Proc. of the 24th IEEE Conference on Decision and Control*, pp. 260-265, Dec. 1985.

[20] Maciejowski, J.M., *Multivariable Feedback Design*, Addison-Wesley, Ma, 1989.

[21] Doyle, J. and K. Glover, "State-Space Formulae for all Stabilizing Controllers that satisfy an H_∞-norm bound and relations to Risk Sensitivity," Systems and Control Letters, 11, pp. 167-172, 1988.

[22] Athans, M., "The Role and Use of the Stochastic Linear Quadratic-Gaussian Problem in Control System Design," *IEEE Trans. on Automat. Contr.*, AC-16, pp. 529-552, Dec. 1971.

[23] Hotz. A.F., "Constrained Variance Control Design - A Multi Objective Control Theory," ACC, Pittsburgh, Pa., pp. 2071-2076, June 1989.

[24] Francis, B.A., A Course in H_∞ Control Theory (Springer-Verlag, Berlin-New York, 1987).

[25] μ-Analysis and Synthesis Toolbox (μ-Tools), supplied by MUSYN Inc.

[26] Bisplinghoff, Raymond L. and Holt Ashley, *Principles of Aeroelasticity*, Dover Publications, Inc. NY, 1962, 395-396.

[27] R. Ramnath. 16.16 Flight Dynamics Course, MIT, 1990.

[28] Nelson, R.C., *Flight Stability and Automatic Control* (McGraw-Hill, NY,1989).

[29] Lunze, Jan, *Robust Multivariable Feedback Control*, (Prentice Hall, NY, 1988).